Universidad de Málaga
Departamento de Física Aplicada II
Escuela Doctoral Internacional en Estudios del Mar (EDEIMAR)
Programa de doctorado: Dinámica de los flujos biogeoquímicos y sus aplicaciones.

Drainage of deep Mediterranean Water, its transition through the Strait of Gibraltar: spatial and temporal variability.

Tesis Doctoral presentada por:
Cristina Naranjo Rosa

Dirigida por:
Jesús García Lafuente

Y codirigida por:
José Carlos Sánchez Garrido

Drainage of deep Mediterranean Water, its transition through the Strait of Gibraltar: spatial and temporal variability

(Drenaje de las aguas profundas del mar mediterráneo, estudio de su tránsito a través del Estrecho de Gibraltar y su variabilidad espacio-temporal)

Tesis Doctoral presentada por:

Cristina Naranjo Rosa

Dirigida por:

Jesús García Lafuente

Y codirigida por:

José Carlos Sánchez Garrido

Para obtener el grado de Doctora por la Universidad de Málaga

Departamento de Física Aplicada II

Grupo de Oceanografía física

Escuela de doctorado:

Escuela doctoral internacional en estudios del mar (EIDEMAR)

Programa de doctorado:

Dinámica de los flujos biogeoquímicos y sus aplicaciones

El Director	El Codirector	La Doctoranda
Jesús García Lafuente	José Carlos Sánchez Garrido	Cristina Naranjo Rosa

D. Jesús García Lafuente, catedrático de la Universidad de Málaga y *D. José Carlos Sánchez Garrido,* investigador del Departamento de Física Aplicada II de la Universidad de Málaga

HACEN CONSTAR:

Que el trabajo recogido en la memoria titulada "*Drainage of deep Mediterranean Water, its transition through the Strait of Gibraltar: spatial and temporal variability*", presentada por *Cristina Naranjo Rosa*, ha sido realizado bajo nuestra supervisión y cumple con la calidad científica suficiente.

Que la presente tesis está avalada por cuatro artículos, dos de ellos ya publicados, un tercero enviado tras una segunda revisión menor y un último en (moderada-menor) revisión. Todos ellos en revistas de alto índice de impacto en su área que no han sido presentados anteriormente en ninguna otra tesis.

Que reúne sobradamente los criterios de calidad establecidos para la lectura de la tesis en el programa de doctorado "Dinámica de los flujos biogeoquímicos y sus aplicaciones", por ello se informa muy favorablemente sobre el trabajo realizado y se autoriza su presentación y defensa para optar al grado de Doctor Internacional por la Universidad de Málaga.

Para ello firmamos la presente en Málaga a 06 de julio de 2015.

Fdo. Director
Jesús García Lafuente

Fdo. Codirector
José Carlos Sánchez Garrido

A mis padres, mis hermanos y
nuestros dos soles, Adri y Guille

TABLE OF CONTENTS

I. PUBLICATIONS ARISING FROM THIS THESIS

The thesis hereby is presented as a "*thesis by published works*". A total of four papers are gathered to this aim, which have been published (a, and b), accepted for publication (c) or under review (d) in scientific journals all of them belonging to the first quartile in the oceanography area. This thesis model has been previously supported by the directors in the corresponding inform. The four papers listed below deal with different aspects of the drainage of deep Mediterranean waters through the Strait of Gibraltar from the Alboran basin to the Atlantic Ocean as well as with the effect that the local tides in the Strait have on larger scale processes taking place in the neighboring basins.

a) *Cristina Naranjo*, Jesús García Lafuente, Jose C. Sánchez Garrido, Antonio Sánchez Román, Javier Delgado Cabello, *The Western Alboran Gyre helps ventilate the Western Mediterranean Deep Water through Gibraltar*. Deep Sea Research Part I: Oceanographic Research Papers, Volume 63, May 2012, Pages 157-163, ISSN 0967-0637, http://dx.doi.org/10.1016/j.dsr.2011.10.003.
Impact factor: 2.825 Quartile in category: Q1

b) *Cristina Naranjo*, Jesús García Lafuente, Gianmaria Sannino, Jose C. Sánchez Garrido, *How much do tides affect the circulation of the Mediterranean Sea? From local processes in the Strait of Gibraltar to basin-scale effects*. Progress in Oceanography, Volume 127, September 2014, Pages 108-116, ISSN 0079-6611, http://dx.doi.org/10.1016/j.pocean.2014.06.005.
Impact factor: 3.986 Quartile in category: Q1

c) Jose C. Sánchez Garrido, *Cristina Naranjo*, Jesús García Lafuente, Diego Macías, Temel Oguz, *Modeling the impact of tidal flows on the biological productivity of the Alboran Sea.* Journal of Geophysical Research: Oceans, submitted under a second minor revision.
Impact factor: 3.440 Quartile in category: Q1

d) *Cristina Naranjo*, Simone Sammartino, Jesús García Lafuente, María J. Bellanco, Isabelle Taupier Letage. *Mediterranean waters along and across the Strait of Gibraltar, characterization and zonal modification*. Submitted to Deep Sea Research Part I: Oceanographic Research Papers. Under review (a first report from the reviewers has been received; two out of three recommend publication with minor or very minor revision and the third reviewer also recommend the publication but with a more in depth revision. Currently, July 6, 2015 we are working in the new version).
Impact factor: 2.825 Quartile in category: Q1

II. GENERAL INTRODUCTION

II.a. Abstract

This Thesis is the outcome of the research carried out in the Strait of Gibraltar and adjacent basins during the last years in the frame of the INGRES research projects conducted by the Physical Oceanography Group of the University of Málaga. A first objective was the understanding of the ventilation of the deep waters in the Alboran Sea and the identification of the mechanisms and processes involved, such as the role of regional-scale structures, the tidal forcing in the Strait or the spatio-temporal pattern of the water masses participating in the exchange through the Strait. These topics provide new insights about the dynamics and properties of the Mediterranean outflow before leaving the Mediterranean Sea. The interesting and relevant issue of the impact of tides in the Strait in the bio-geochemistry of the Alboran Sea is the last topic addressed in the Thesis[1].

II.b. State of the art

Early questions about the origin of the Mediterranean outflow were investigated by *Stommel et al.* [1973]. The authors ascribed the uplift of deep Mediterranean water in the Alboran Sea to the Bernoulli suction driven by the high velocities occurring in the main sill of the Strait of Gibraltar, and concluded that even the deepest water in the Mediterranean could flow upward and out through the Strait. These authors measured potential temperature of θ=12.84ºC, which corresponds to the Western Mediterranean Deep Water (WMDW), in the eastern entrance of the Strait. Nevertheless they acknowledged that the θ-S characteristics of this water would be eroded inside the Strait and that its observation on the Atlantic side of the Strait, beyond the Camarinal sill (CS hereinafter, see Figure 1), would not be an easy task. The mentioned work found also that isotherms are banked steeply against the southern continental slope of the Western Alboran Sea. Such structure cannot be explained by Bernoulli suction, so that the authors speculated about a permanent geostrophic eddy as the responsible for that pattern.

[1] Every topic listed above is the subject of a publication in a peer reviewed journal (See section I).

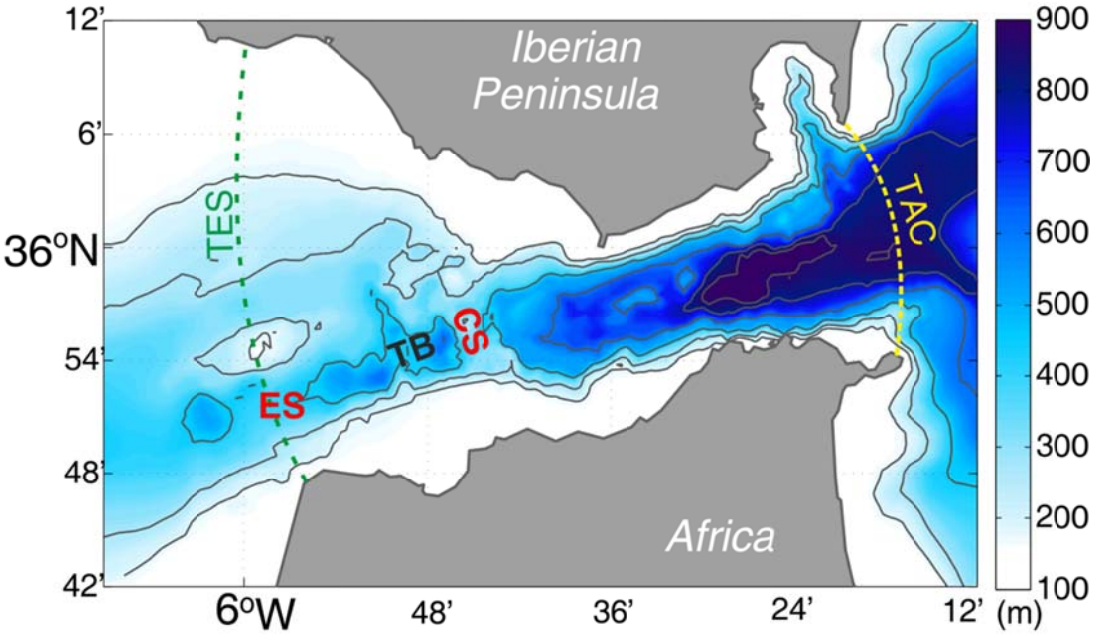

Figure 1. Detail of the Strait of Gibraltar, contours are drawn for 100 to 800 m each 200m, 900 m isobaths have been also added. Main geographical features named in the manuscript are indicated; ES and CS represent Espartel and Camarinal Sill respectively while TB indicates the near location of Tangier basin. The hydrological sections TAC and TES, mentioned in Sections II, VII and IX, have been also represented with yellow and green dashed lines respectively.

A later work by *Bryden and Stommel* [1982] extended the study of this topic and suggested that the Western Alboran Gyre (WAG) was involved in the ventilation of the WMDW by providing energy to uplift this water toward the sill of the Strait. Also, laboratory experiment performed by *Whitehead* [1985] confirmed that a selective withdrawal of Mediterranean Water exists due to Bernoulli suction. Shortly after, *Kinder et al.* [1986] studied the role of a shoaling bottom using a rotating tank experiment with a sloping bottom; results from this experiment showed a narrow boundary current developing on the left side (westward current) of the Bering Sea, and so authors concluded that the bathymetry would dominate the potential vorticity gradient. The same conclusion was drawn by *Parrilla et al.* [1986] and [*Preller*, 1986] using a numerical approach. Their results showed a narrow outflow along the Moroccan slope which they attributed to the dominant effect of the bottom shoaling on the potential vorticity.

New datasets collected during the Gibraltar Experiment (between October 1985 and October 1986, see *Kinder and Bryden* [1987]) disclosed a certain relationship between the westward flow and potential temperature lower than 12.9°C over CS [*Pettigrew*, 1989]; these observations also revealed that some WMDW returned across the CS to the Mediterranean when the

tidal flow reversed. *Kinder and Bryden* [1990], making use of the data set collected so far, analyzed the short time variability and found that the WMDW could flow over CS sill almost every semidiurnal tidal cycle during both spring and neap tides, although it was more often detected in spring tides logically.

The topic was revisited in *García Lafuente et al.* [2007], who showed evidence of the direct drainage of WMDW employing observations gathered at Espartel sill (ES hereinafter), in the western boundary of the Strait (see Figure 1). Their work presented proofs of a seasonal cycle in the outflow, which was warmer and lighter in winter and cooler and denser in spring-summer. More specifically, the authors reported a drop in the observed θ at ES shortly after the very cold March 2005, a harsh winter whose climatic conditions favored the formation of a great amount of WMDW that reached the bottom of the basin, as reported in *Schröder et al.* [2006] and *López-Jurado et al.* [2005]. They ascribed the cycle observed in ES to the subsequent uplift of older and slightly lighter WMDW to depths from which it was easily suctioned over CS. The signature of this water would be also detected in ES shortly after the event of formation of the new WMDW. The role played by the Alboran basin mesoscale structures in evacuating WMDW was addressed in *García Lafuente et al.* [2009]. The authors found a significant correlation between the near-bottom θ series collected in ES and the time coefficients of the second empirical mode identified in an Empirical Orthogonal Functions analysis of altimetry data of the Alboran Sea, whose spatial pattern captured the WAG structure. These results supported the hypothesis of *Bryden and Stommel* [1982] concerning the role of the WAG in the uplift of WMDW in the Alboran basin.

Another important issue related to the exchange through the Strait of Gibraltar is the analysis and identification of the water masses contributing to the inflow and the outflow. For its climatic implications, which are not well understood yet, the water masses in the outflow have been more extensively studied, as it can also be deduced by the previous paragraphs. To this respect, *Millot et al.* [2006] brought into play the suggestion of considering more water masses than the two traditionally taken into account in the outflow, the Levantine Intermediate Water (LIW hereinafter) and the WMDW. In his study Millot put forward the presence of the so-called Tyrrhenian Dense Water (TDW), formed by the mixing of old resident WMDW in the Tyrrhenian Sea

with LIW coming from the Eastern Mediterranean after overflowing the Strait of Sicily. According to Millot's results, this TDW would have been present in the outflow in 2003 and 2004. Following the same thread, in a later paper *Millot* [2009] suggested the participation of a fourth Mediterranean water in the outflow, the Winter Intermediate Water (WIW), that is formed by the cooling of Modified Atlantic Water (MAW) during cold winters in the continental shelf of the north western region of the Western Mediterranean. WIW is identifiable in the potential density interval $28<\sigma_\theta<29$ in a θ-S diagram by a minimum of salinity and occupies a layer located between the NACW and the other three Mediterranean Waters (WMDW, LIW and TDW, see Figure 2). More recently *Millot* [2014] revisited the issue stressing the idea of an outflow formed by different proportions of four Mediterranean water masses that were distinguishable even after crossing the main sill of Camarinal in their path toward the Atlantic. The author supported this conclusion in the analysis of the slope of the mixing lines defined in a θ-S diagram by Conductivity-Temperature-Depth (CTD) profiles of the casts being analyzed. However, the undisputable identification of the different Mediterranean waters beyond CS is a controversial result [*García Lafuente et al.*, 2011].

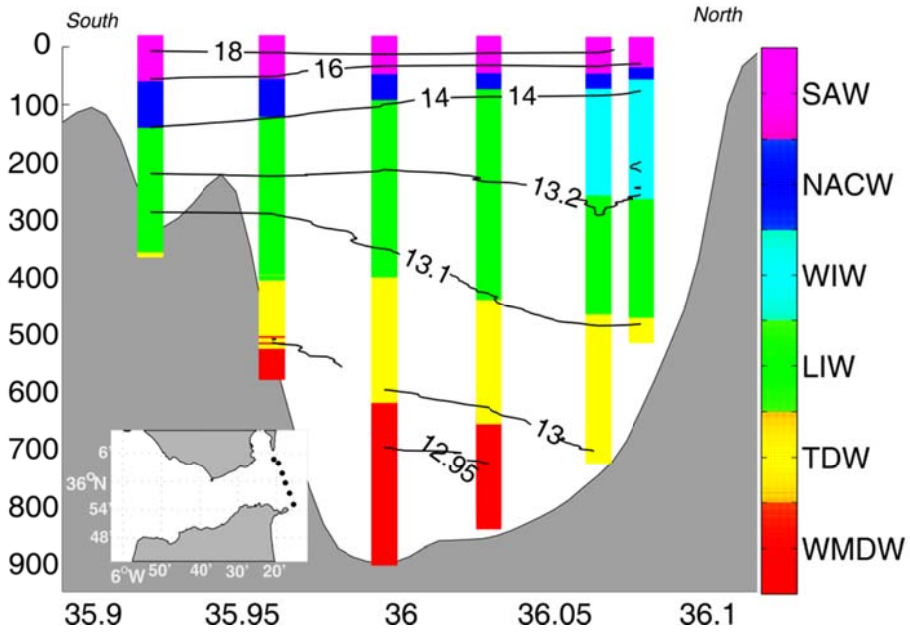

Figure 2. Scheme of the zonal and vertical distribution of Mediterranean and Atlantic waters flowing through the eastern boundary of the Strait of Gibraltar (named TAC in Figure 1). Each color indicates a water mass identified by its acronym in the legend at the right. Enclose map shows the location of the casts used to make this figure.

The inflow of Atlantic water into the Mediterranean Sea, usually referred as the Atlantic Jet, determines the surface circulation of the Alboran Sea, the westernmost sub-basin of the Western Mediterranean. The typical pattern of the surface circulation in this sub-basin is the co-existence of two anticyclonic gyres, the already mentioned WAG and the Eastern Alboran gyre (EAG) [*Seco*, 1959; *Donguy*, 1962; *Lanoix*, 1974]. The Atlantic Jet follows a meandering path around both gyres and originates intense density fronts repeatedly studied in the literature [*Tintore et al.*, 1988; *Tintoré et al.*, 1991; *Viúdez et al.*, 1996] when it meets the denser and saltier MAW residing in the Mediterranean Sea. Associated with the frontal activity of these structures, satellite data show high chlorophyll concentrations along the Jet [*Navarro et al.*, 2011], suggesting an enhanced productivity sustained by the ageostrophic circulation in the front [*Oguz et al.*, 2014]. This pattern is more noticeable in the western Alboran Sea, where westerly winds can further cause upwelling along the Spanish shore and give rise to phytoplankton blooms [*Sarhan et al.*, 2000; *Ramírez et al.*, 2005; *Reul et al.*, 2005; *Macías et al.*, 2007; 2008]. These processes are essential to explain why the Alboran Sea is the most productive sub-basin of the Mediterranean Sea [*Uitz et al.*, 2012]. The role played by the frontal dynamics in the biological productivity of the Alboran Sea was recently addressed by *Oguz et al.* [2014] using a 3D numerical model. Their model did not include tides, which is a considerable drawback since tidal currents can fertilize the surface inflowing waters through the enhancement of the vertical mixing at the western side of CS [*García Lafuente et al.*, 2013]. The strong interaction between tidal currents and the abrupt bottom topography of the Strait of Gibraltar originates hydraulic transitions [*Sánchez Garrido et al.*, 2011] that favors vertical motions, particularly in the Tangier basin downstream of CS (Figure 1), and the subsequent mixing of the relative impoverished Atlantic water with the nutrient rich deep Mediterranean waters that had been previously uplifted from the Alboran basin. A good deal of the mixed water returns toward the Mediterranean when the tide reverses and could fuel the production in the photic layer, helping to maintain the high rates of primary productivity observed in the northern area. However, the topic has not been addressed yet.

II.c. The objectives of this dissertation and its organization

The previous section has raised several important and relevant issues concerning different processes of the Strait of Gibraltar and its neighboring basins, especially the Alboran basin in the Mediterranean Sea. These issues are the body of this dissertation, which aims at providing responses to questions like whether or not the WAG is involved in the final drainage of the WMDW and, if yes, which is its role in the process (Chapter III[2]), or which is the role of the tides in the Strait of Gibraltar in the aspiration of this water (Chapter IV [3]). Other appealing issues are the remote effect of the tides in the Strait on large scale processes taking place inside the Mediterranean Sea, such as the winter deep convection in the Gulf of Lion (also addressed in Chapter IV) or in the fertilization of the Alboran basin (Chapter V[4]). There is also the ongoing debate about the composition of the outflowing waters through the Strait of Gibraltar. Based on a comprehensive dataset acquired in this area recently, Chapter VI [5] describes new outcomes about this composition. The dissertation finishes with a short summary of the main findings reported in the mentioned Chapters.

All this research has been carried out in the frame of the sequence of INGRES projects funded by the Spanish Ministry of *Economía y Competitividad* (projects REN2003_01608, CTM2006_02326 and CTM2010_21229), although most of the effort has been done within INGRES-3 project (CTM2010_21229), the last also granted the author of the present dissertation with a "Formación de Personal Investigador" (BES-2011-043421) fellowship, both of which are specially acknowledged.

[2] This Chapter corresponds to paper "*The Western Alboran Gyre helps ventilate the Western Mediterranean Deep Water through Gibraltar*" (see section I).

[3] This Chapter corresponds to paper "*How much do tides affect the circulation of the Mediterranean Sea? From local processes in the Strait of Gibraltar to basin-scale effects*" (see section I).

[4] This Chapter corresponds to paper "*Modeling the impact of tidal flows on the biological productivity of the Alboran Sea*" (see section I).

[5] This Chapter corresponds to paper "*Mediterranean waters along and across the Strait of Gibraltar, characterization and zonal modification*" (see section I).

II.d. Methodology

To address the first of the above mentioned topics, Chapter III examines the presence of WMDW in the outflow by analyzing a five-year long time series of potential temperature collected at ES. The sensor was placed near the bottom to ensure that it was measuring the densest water leaving the Strait, which is the WMDW. Altimetry data of the Alboran Sea were utilized to detect surface structures, such de anticyclonic gyres, and follow their evolution, which allowed us to investigate the relation between the WAG and the drainage of WMDW at ES as indicated by the θ time series. Historical CTD data from MEDATLAS database [*MEDAR-Group*, 2002] were used to estimate the depth from which deep waters in the Alboran Sea could be suctioned. Finally, a numerical model was run under two different configurations: in one of them the Strait of Gibraltar was closed and the outputs of the model were compared with a run in which the Strait was present. The comparison clarifies the role that the dynamics within the Strait plays in the aspiration of WMDW.

Chapter IV investigates the effects that the tidal forcing in the Strait of Gibraltar could have not just in the near Alboran basin but also farther east, in the interior of the Mediterranean Sea. Two process-oriented model experiments were conducted to this aim: the first one was a regional (Strait of Gibraltar and neighbor basins) and the second one was basin-wide (Mediterraneam Sea). Both models were run twice, with and without tidal forcing. The regional model revisited the effect of tides on the exchanged flows through the Strait and the modification of the hydrological properties of the Altantic inflow by contrasting the outputs from the runs with and without tides. The last issue is relevant for the deep formation processes in the Gulf of Lions since the mixing induced by tides in the Strait makes a first preconditioning of the Atlantic water that will be transformed in different Mediterranean waters. This important issue was further addressed with a basin scale model with a comparable configuration in the Strait region. The comparison between both runs highlights the role of the tides in the deep convection processes forming WMDW in the Gulf of Lion and also in the ventilation of this water in the Alboran Sea.

As commented above, the Alboran Sea displays high rates of primary productivity, especially if compared with the rest of the Mediterranean Sea. Vertical mixing induced by tides in the Strait of Gibraltar has been proposed [*García Lafuente et al.*, 2013] as a source of nutrients to this basin. The issue

is further discussed in Chapter V by the implementation of a high resolution circulation model coupled to an ecosystem model. The same procedure followed in Chapter IV is repeated here: a reference numerical experiment in which tidal forcing is suppressed (but yet reproducing the basic circulation in the area of the Strait of Gibraltar and Alboran Sea) is compared with a similar run including tidal forcing in order to evaluate the biological consequences that the tidal dynamics in the Strait could have on the biological processes in the Alboran basin.

The last of the works, presented in Chapter VI, deals with the classification of the water masses involved in the exchange through the Strait of Gibraltar. The θ-S characteristics of the Mediterranean waters differ very slightly and, moreover, their presence or position in a determined section is highly variable and depends noticeably on the tidal phase. The Gibraltar International campaign (see Chapter VI for details) was conducted to acquire new data with a Moving Vessel Profiler (MVP), which allows a high spatial resolution and relatively fast accomplishment of hydrological transects and, therefore, provides datasets that minimize that variability. These data were processed by cluster analysis specifically developed for these data, which assigned a membership to each point of every CTD cast in function of the distance to centroids with θ-S-σ_θ characteristics predefined for each of the possible water masses that are susceptible to flow through the Strait. Time variability was assessed using the collection of CTD measurements in the western and eastern limiting sections of the Strait that have been repeated since 2005 within the INGRES projects.

Further details about the methodology are described in more detail in each of the following Chapters.

III. The Western Alboran Gyre helps ventilate the Western Mediterranean Deep Water through Gibraltar

Cristina Naranjo*, Jesús García Lafuente, Jose C. Sánchez Garrido, Antonio Sánchez Román, Javier Delgado Cabello

Physical Oceanography Group, ETSI Telecomunicación, University of Málaga, Campus Teatinos, 29071 Málaga, Spain

Published in Deep-Sea Research I doi:10.1016/j.dsr.2011.10.003

ARTICLE INFO

Article history:
Received 27 April 2011
Received in revised form
19 October 2011
Accepted 24 October 2011
Available online 29 October 2011

Keywords:
Western Mediterranean Deep Water
Deep water ventilation
Strait of Gibraltar
Alboran Gyre

ABSTRACT

Variable properties of the Mediterranean outflow and the variability of the Western Alboran Gyre are analyzed by means of 5-year long time series of near bottom potential temperature at Espartel sill in the Strait of Gibraltar and altimetry data in the Alboran Sea. Geostrophic velocity at the southern edge of the gyre and potential temperature at Espartel sill are significantly correlated (correlation coefficient 0.67), suggesting that the intensification of the Alboran Gyre favors the ventilation of Western Mediterranean Deep Water. The analysis of historical temperature profiles shows that Western Mediterranean Deep Water in the Alboran Sea can be suctioned from a layer between 500 and 700 m depth for typical changes of the gyre intensification.

1. Introduction

The question of how the Western Mediterranean Deep Water (WMDW) is ventilated through the Strait of Gibraltar is of key importance for the renewal of the Mediterranean Sea. WMDW has to flow over Camarinal sill (CS, see Fig. 1) whose depth (290 m) is less than the depth of the interface between WMDW and the overlying waters in the Alboran Sea. The Mediterranean outflow is formed by the WMDW, the Levantine Intermediate Water (LIW, by far the most important contributor) and other waters of Mediterranean origin (Millot, 2009). WMDW is the densest, hence the deepest, of all the Mediterranean waters and therefore the most energy-demanding to be drained out to the Atlantic Ocean over the depths of CS. In a pioneering paper by Stommel et al. (1973), using Bernoulli equation arguments, showed that WMDW could be aspired from depths as great as 700 m in the Alboran basin, a possibility confirmed few years later by Whitehead (1985) in laboratory simulations and by Kinder and Parrilla (1987) who presented for the first time experimental evidence of WMDW west of CS thus proving that this water had overflowed the sill.

Bryden et al. (1994) and Vargas et al. (2006) showed that the outflow over CS occurs in a pulsating way driven by tidal forces that move back and forth a volume of water three to five times larger than the mean flow (García Lafuente et al., 2000). Tide is also the main source of energy to suction deep waters located in the eastern approach of the Strait and to bring them west of CS into the Atlantic Ocean. Actually, the ventilation of WMDW would comprise two separated, though linked, set of processes. The first one would include all processes leading to make WMDW available for suction in the westernmost part of the Alboran basin close to the Strait of Gibraltar or, in other words, to carry WMDW towards the eastern approach of the Strait. García Lafuente et al. (2009) identified some of these processes such as the re-filling of the western Mediterranean basin with newly formed WMDW, or favorable meteorological conditions able to diminish the net barotropic flow through the Strait of Gibraltar, or the presence of a large Western Alboran Gyre (WAG). The second set of processes comprise all physical forcing that influence the total current over CS since the larger the current here, the greater the depth from which deep water in the eastern approach of the Strait can be suctioned. Tidal strength (the fort-nightly cycle) plays a relevant role in this mechanism, a fact acknowledged by Kinder and Bryden (1990) who suggested that pure WMDW overflows CS during all spring tide periods.

Bryden and Stommel (1982) presented currentmeter observations at 500 m depth in the southwestern Alboran Sea (see the black triangle in Fig. 1) showing a rather permanent flow of WMDW (mean $=4.6 \pm 4.3$ cm s^{-1}) heading towards the Strait of Gibraltar with potential temperature (θ hereafter) ranging from 12.81 °C to 13.01 °C, typical of this water. They also observed a marked upwards slope of the isotherms towards the African shore, suggesting that the main path of WMDW ventilation follows the southern part of the Alboran Sea, a result further confirmed by numerical models (Parrilla et al., 1986; Speich et al., 1995 and references therein) and reproduced by the model used in this work as well. On the basis

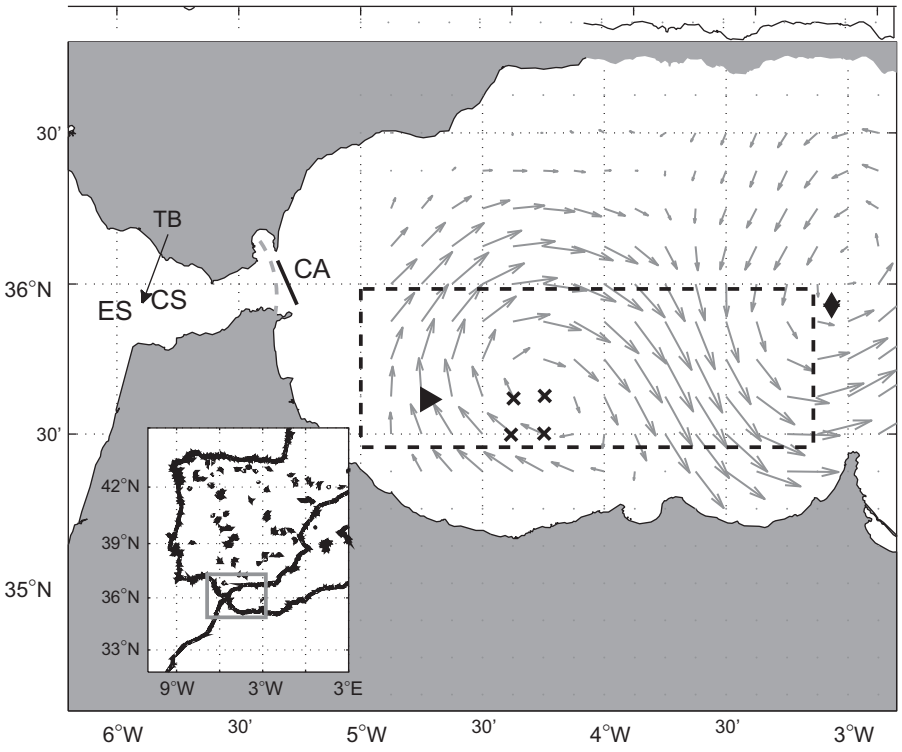

Fig. 1. Map of the Strait of Gibraltar. ES and CS indicate the location of Espartel and Camarinal sills; TB is Tangier Basin and CA indicates the Ceuta-Algeciras CTD section mentioned in the text. Dashed gray line shows the model section used in Fig. 3. Dashed black rectangle in the Alboran Sea indicates the area where MEDATLAS profiles have been selected. Arrows depict the Western Alboran Gyre and indicate surface velocity in August 2008 from altimetry data. Crosses indicate the positions to compute U_{SWAG} (see text Section 2.2). Black triangle indicates the currentmeters' site in Bryden and Stommel (1982). The diamond represents the Alboran Island.

of these observations Bryden and Stommel (1982) put forward for the first time the idea that the WAG may facilitate the drainage of WMDW, as the gyre provides energy to uplift deep water to depths where it can be easily aspired when they eventually reach the eastern entrance of the Strait.

New experimental evidence of direct WMDW suction over CS has been provided by García Lafuente et al. (2007), who showed two cold pulses typical of WMDW in a time series of θ measured at Espartel sill (ES, Fig. 1) during the winters of years 2005 and 2006. More recently, García Lafuente et al. (2009), using a longer series θ at ES, re-visited the role of the WAG in facilitating the aspiration of WMDW through the Strait. They carried out an Empirical Orthogonal Function analysis of altimetry data of the Alboran Sea and showed that the time coefficients of the second empirical mode were significantly correlated with θ at ES. Since this mode captured a significant fraction of the temporal variability of the WAG, they conclude that the presence of a well developed gyre facilitated the suction of WMDW—identified by relative minima of θ in the time series—through ES (and, hence, through CS) supporting the Bryden and Stommel (1982) hypothesis. However, part of the WAG variability in García Lafuente et al. (2009) was also explained by the first empirical mode, which was uncorrelated with θ at ES. The question deserved further attention and has been addressed in this work using long time series of θ and Sea Surface Height (SSH) from altimetry in the Alboran Sea. The Massachusetts Institute of Technology general circulation model (MITgcm, Marshall et al., 1997) has also been run to illustrate some basic aspects of the whole process.

2. Data and data processing

2.1. In situ measurements

In October 2004 an oceanographic station was deployed in ES to monitor the Mediterranean outflow. A conductivity–temperature (CT) probe installed 10 m above the sea floor measured the θ–S characteristics of the outflow at a sampling rate of 30 min. Due to its proximity to the bottom, the probe detected the densest water flowing out from the Mediterranean Sea. Six conductivity–temperature–depth (CTD) casts along the cross-section CA (Fig. 1) were carried out in June 2009 to show the spatial structure of the Mediterranean water masses in the eastern part of the Strait. The CTD probe was lowered as close as possible to the bottom to register the characteristics of the deepest, densest water. Historical CTD data of the Alboran Sea from the MEDATLAS database (MEDAR group, 2002) have also been used in this study.

As in García Lafuente et al. (2009), θ series at ES is used here to follow the variability of the WMDW in the outflow. Salinity was another possibility that was discarded because temperature is a better choice to discriminate WMDW against LIW, the other important water mass in the outflow. The θ series shows large tidal fluctuations that act as noise for long-term variability on which this work focuses. Following García Lafuente et al. (2007, 2009), tides have been removed by selecting the sample of minimum θ within each semidiurnal cycle, which decimates the series to about a value every 12 h. Since it will be correlated to SSH data from AVISO, whose sampling interval is a week, θ series has been further decimated to weekly values by extracting the coldest sample every week. The resulting series will be referred to as θ_{min} series hereafter.

2.2. Satellite data

Geostrophic surface velocities derived from altimetry provided by AVISO have been used to determine the WAG variability. These data have spatial and temporal resolutions of 1/4 degree and one week, respectively, and span the period from October 2004 to October 2009, which coincides with the CT time series. For the purpose of this work, the variable U_{SWAG} defined as the spatial average of the zonal component of the geostrophic velocity in the

grid points marked in Fig. 1 has been used as a proxy of the WAG variability. Large absolute values of U_{SWAG} correspond to a well-developed gyre that, in our hypothesis, has more potential to uplift WMDW from greater depths in the Alboran Sea.

3. Experimental results

3.1. The WAG and the temperature in ES

Fig. 2 shows the time evolution of U_{SWAG} and θ_{min} and their low-passed contributions. Its mean value is 24 cm s^{-1} with a standard deviation (STD) of $\pm$11 cm s^{-1}, and does not exhibit a well-defined seasonality although the low-passed series suggests greater westward velocity in summer months. Taking into account that AVISO geostrophic velocities are inferred from sea level gradients, summer maximum would correspond to a well-developed WAG, in good agreement with previous works dealing with the WAG variability (Vargas-Yáñez et al., 2002).

More than six year long time series of θ_{min} in ES shows cold peaks close to 13 °C (Fig. 2b) that roughly match the time evolution of U_{SWAG}. Warmer values above 13.2 °C are found by the end of the different years when U_{SWAG} also presents (absolute) minimum values associated with a weaker WAG. The cross correlation coefficient between both series is 0.46 at the 95% significance level. The coefficient raises to 0.61 if high-frequency variability is removed (low-passed series) and it further increases to 0.67 if θ_{min} series is shifted back 2 weeks with respect to U_{SWAG}. This fact is interpreted as a time-delayed response if the WAG intensity is a driving force for uplifting WMDW in the Alboran Sea.

3.2. Spatial evolution of potential temperature depth

The mean value of θ_{min} at ES is 13.10 °C, a value that can be taken as representative of the WMDW that leaves the Strait of Gibraltar through ES. Using long time series of simultaneous observations in CS and ES, García Lafuente et al. (2011) showed that vigorous tidal

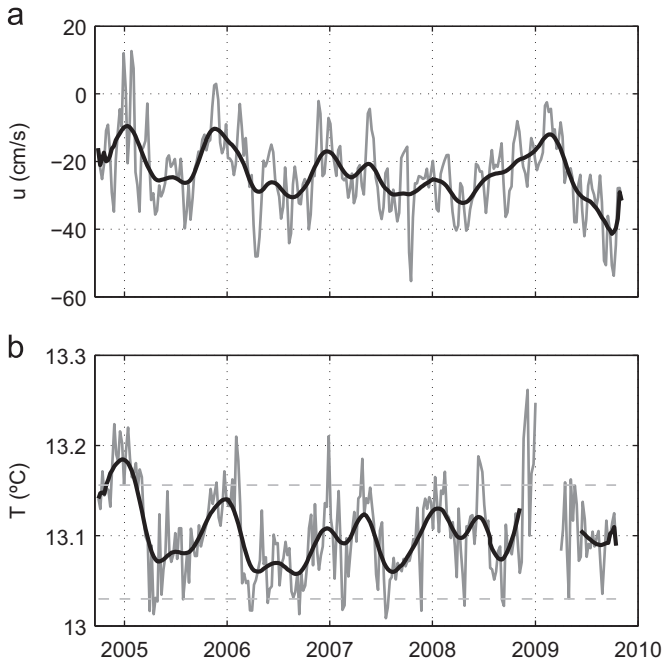

Fig. 2. (a) Gray line: U_{SWAG} time series derived from altimetry data. Black line: low-pass filter signal. (b) Gray line: θ_{min} time series in Espartel sill. Black line: low-pass filter signal. Dashed line: the mean minimum and maximum values of θ, 13.05 and 13.15 °C, respectively ($\theta \pm$ STD).

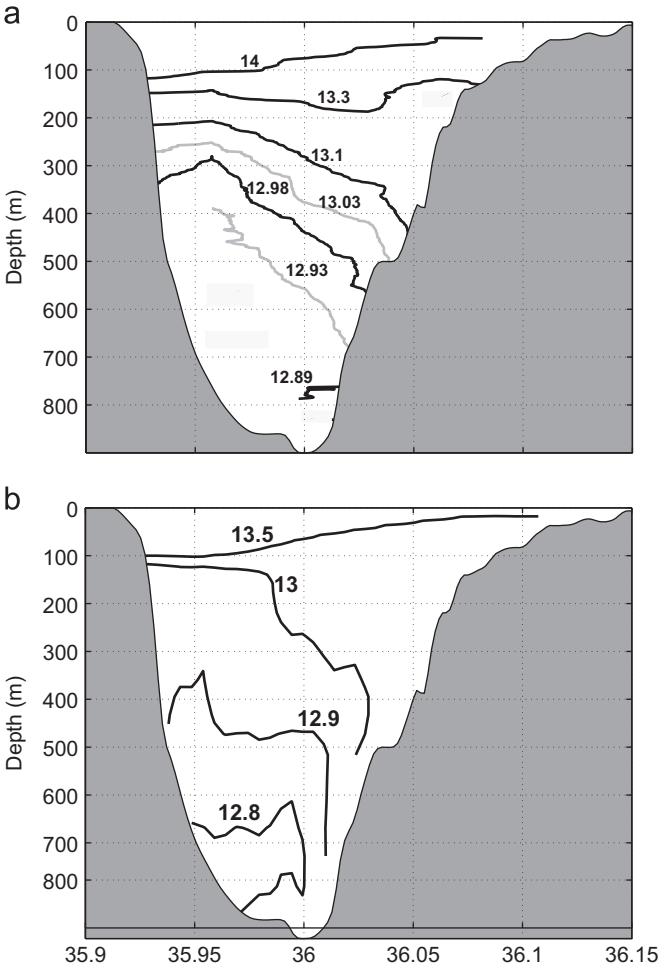

Fig. 3. (a) Potential temperature measure in cross-section CA marked in Fig. 1, *x*-axis is latitude (°N); CTD data were collected from 10:16 to 14:09 h in June 16th, 2009. (b) Model results in a similar section (dashed gray line in Fig. 1).

mixing in Tangier basin (TB, Fig. 1) increases the WMDW temperature by 0.12 °C on its way from CS to ES, so that the representative θ_{min} at CS would be 12.98 °C. Eastwards of CS the cross-area of the outflow increases markedly and the Mediterranean layer flows rather slowly. This fact reduces greatly water mixing, so we can assume that θ remains constant along streamlines. Fig. 3a shows that, in the eastern approach of the Strait, WMDW still maintains the tendency of remaining attached to the African side and that θ=12.98 °C can be found in the depth range 300–600 m, shallower in the south. Historical MEDAR θ data in the southern half of the western Alboran Sea (Fig. 4) show that this water resides, on average, at 520 m depth, although the banking of WMDW against the African slope would allow this water to be found at shallower depths more to the south. This description shows the continuous uplifting of the WMDW from the Alboran Sea to the west until it finally crosses ES and flows out to the North Atlantic Ocean.

3.3. Temporal variability

Taking the STD as representative of the typical variability, θ_{min} at ES would be 13.10 $\pm$ 0.05 °C although Fig. 2b shows that it fluctuates between 13.01 °C and an anomalous maximum of 13.26 °C by the end of 2009. Correcting these values for mixing in Tangier basin, θ_{min} at CS would be 12.98 $\pm$ 0.05 °C (from 12.93 °C to 13.03 °C interval), which would be also representative of θ_{min} variability eastwards of CS in our hypothesis of very reduced mixing. Isotherms 12.93 °C and 13.03 °C are marked with

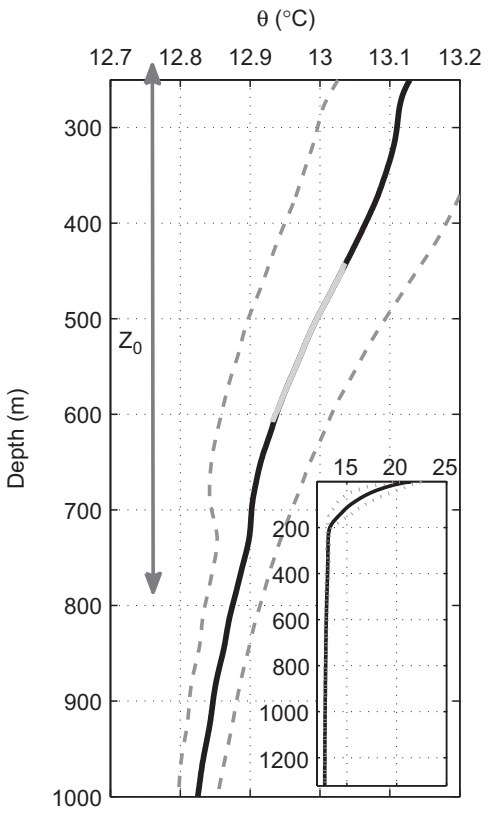

Fig. 4. Spatially-averaged vertical profiles of potential temperature below 260 m depth from the MEDATLAS database in the southern part of the western Alboran basin (the inset shows the whole profile). Dashed lines indicate ± 1 STD, shadow area indicates de θ_{min} interval variation in ES corrected by the mixing factor.

gray lines in Fig. 3a and indicate the layer in the eastern part of the Strait that would be evacuated to the North Atlantic under the typical fluctuations of the forcing responsible for the observed variability at ES. It occupies the depth range between 670 m and 250 m depth. However, extreme θ_{min} values at ES of 13.01 °C in Fig. 2a, which would reduce to 12.89 °C at CS and eastwards, would displace the lower bound to the sea bottom (Fig. 3a), suggesting that all the Mediterranean layer in the eastern approach of the Strait is potentially drainable to the Atlantic under extreme forcing.

Further east, the depth range associated with the STD-size fluctuations at ES is from 440 to 600 m if we only consider the mean profile (gray portion of the mean profile in Fig. 4) but increases from 230 to 780 m if the variability of the profile, indicated by the dashed lines, is taken into account (double-headed arrow in Fig. 4). In case of extreme fluctuations, this depth could exceed 800–900 m.

4. Numerical model

The correlation between U_{SWAG} and θ_{min} supports the hypothesis of Bryden and Stommel (1982) that the WAG helps to uplift WMDW. For that, the WMDW in the western Alboran Sea must flow westwards along the African slope in the same direction as the overlaying Atlantic layer in the southern part of the WAG. The observations of Bryden and Stommel (1982) confirm they do but whether this preferred path of the WMDW is determined by the general circulation of the Mediterranean Sea (remote influence) or it is more a consequence of the water exchange through the Strait (local influence) remains unclear. A second issue to investigate is to which extent the uplifting of WMDW in the southern Alboran Sea is directly influenced by the dynamic of the Strait. Both topics have been addressed by process-oriented numerical simulations using the MITgcm.

The model domain extends from 9°W to 1°E and is horizontally discretized by a curvilinear orthogonal grid with minimum grid size in the Strait (Δx, Δy=500 m), gradually increasing to 4–5 km in the Alboran Sea, and 8–10 km near the open boundaries (Fig. 5a). The vertical spatial coordinate is discretized with 46 z-levels.

The model was run from a very simplified initial state in which the Mediterranean side was filled with two water masses representing LIW and WMDW of θ–S characteristics (13.2 °C, 38.55) and (12.8 °C, 38.45), respectively. Initially LIW occupied the 600 uppermost meters, the rest being filled with WMDW. The Atlantic side was occupied by Atlantic water of (15.5 °C, 36.2) θ–S characteristics. Both basins, initially at rest, were separated by a barrier that was removed at t=0 (lock-exchange initial condition). Orlanski radiation boundary condition (Orlanski, 1976) for both velocity and tracers was imposed at the open boundaries. No other external forces (meteorological, tides) were applied.

The model evolves to a final state characterized by a well developed WAG occupying the western Alboran Sea encircled by a swift Atlantic jet of 1 ms^{-1} typical speed (Fig. 5b) that leaves the domain by the eastern boundary to form eventually the Algerian current. The deep circulation (Fig. 5c) shows a vein of LIW/WMDW at 500 m depth that enters the western Alboran basin along the trough located north of the Alboran Island and flows southwestwards to the African continental slope where it veers towards the Strait to contribute to the outflow. Its mean speed at the grid points used to compute U_{SWAG} is 4.8 cm s^{-1}, quite close to the mean value of 4.6 cm s^{-1} provided by Bryden and Stommel (1982) at the same depth at a short distance to the west. The spatial distribution of isotherms across the Alboran basin (Fig. 5d) reproduces the pattern reported by these authors and illustrates the uplift of WMDW in the south where it is noticeably shallower ($<$300 m) than it was initially (600 m). Fig. 3b shows that the model also accumulates WMDW in the southern part of the Strait, matching the observations in Fig. 3a. Since no forcing was imposed on the open boundaries, this pattern would be linked to the dynamics of the exchange rather than to remote forcing acting across the boundaries.

To assess the direct influence of the Bernoulli aspiration caused by high velocities over CS on the uplifting of WMDW in the Alboran Sea, another numerical experiment was carried out in which the WAG was isolated from the strait dynamics by closing the strait at t=100 day, 50 days before the situation presented in Fig. 5b. The surface circulation 50 days later is yet characterized by a large WAG (Fig. 6a), now extending more to the north as it is not constrained by the Atlantic jet. Fig. 6b and c shows that the depth of the isotherm 12.85 °C is fairly similar in the closed and open-strait experiments except for the small area in front of the Strait's entrance where the closed-strait simulation shows it deeper and somewhat displaced northeastwards (consequence of the new enlarged shape of the WAG). Farther away from this area the circulation appears to be quite independent of the strait status indicating that the gyre is mainly responsible for the banking of WMDW against the African slope. On the other hand, the shallowness of the isotherm in front of the strait in the open-strait run is attributable to the Bernoulli suction, whose effect is only noticeable around this area.

5. Discussion and conclusions

The analysis of the different datasets in this work has showed the good correlation between the geostrophic velocity of the WAG

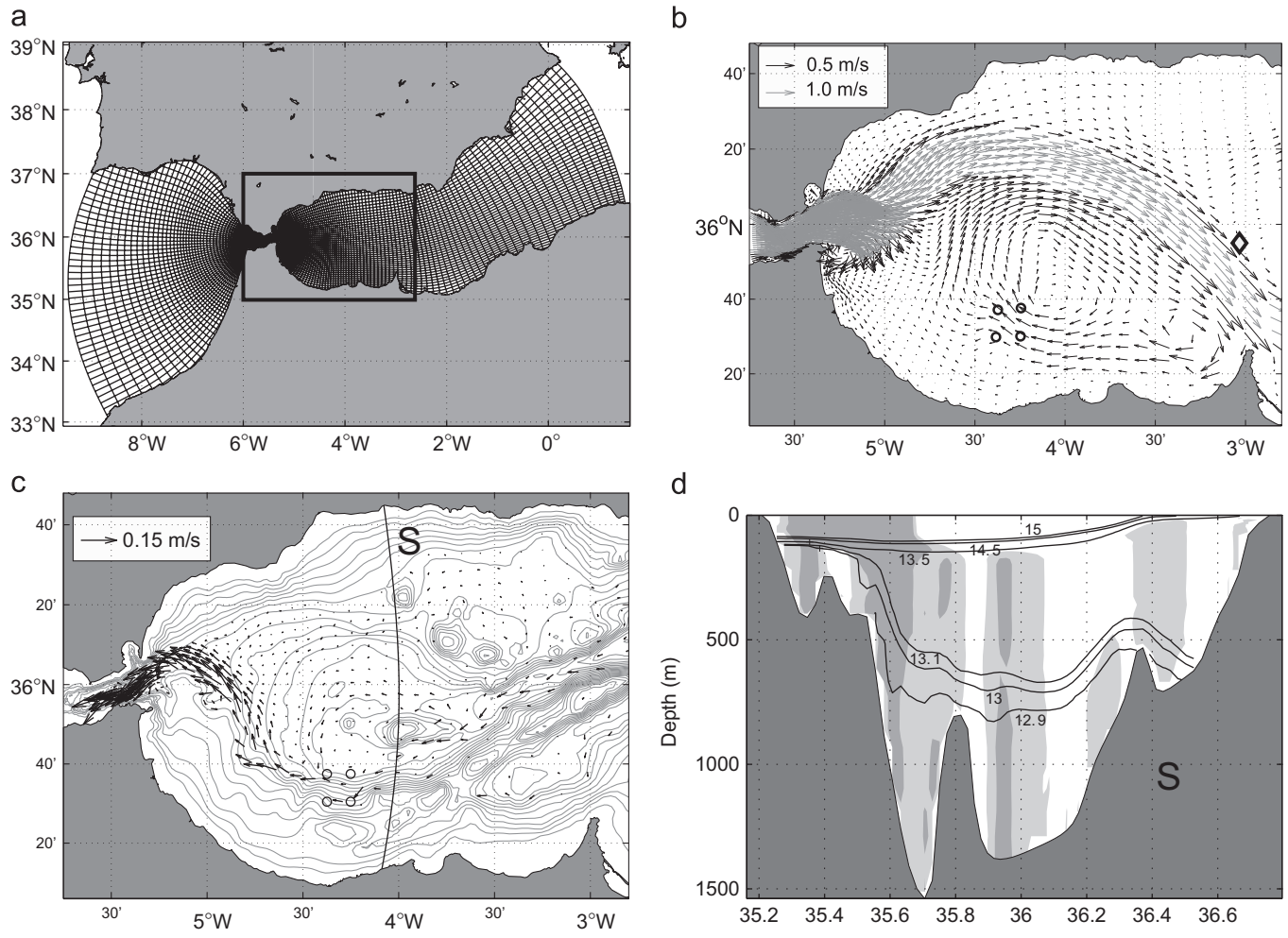

Fig. 5. (a) Computational grid used in the study (only 50% of the grid points are shown for the sake of clarity), the black rectangle encloses the Strait of Gibraltar and the Western Alboran Sea. (b) Modeled surface velocity. The diamond represents Alboran Island. (c) Same as (a) at $z=500$ m depth. Isobaths $z=100, 200, \ldots, 2000$ m are given by gray lines. (d) Cross section S, (panel c) of temperature and zonal velocity. Light contours are for negative velocities. Darker contours indicate areas of $u < -0.02$ m s^{-1}.

and the near-bottom potential temperature at ES, which gives support to the hypothesis that a well developed WAG helps ventilate WMDW from the Alboran Sea and, hence, from the Mediterranean Sea. The ventilation is a two-step process starting with the uplift of WMDW produced by the WAG, whose final result is to facilitate the arrival of WMDW to the eastern entrance of the strait from where it is eventually aspired by the enhanced currents over CS. Once the sill has been surpassed, the WMDW flows without major topographic restrictions towards the Atlantic Ocean while mixing with the surrounding waters.

Some attempts have been made to investigate the depth from which WMDW can be aspired by this two-step mechanism. Using θ as a tracer, historical data from MEDAR in the southern half of the western Alboran basin (Fig. 4) indicate that $\theta_{min}=12.98$ °C (the mean value of θ_{min} at CS) is found at $z_0=520$ m. This would be the representative depth from which the coldest/densest WMDW can be suctioned. Numerical results presented in Fig. 5c strongly suggest that water at 500 m depth flowing at 4.8 cm s^{-1} leaves the Mediterranean Sea. The coincidence in turn suggests that this velocity would correspond to the minimum value able to uplift resident WMDW in Alboran over the sills of the Strait.

When the time variability of θ_{min}, scaled by its STD at ES, is incorporated into the analysis then z_0 becomes a layer between 440 and 610 m (thick gray line in Fig. 4). If the correlation between θ_{min} and U_{SWAG} stands, the upper bound of this layer would coincide with the maximum depth from which a weakened WAG of $U_{SWAG}=11$ cm s^{-1} (the mean, 24 cm s^{-1}, minus the STD, 13 cm s^{-1}) could uplift, on average, water for feeding the outflow. Similarly, the lower bound would be the maximum depth from which a strengthened WAG of $U_{SWAG}=37$ cm s^{-1} (mean+STD) would suction water. Obviously the WMDW characteristics in the suctioned water will be much clearer in the second case. Under extreme situations, both the lower and upper ends of the depth interval will change. For instance, judging from the θ transect in Fig. 3a, the lower bound can move downwards to 800–900 m if we consider the extreme situations that forces the periodically observed presence of θ_{min} as low as 13.01 °C in the Mediterranean outflow at ES (Fig. 2b). On the contrary, there are unusual situations in which the WAG in the western Alboran Sea disappears and is replaced by a coastal jet of Atlantic water flowing attached to the African shore (Vargas-Yáñez et al., 2002). In this case, the downwards transfer of momentum would act to stop the flow of WMDW towards the Strait while the general circulation would facilitate a major drainage of the LIW residing at intermediate depths in the northern part of the Alboran basin, thus changing markedly the proportion of the different Mediterranean waters in the outflow.

It must be noticed that the water exchange is responsible for the WAG generation, which in turn uplifts WMDW from the deep part of the Alboran basin and makes it available for suction at the eastern approach of the Strait. From this point of view, the two-step process of WMDW evacuation from the western Alboran

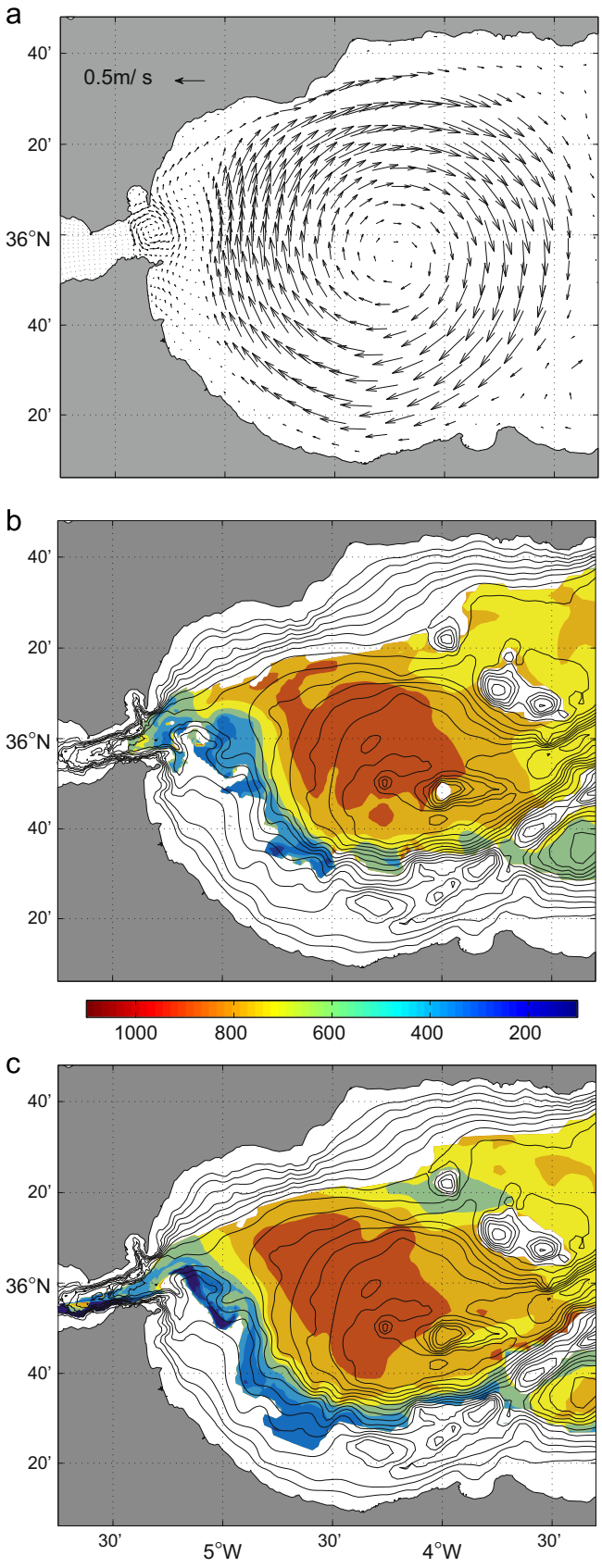

Fig. 6. (a) Surface velocity of the Western Alboran Sea in the closed-Strait experiment. (b) Depth of the isotherm surface $\theta = 12.85\ ^{\circ}C$ (in meters) after 50 days of the Strait closure. (c) Same as (b) for the open-Strait run.

Sea is triggered by the internal dynamics of the exchange whose spatial reach exceeds the Strait dimensions. This conclusion is supported by the simple lock-exchange experiment that reproduces the well-documented deep circulation of the western Alboran Sea (Bryden and Stommel, 1982; Parrilla et al., 1986), with WMDW being uplifted and flowing towards the Strait over the African shelf. The closed-Strait experiment confirms that this uplift is driven by the WAG although the final escape of the WMDW from the Mediterranean Sea needs the Bernoulli suction triggered by the very high velocities over CS.

The aspiration of WMDW depends on the availability of this water at the depths from which it can be suctioned. The WAG forcing discussed here is one mechanism but it is not the only one. There are some others as commented in Section 1. Should any of them prevail over the WAG forcing, the correlation between θ_{min} and U_{SWAG} would diminish. Most probably, this was the case by the end of the winter of year 2005 (and to a lesser extent of year 2006), when an extraordinary production of new and very dense WMDW reached the bottom of the western Mediterranean basin and uplifted old WMDW to shallower depths (Schroeder et al., 2008). Its footprint was a very cold pulse in θ_{min} at ES (Fig. 2b) that was not echoed by a similar fluctuation of U_{SWAG} (Fig. 2a). The signal that a fluctuating WAG could have induced in θ_{min} would have been masked by this process, as discussed in García Lafuente et al. (2009).

The last remark concerns the meteorological variability that acts at – relatively – short time scale. It has been discussed above since it is implicitly included in both θ_{min} and altimetry time series. However, it is not included in the numerical simulations for two reasons. First, the main objective of the model was to address process-oriented studies to assess the role of the WAG in the ventilation of WMDW. Meteorological forcing would obviously modulate the whole process, but it is not expected to produce significant changes. The second and more important reason is that the main factor driving subinertial variability in the Strait of Gibraltar and, hence, in the western Alboran Sea is the atmospheric pressure variability over the whole Mediterranean basin, whose parameterization in a reduced model domain such as the one used in this work is far from being trivial (see García Lafuente et al., 2002). The detailed numerical analysis of the meteorological forcing on the exchange through the Strait requires the nesting of a Mediterranean basin-scale model, like the barotropic model used in García Lafuente et al. (2002), with a reduced-domain model like the one used in this work. Such study is presently under way and it is not addressed here as it is out of the scope of this work.

Acknowledgments

Authors acknowledge the Spanish Ministerio de Ciencia e Innovación for the financial support of INGRES projects (CTM2006-02326 and CTM2010-21229), Acciones Complementarias (CTM2009-05810/E and CTM2009-05885-E) and partial funding of regional government of Junta de Andalucía through excellence project RNM-3738. We are grateful to AVISO for the free use of their databases and to the crew of the Spanish R/V Odón de Buen for their help and assistance during the oceanographic cruises. Computer resources and technical support provided by the Supercomputing and Bioinformatics (SCBI) center of the University of Malaga are also acknowledged.

References

Bryden, H.L., Candela, J., Kinder, T.H., 1994. Exchange through the Strait of Gibraltar. Prog. Oceanogr. 33, 201–248.
Bryden, H.L., Stommel, H.M., 1982. Origin of the Mediterranean outflow. J. Mar. Res. 40, 55–71.

García Lafuente, J., Vargas, J.M., Plaza, F., Sarhan, T., Candela, J., Baschek, B., 2000. Tide at the eastern section of the Strait of Gibraltar. J. Geophys. Res. 105, 14197–14213.

García Lafuente, J., Alvarez Fanjul, E., Vargas, J.M., Ratsimandresey, A.W., 2002. Subinertial variability in the flow through the Strait of Gibraltar. J. Geophys. Res. 107, 32.1–32.9. doi:10.1029/2001JC0011004.

García Lafuente, J., Sanchez Román, A., Sannino, G., Díaz del Río, G., Sánchez Garrido, J.C., 2007. Recent observations of seasonal variability of the Mediterranean outflow in the Strait of Gibraltar. J. Geophys. Res. 107 (C10), 32.1–32.9. doi:10.1029/2001JC0011004.

García Lafuente, J., Delgado, J., Sánchez Román, A., Soto, J., Carracedo, L., Díaz del Río, G., 2009. Interannual variability of the Mediterranean outflow observed in Espartel Sill, Western Strait of Gibraltar. J. Geophys. Res. 112 (C10005). doi:10.1029/2006JC003992.

García Lafuente, J., Sánchez-Román, A., Naranjo, C., Sánchez-Garrido, José C., 2011. The very first transformation of the Mediterranean outflow in the Strait of Gibraltar. J. Geophys. Res. 116 (C07010). doi:10.1029/2011JC006967.

Kinder, T.H., Parrilla, G., 1987. Yes, some of the Mediterranean outflow does come from great depth. J. Geophys. Res. 92 (C3), 2901–2906.

Kinder, T.H., Bryden, H.L., 1990. Aspiration of deep waters through straits. In: Pratt, L.J. (Ed.), The Physical Oceanography of Sea Straits, vol. 318, The Netherlands, pp. 295–319.

Marshall, J., Adcroft, A., Hill, C., Perelman, L., Heisey, C., 1997. A finite-volume, incompressible Navier Stokes model for studies of the ocean on parallel computers. J. Geophys. Res., 5753–5766.

MEDAR Group, 2002. MEDAR 2002 Database Mediterranean and Black Sea cruise Inventory, Observed Data, Analysed Data and Climatological Atlas (4 CD-ROMs).

Millot, C., 2009. Another description of the Mediterranean Sea outflow. Prog. Oceanogr. 82, 101–124. doi:10.1016/j.pocean.2009.04.016.

Orlanski, I., 1976. A simple boundary condition for unbounded hyperbolic flows. J. Comput. Phys. 211, 251–269.

Parrilla, G., Kinder, T.H., Preller, R.H., 1986. Deep and intermediate Mediterranean water in the western Alboran Sea. Deep-Sea Res. 33, 55–88.

Schroeder, K., Ribotti, A., Borghini, M., Sorgente, R., Perilli, A., Gasparini, G.P., 2008. An extensive western Mediterranean deep water renewal between 2004 and 2006. Geophys. Res. Lett. 35, L18605. doi:10.1029/2008GL035146.

Speich, S., Madec, G., Crépon, M., 1995. A strait outflow circulation process study: the case of the Alboran Sea. J. Phys. Oceanogr. 26, 320–340.

Stommel, H., Bryden, H.L., Mangelsdorf, P., 1973. Does some of the Mediterranean outflow come from great depth? Pageoph 105, 879–889.

Vargas, J.M., García Lafuente, J., Candela, J., Sánchez-Román, A.J., 2006. Fortnightly and monthly variability of the exchange through the Strait of Gibraltar. Prog. Oceanogr. 70 (2–4), 466–485.

Vargas-Yáñez, M., Plaza, F., García-Lafuente, J., Saran, T., Vargas, J.M., Vélez-Belchi, P., 2002. About the seasonal variability of the Alboran Sea circulation. J. Mar. Syst. 35, 224–248.

Whitehead, J.A., 1985. A laboratory study of gyres and uplift near the Strait of Gibraltar. J. Geophys. Res. 90 (C4), 7045–7060.

IV. How much do tides affect the circulation of the Mediterranean Sea? From local processes in the Strait of Gibraltar to basin-scale effects

C. Naranjo [a,*], J. Garcia-Lafuente [a], G. Sannino [b], J.C. Sanchez-Garrido [a]

[a] Physical Oceanography Group, University of Málaga, CEIMAR, Málaga, Spain
[b] ENEA, Ocean Modelling Unit, via Anguillarese 301, 00123 Rome, Italy

Published in Progress in Oceanography http://dx.doi.org/10.1016/j.pocean.2014.06.005

A B S T R A C T

The effects of tidal forcing on the exchange flow through the Strait of Gibraltar and the circulation in the near-field region are revisited with a regional numerical model. Also a basin-scale model run is conducted in a first attempt to assess the impact of these local processes on the Western Mediterranean thermohaline circulation. In the Strait of Gibraltar, tides are found to (1) increase the exchange flow volume transport, (2) modify the hydrological properties of Atlantic inflowing waters through the enhancement of mixing, and (3) facilitate the drainage of Mediterranean deep water. In the far-field, the model reveals that these local processes can favor deep convection in the Gulf of Lion. Some thoughts are provided offering possible explanations.

Introduction

The baroclinic exchange through the Strait of Gibraltar (SoG hereinafter) is forced by the buoyancy losses in the Mediterranean Sea (MS). They give rise to the characteristic anti-estuarine thermohaline circulation of the MS that starts at the SoG with the surface Atlantic Jet and ends at the same location with the deep outflow of Mediterranean waters. The average properties of the latter are basically determined by the buoyancy losses and the constraining topography of the SoG (Fig. 1), which drives the intervening flows to the hydraulic limit and to a situation of maximal exchange (Armi and Farmer, 1985, 1986; Farmer and Armi, 1988). Within this theoretical frame, Bryden and Kinder (1991) resolved the steady, two-layer maximal exchange problem for a simple but yet realistic geometry of the SoG by imposing the mean net evaporation over the MS as the proper reservoir condition. Despite ignoring some of the relevant driving forces, the approach gives realistic predictions of the exchange.

The exchange involves different time-scales (Garcia-Lafuente et al., 2000, 2002a, 2002b) and the forces ignored in the previous models, essentially tidal forces and meteorologically-driven pressure gradients should be included to obtain more accurate predictions. Theoretical (Farmer and Armi, 1986; Helfrich, 1995), laboratory (Helfrich, 1995), numerical (Wang, 1993; Sannino et al., 2004) and observational (Bryden et al., 1994; Vargas et al., 2006) studies show that tides increase the long-term exchange flow by means of eddy-fluxes. The easiest way to visualize this process is by decomposing the velocity and the layer thickness in slowly varying (overbar) and fluctuating (primed) components according to $u = \bar{u} + u', h = \bar{h} + h'$ (in practice, the decomposition is achieved by applying a suitable filter). The slow-varying flow, often called long-term flow, is defined as the exchange resulting from the time-average of the flow over a time window considerably longer than the tidal scale and is obtained as

$$\bar{q}_l = W\left(\bar{u}_l\bar{h}_l + \overline{u_l'h_l'}\right) \quad (1)$$

The first term of the right hand side is the quasi-steady contribution due to the mean fields whereas the second term is the eddy fluxes. Here W is a representative width and $i = 1, 2$ indicates the Atlantic and Mediterranean layers. According to the observational analysis by Bryden et al. (1994), eddy-fluxes may account for up to 40% of the estimated long term flow. Subsequent experimental studies show that they depend on the location of the cross-section where they are computed (Garcia-Lafuente et al., 2000; Baschek et al., 2001; Sanchez-Román et al., 2009), a result also reported in the numerical study by Sannino et al. (2004). Eddy fluxes show a clear dependence on the fortnightly tidal cycle (Vargas et al., 2006). The total flow, however, is less sensitive to the fortnightly tide since the enhanced mixing driven by strong currents during spring tides diminishes the quasi steady term in (1) and counterbalances the increased eddy-flux (Bryden et al., 1994; Vargas

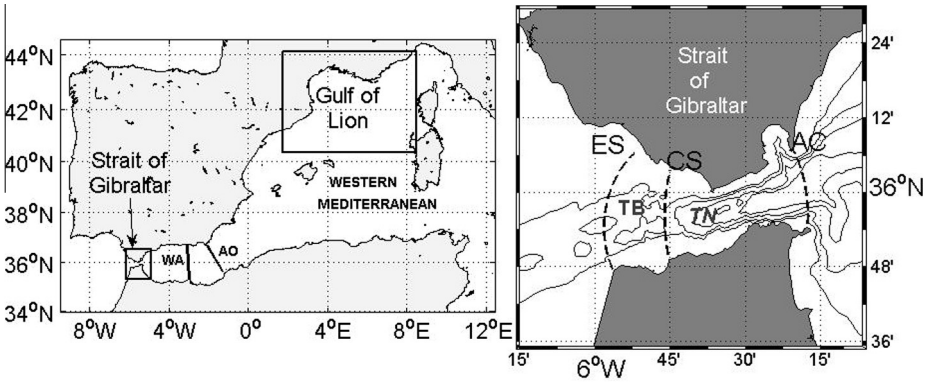

Fig. 1. Left panel shows the Western Mediterranean Sea. The upper rectangle indicates the control volume in the Gulf of Lion used to compute the results of Section 'Basin scale processes, WMDW formation'. WA in the Alborán Basin indicates the Western Alborán section mentioned in the text, and AO indicates the Almería-Orán front. The lower small rectangle encloses the Strait of Gibraltar (SoG), which is zoomed on in the right panel. In this panel, ES, CS and AC indicate Espartel Sill, Camarinal Sill and Algeciras–Ceuta sections, respectively, which are used for doing computations. TN represents Tarifa Narrows and TB is the Tangier Basin that extends from CS to ES. Isobaths every 200 m are shown from the surface to 1000 m.

et al., 2006). This result agrees with the findings of Helfrich (1995) who shows that the exchange increases with the frequency and the strength of the barotropic fluctuations.

While the effect of tides on the volume transport is relatively well known, other processes are not. Tidally-induced mixing in the Camarinal sill area (CS hereinafter, Fig. 1) is remarkably pronounced across the internal hydraulic jump at the western flank of the sill, and grows particularly vigorously when the shear between Atlantic and Mediterranean layer is enhanced by tidal flows. This leads to flow instability and turbulence as revealed by the observation of Kelvin–Helmholtz billows and energy dissipation rates as large as 10^{-2} W kg^{-1} (Wesson and Gregg, 1994), which are among the greatest ever recorded in the ocean. Sanchez-Garrido et al. (2011) show that the flow instabilities keep occurring in additional hydraulic transitions downstream of smaller-scale topographic features located in the Tangier Basin (Fig. 1), which enlarges the mixing area to the west. As a result, this basin is a remarkable source of Atlantic–Mediterranean mixed water that can be advected in either direction (Garcia-Lafuente et al., 2013). Furthermore, tides are the origin of propagating internal bores and large amplitude nonlinear internal waves (Farmer and Armi, 1988; Vázquez et al., 2008; Sanchez-Garrido et al., 2013) with clear potential to increase mixing elsewhere in the SoG (Garcia-Lafuente et al., 2013). Whatever the specific process involved, mixing is so strong that it invalidates the simple description of the exchange in terms of two layers and requires the inclusion of a third interface mixing layer, which participates actively in the dynamic of the exchange (Bray et al., 1995; Sannino et al., 2007).

The physical and biological consequences of this mixing in the nearby Alborán Sea basin and further east in the MS are poorly addressed and are awaiting for more in depth studies. According to several authors (Macías et al., 2007, 2008; Vázquez et al., 2009; Garcia-Lafuente et al., 2011, 2013) and as mentioned previously, a considerable volume of the biologically enriched waters in the area of strong mixing in CS is advected eastward, and eventually helps fertilize the Alborán Sea. In his paleoclimate study of the MS, Mikolajewicz (2011) found that the numerically modeled sea surface temperature in the Alborán Sea was greater than the observed climatology. He attributed this mismatch to the absence of tidal forcing in his model, which reduces the vertical turbulent fluxes of heat and salt. The result is a slightly warmer and more buoyant inflowing Atlantic surface water when tides are not included. The effect might be far-reaching taking into account that this inflow will be finally transformed into intermediate and/or deep Mediterranean water.

Another relevant issue for the MS circulation is the renewal of deep Mediterranean waters and the ventilation of the bottom layer. Western Mediterranean Deep Water (WMDW), which is formed in the Northwestern MS and spreads later over the Western Mediterranean basin, resides well below the main sill of Camarinal and must be uplifted above the sill depth in order to leave the MS. The required energy would be supplied by the spatial acceleration that the flow undergoes as it approaches the SoG (Bernoulli suction), a topic which has been addressed in different studies (Stommel et al., 1973; Bryden and Stommel, 1982; Whitehead, 1985; Garcia-Lafuente et al., 2007, 2009; Naranjo et al., 2012). The remarkable intensity of tidal currents in the SoG is a relevant energy source for the aspiration of deep water that has not been mentioned in the literature except for the paper by Kinder and Bryden (1990). These authors detected traces of WMDW in the ocean side of the sill at the end of the west-going phase of some tidal cycles in spring tides, and speculated about the possibility that WMDW were routinely uplifted by tides. The authors left the issue open for further research.

The present work addresses these topics with the help of two numerical models that have been run with and without tidal forcing in order to compare their outputs and thus assess the influence of tides on several hydrodynamic relevant features. The work is organized as follows. Section 'Numerical models' describes the most relevant aspects of the numerical models already used in previous studies, which the readers are referred to for details. Section 'Tides increase the long-term exchange flows' revisits the relevant issue of the tidally-forced eddy fluxes in the SoG in the light of the new results provided by the models. Section 'Tides modify the hydrological properties of inflowing water' addresses the changes that tidally-induced mixing cause in the Atlantic inflow in the Alborán Sea and further east. Section 'Tides favor Mediterranean deep water ventilation through the SoG' analyses the influence that tides could possibly have on the ventilation of WMDW near the SoG due to an enhanced Bernoulli suction. All these topics are of rather local or regional nature. In contrast, Section 'Basin scale processes, WMDW formation' addresses the far-field influence of tides by analyzing hindcast events of WMDW formation during the decade of 1960. Section 'Discussion and conclusion' summarizes the findings and conclusions of the study.

Numerical models

The results of two numerical models based on the Massachusetts Institute of Technology general circulation model (MITgcm; Marshall et al., 1997a, 1997b) have been used in this study.

The first model (RSGM, hereinafter) is sub-basin scale and it is described in detail by Sanchez-Garrido et al. (2013). Just a brief summary is given here. The model uses the free-surface and hydrostatic configuration of the MITgcm and its domain covers the Gulf of Cádiz and the Alborán Sea. It is horizontally discretized with a curvilinear grid of variable spatial resolution. In order to better reproduce the mixing processes and the vorticity field in the SoG, the maximum resolution is achieved in the strait with a horizontal mesh size of around 300–500 m for both Δx and Δy, which gradually increases to some kilometers toward the east and west open boundaries. In the vertical the model has 46 unevenly distributed z-levels, with minimum cell thickness at the surface ($\Delta z = 5$ m). Vertical eddy viscosity and diffusivity coefficients are calculated according to the parameterization of Pacanowski and Philander (1981), whereas the turbulence closure scheme by Leith (1968) is chosen for the horizontal viscosity. The model is driven at the lateral open boundaries by the tracer and velocity fields provided by the Mediterranean forecast model (Oddo et al., 2009), whereas tides are introduced by forcing the model laterally with the tidal velocities produced by the barotropic tidal model of Carrère and Lyard (2003). The model was run for a two-year spin-up period after which it produces realistic outputs.

The second model (GMSM, hereinafter) covers the whole MS, a brief overview is given here. Its grid is non-uniform, curvilinear orthogonal as well, with maximum horizontal resolution of about $1/200^\circ \times 1/200^\circ$ (456 m) in the SoG. Eastwards and westwards of the SoG the resolution diminishes progressively until it reaches a grid size of $1/16^\circ \times 1/16^\circ$ (5.7 km) in the rest of the domain. To resolve the dynamics of the different water masses in the MS adequately, 73 unevenly spaced vertical z-levels were used, whose thickness range from 3 m at the surface to 300 m at the ocean bottom. The model is forced at the surface by the wind stress and the heat and fresh water fluxes derived from the dynamical downscaling of ECMWF ERA40 reanalysis performed with the regional atmospheric model RegCM (Artale et al., 2009). A surface relaxation to climatological temperature (5 days) and salinity (30 days) are also applied. Tides are incorporated in the model and tidal forcing includes both the tide generating potential as a body force in the momentum equations, and the lateral boundary condition in the open Atlantic boundary, which is imposed in the same way as in the RSGM model.

Both models have been run with and without tidal forcing in order to assess the local, regional and far-reaching effects of the tides. The characteristics of RSGM model make it more suitable for addressing local and regional issues as it produces hourly values compared to daily-means in GMSM; its outputs are used throughout Sections 'Tides increase the long-term exchange flows' and 'Tides modify the hydrological properties of inflowing water'. Although the simulation run covered the years 2010–2011, only the period from September to December 2011 has been used in this study. The period has been intentionally chosen because it coincides with the period analyzed in Sanchez-Garrido et al. (2013) and Sammartino et al. (2014), during which a comprehensive model validation was carried out. The GMSM model is used to address the question of how tides in the SoG could possibly affect relevant physical processes in the MS far away from the very strait, namely the deep water formation processes in the Gulf of Lion. This study makes use of the 1958–1968 hindcast in Sections 'Tides favor Mediterranean deep water ventilation through the SoG' and 'Basin scale processes, WMDW formation'.

Tides increase the long-term exchange flows

This section revisits the issue of how tide-induced eddy-fluxes increase the exchanged flows, with the help of the RGSM model, which has proven to be more accurate than the one presented by Sannino et al. (2004) (see model comparison in Sannino et al., 2014). Following Garcia-Lafuente et al. (2000) and Baschek et al. (2001) the volume transport through a given cross-section is calculated by taking as the interface between Atlantic and Mediterranean waters the isohaline that maximizes the transport. A fresher isohaline would ascribe eastward-flowing Atlantic water to the Mediterranean layer, thus diminishing both the estimated inflow and the outflow. The same would occur if a saltier isohaline were selected, since westward-flowing Mediterranean water would be ascribed to the Atlantic layer. Fig. 2 shows that this isohaline can always be found, although its specific value changes with the location. It also changes in the tidal and non-tidal runs at the same location. Table 1 shows the computed volume transport at CS section and at the two boundaries of the SoG, namely Espartel (ES, see Fig. 1) and Algeciras–Ceuta (AC) sections, along with the isohaline that maximizes the exchange in both runs.

Focusing on section CS, the maximum exchange is achieved for isohalines 37.3 and 37.1 for the tidal and non-tidal runs, respectively, and the corresponding transports are 0.84 Sv and 0.79 Sv, respectively, 6% higher in the tidal run. At ES, the isohaline that maximizes the flow is 36.6 (Fig. 2, Table 1) in both runs, an expected lower salinity than at CS. The transport at ES in the two experiments is larger than at CS, with the tidal run still giving a ~6% greater value (0.98 Sv versus 0.93 Sv). The lower salinity of the isohaline used as interface and the larger flow at ES compared with CS section are attributable to the entrainment of AW by the swift Mediterranean undercurrent in the western part of the SoG (Garcia-Lafuente et al., 2011). Likewise, the entrainment of MW by the overlying Atlantic jet leads to a more saline interface (around 37.4) and greater flows through AC section than at CS. The tidal run keeps on providing greater transports than the non-tidal run also in this section (0.89 Sv against 0.82 Sv, ~8% increase).

It is interesting and illustrative to explore the decomposition of transport in terms of the slowly-varying and eddy-fluxes contributions (Eq. (1)). Table 1 indicates that the contribution of eddy-fluxes to the total flow at CS is very large (0.32 Sv or 38%), whereas they decrease dramatically to 3% and 1.4% at the bounding sections of ES and AC respectively. These results agree with the findings of Bryden et al. (1994) who reported eddy-fluxes as high as 50% at CS, and with Vargas et al. (2006) who estimated eddy-fluxes of 0.3–0.4 Sv from observations at the same section. The very small eddy fluxes at the ending sections of AC and ES (Table 1) are also in agreement with Garcia-Lafuente et al. (2000) and Baschek et al. (2001) who found eddy-fluxes reduced to less than 5% in a cross section nearby AC, and with Sanchez-Román et al. (2009) who estimated similar percentages at ES. The reason why eddy fluxes are so significant at CS and almost negligible at the ending sections of the strait is related to the internal hydraulics of the SoG. As shown in Sannino et al. (2007) and Sanchez-Garrido et al. (2011) the hydraulic control at CS is not as permanent as at ES or at Tarifa Narrows (Farmer and Armi, 1988), and it is when the hydraulic control at CS is lost that eddy-fluxes participate actively in the mean transport. As long as the hydraulic controls at ES and Tarifa Narrows are not flooded, eddy-fluxes at AC and ES may be neglected (Vargas et al., 2006; Sannino et al., 2007; Sanchez-Garrido et al., 2011).

Another result worth noting in Table 1 is that the exchanged flows in the non-tidal run do not coincide with the slowly-varying contribution of the flows in the tidal run (compare columns 4 and 6 in Table 1). Thus, the result of including tides is not the mere addition of an eddy-flux contribution to the flows computed in the non-tidal run, because this sum does not match the flows in the tidal run. At ES and AC, the quasi-steady part of the flows in the tidal run is already greater than the flows in the non-tidal run, but at CS, however, it is much lower. All this highlights the complexity that tides bring to the actual exchange.

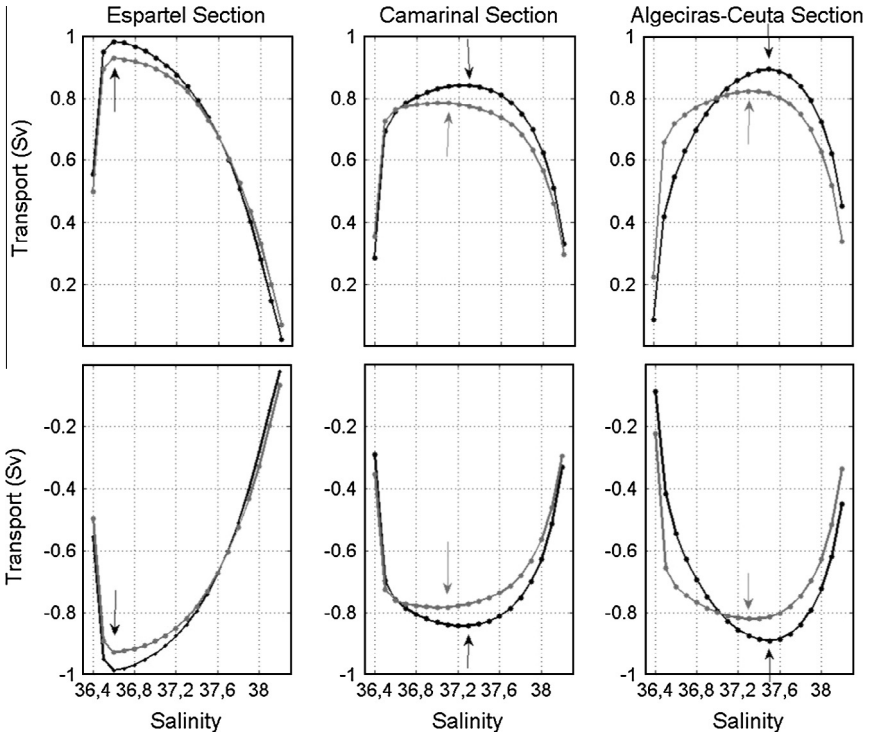

Fig. 2. Atlantic and Mediterranean transports versus the salinity of the isohaline used to calculate it. Black and gray lines correspond to tidal and no-tidal runs, respectively. Arrows indicate the maximum transport with the same color code. Only one arrow is seen at ES because the isohaline that maximizes the transport is the same in both runs.

Table 1
Computed transports (in Sv) at ES, CS and AC sections (see Fig. 1). The first two columns indicate the isohalines that maximizes the transports in each section (see Fig. 2). The third and fourth columns are the mean transport in the tidal and non-tidal runs, respectively, and the fifth column gives the increment (percentage) that tides cause on the transports. The term $(\bar{u}_i\bar{h}_i)$, which is representative of the slow-varying term in Eq. (1), is shown in the sixth column. Eddy-fluxes $(\overline{u_i'h_i'})$ and the percentage of the total flow that they account for are shown in the last two columns.

	S_{Tid}	$S_{\text{No-Tid}}$	$\overline{Q}_{\text{Tid}}$	$\overline{Q}_{\text{No-Tid}}$	Δ (%)	$\bar{u}_i\bar{h}_i$	$\overline{u_i'h_i'}$	% $\overline{u_i'h_i'}$
ES	36.6	36.6	0.988	0.935	5.7	0.957	0.031	3.0
CS	37.3	37.1	0.844	0.793	6.4	0.522	0.322	38
AC	37.5	37.3	0.893	0.823	8.5	0.880	0.013	1.4

Tides modify the hydrological properties of inflowing water

The most apparent local effect of tides in the SoG is the enhanced mixing driven by shear instabilities and turbulence, whose most noticeable results are the thickening of the interfacial layer and the modification of the hydrological properties of their water. Both issues are addressed in this section using the RGSM model under tidal and non-tidal runs.

The upper panels of Fig. 3 show the interfacial layer thickness produced by each run, calculated by fitting a hyperbolic tangent function to the vertical salinity profiles, following Sannino et al. (2007). Lower panels indicate the depth of the middle interface, which coincides with the inflection point of the fitted hyperbolic tangent function. The panels show that the interfacial layer is shallower in the tidal run and, consequently, covers a greater horizontal extension. Despite this increment, west of CS the thickness of the interfacial layer is much the same in both runs, but the layer becomes markedly thicker (up to 90 m in certain regions) eastwards of CS in the tidal run (Fig. 3a and b). As analyzed in Garcia-Lafuente et al. (2013), the reason for this pattern is the eastward advection of the waters that had been mixed in the Tangier basin during the previous rising tide and in the subsequent release and eastward progression of the internal hydraulic jump formed leeward of CS, which provides energy for maintaining high rates of mixing. The shoaling of the interface is primarily noticeable in north-eastern part of the Strait, where the depth of the middle interface changes from 70 m in non-tidal run to near the surface in the tidal one. The joint effect of the shoaling and thickening of the interface in the eastern half of the SoG in the tidal run is to carry water from below to the surface layers in a more effective way than in the non-tidal run. In other words, AWs are expected to be saltier and colder under tidal forcing and, hence, denser and less buoyant.

These AWs are directly advected into the adjacent Alborán Sea basin so that the tidal run gives colder temperatures not only within the dimensions of the SoG but also beyond its limits. Fig. 4 shows the surface temperature difference between the tidal and non-tidal simulations. The greatest differences are found in the eastern exit of the SoG and along the expected path of the Atlantic Jet in the western Alborán Sea, which confirms that in the tidal run the Jet carries colder water because of the enhanced tidal mixing in the SoG. Even when reduced, this difference is still detectable in the area of the Almería-Orán front at the eastern end of the Alborán basin and along the path of the Algerian current further east. These visual results are confirmed by computing the mean temperature of the incoming AWs across AC section: the inflow is 0.37 °C colder in the tidal run (15.42 °C versus 15.79 °C) and also 0.47 units saltier (36.63 versus 36.16). The joint effect is an inflow 0.45 kg m^{-3} denser in the case of the tidal run and, consequently, the flux of advected buoyancy into the Alborán Sea diminishes. For instance, the advected buoyancy within the 100 upper meters of the water column, computed at the AC section, is 1.13 times lower in the tidal run (2.505 ms^{-2} versus 2.235 ms^{-2}), which may have far-field significant consequences, as the cold and salty signature generated in the SoG is exported by the Algerian current to the interior of the MS.

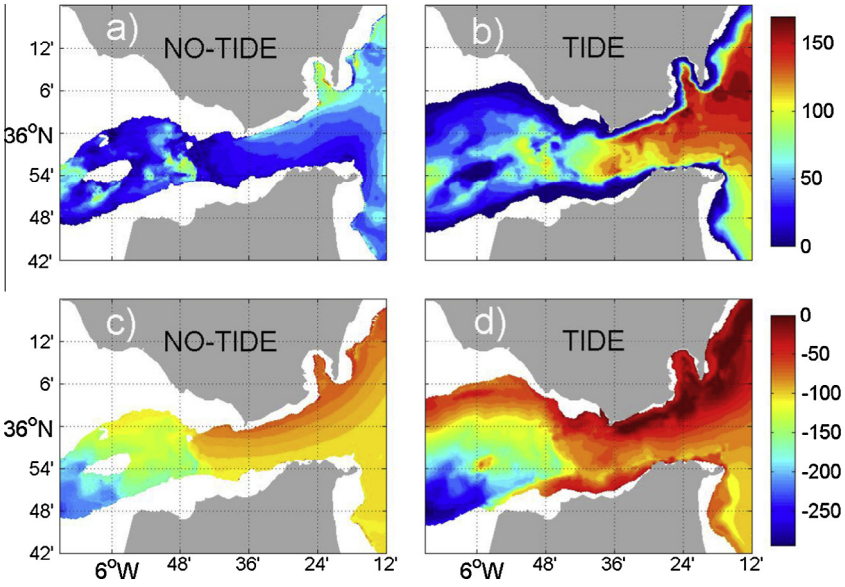

Fig. 3. (a) Interface thickness, in meters, for the non-tidal run. (b) Same as (a) for the tidal run. (c) Mean depth of the interface, in meters, for the non-tidal run. (d) Same as (c) for the tidal run. See text for details about the way they are computed.

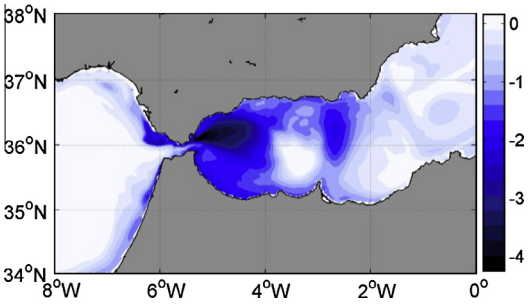

Fig. 4. Surface temperature difference ($\theta_{\text{tides}} - \theta_{\text{no-tides}}$, in °C) between the tidal and non-tidal run in the Alborán Sea.

Tides favor Mediterranean deep water ventilation through the SoG

The GMSM model outputs are examined in this section to address the influence of tides on the draining of the WMDW toward the Atlantic Ocean through the shallow SoG. Prior to investigating the topic, it is convenient to check the model performance, which can be assessed from Fig. 5. The left panel shows the mean temperature and salinity in the AC section (see Fig. 1) provided by the model, whereas panel b) presents observations collected in a nearby cross section. The hydrological properties of the modeled water masses as well as their spatial distribution match remarkably well the observations, particularly in the lower layer, which supports the use of the GMSM model to accomplish the study of the WMDW drainage.

The influence of tides is assessed by comparing the volume of WMDW flowing across the AC section computed for the tidal and non-tidal runs. In the present study, water colder than 13 °C (potential temperature) in the SoG area is considered as WMDW. This criterion, which has been traditionally assumed in the literature (Bryden and Stommel, 1982; Kinder and Parrilla, 1987; Kinder and Bryden, 1990; Garcia-Lafuente et al., 2007, 2009; Naranjo et al., 2012), is convenient in this case because the isotherm $\theta = 13$ °C is sufficiently far from the bottom in both the model and the observations (see Fig. 5) to ensure that it always lies well outside of the bottom boundary layer. Therefore, the estimated flows of WMDW are not critically dependent on the physics of the bottom boundary layer, which is not as well resolved as the ocean interior in the numerical models. Consequently, this weakness is not a major concern for our results.

Table 2 shows the estimated WMDW flow across AC section using the five last years of the GMSM hindcast. Results for the entire 5-year period along with the values for each single year are presented in Table 2. The 5-year average is 28% (0.051 Sv)

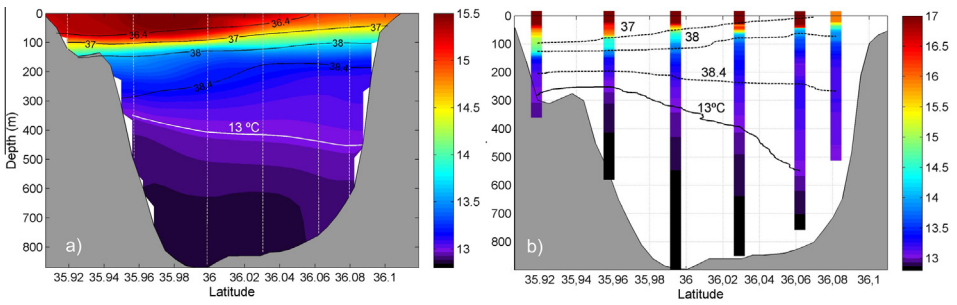

Fig. 5. (a) Mean potential temperature and salinity in section AC (see Fig. 1) derived from the GMSM model outputs. The filled color contours are potential temperature (color bar on the right), while the labeled black contours show the salinity. The white contour is the isotherm $\theta = 13$ °C used as the upper limit of WMDW (see text). (b) CTD profiles collected at the – nearly – same section as in panel (a). The color bar is again for temperature, the dashed black contours are salinity, and the solid black line is the isotherm $\theta = 13$ °C. (For interpretation of the references to color in this figure legend, the reader is referred to the web version of this article.)

Table 2
Time-averaged outflow of water with $\theta < 13$ °C across the AC section (see Fig. 1), which is identified with WMDW in this study. The first row is the five-year average and the remaining rows indicate the year-averaged WMDW outflow. Transport with and without tides are shown in the first two columns. Last column gives the increment between tidal and non-tidal run (ΔQ) and its percentage (%).

Period	Block 1: $\theta < 13$ °C		
	Q_{TID} (Sv)	Q_{NOT} (Sv)	ΔQ (Sv)/%
(1963–1968)	0.233	0.182	0.051/28
1963	0.091	0.060	0.031/51
1964	0.285	0.236	0.049/21
1965	0.307	0.230	0.077/33
1966	0.334	0.303	0.031/10
1967	0.211	0.158	0.052/33

higher in the tidal run, although the percentage fluctuates between 10% and 50% depending on the year. The relevant result regarding this study is the visible enhancement of the WMDW aspiration in the tidal run, but the high year-to-year variability during the simulated period, which we ascribe to the internal variability of the MS and of the WMDW formation processes should also be noted.

A similar procedure has been carried out to estimate the WMDW flow through section WA at 3°W in the Alborán Sea (see Fig. 1). Although the overall estimates point at a slight increase of WMDW volume transport toward the SoG in the tidal run, the analysis is not statistically conclusive. The fact that the comparison of tidal and non-tidal runs does not clearly detect the effect of tides on the WMDW flow through this section, located around 200 km to the east of the SoG, is interpreted as the weakening with the distance of the direct suction by tides.

Basin scale processes, WMDW formation

Deep convection that leads to the formation of WMDW in the northwestern MS is among the most relevant oceanographic processes taking place in this Sea and, as such, it has been extensively discussed in the literature (MEDOC Group, 1969; Schott et al., 1996; Herrmann et al., 2008; Gascard, 1991; Smith et al., 2008; Marshall and Schott, 1999). The convection process involves several phases. The first one is the preconditioning phase (Gascard and Richez, 1985; MEDOC Group, 1969), which comprises the densification processes (buoyancy losses) that the Atlantic surface water undergoes since entering the MS through the SoG until it sinks in winter during the second phase of the convection process. Section 'Tides modify the hydrological properties of inflowing water' of this study has shown that the AW inflow is colder and saltier, i.e., less buoyant, when tides are included in the model and that those signatures are carried eastwards by the Algerian current (Fig. 4). In other words, the AW in the tidal run is more strongly preconditioned than in the non-tidal run.

This section investigates whether or not this difference at the source point (SoG) has a far-field influence on the formation of WMDW in the Gulf of Lion area (Fig. 1). The outputs of the GMSM model run with and without tides are compared to address the issue. Two bulk variables or proxies are analyzed herein: the mixed layer depth (MLD) and the surface area susceptible to participate in the deep convection event (hereinafter DCA). The MLD at each grid point has been defined as the distance from the surface to the depth where the vertical diffusion coefficient reaches a threshold value of 0.04 $m^2 s^{-1}$, following Herrmann et al. (2008). DCA has been estimated as the area where the surface water is denser than 1029.10 kg m^{-3}, a criterion widely used in the literature of deep convection (Schott et al., 1996; Smith et al., 2008; Pinardi et al., 2013).

Fig. 6 shows the MLD averaged from January to the end of April for every year from 1963 to 1967. Maximum mean MLD reaches 1500 m during 1963, 1964 and 1965, values that are quite similar to those presented by Schott et al. (1996) and Herrmann et al. (2008) in the same area. Except for 1963 MLD in the tidal run is always greater than in the non-tidal run, which is expected if tidal runs better precondition the inflowing AW. Fig. 7 presents the evolution of the estimated DCA during the winter months (January to end of April). The greatest DCA is reached in March 1965 (almost 10×10^{10} m^2 in the tidal run, 2×10^{10} m^2 more than in non-tidal run) followed by 1963; during this year, the DCA is larger in the non-tidal run as was the case for the MLD as well. During the other years, however, the tidal run provides larger DCA than the non-tidal run. A deep water formation rate has been calculated following Lascaratos and Nittis (1998) and is presented in Fig. 8a. Since it combines the former MLD and DCA variables, the comparison of tidal and non-tidal runs does not provide new results but confirms the previous ones, the non-tidal run gives higher formation rates in 1963 and lower rates in all the other years.

The results presented in Figs. 6 and 7 deserve some comentaries despite the topic not being the scope of this work. Focussing on the tidal run, the model simulations predict a great year-to-year variability in all variables, namely MLD, DCA and rate of formation. Notice the reduced DCA in years 1966 and 1967, which is in agreement with the also diminished MLD during these years shown in Fig. 6, which in turn gives the minimum formation rate of barely 0.2 Sv in 1967 (Fig. 8a). On the opposite end is 1965 when the rate of formation approaches 4 Sv, a rather high value that would correspond to an exceptionally productive year. In any case, they fall inside the interval of deep water formation rates reported by other authors that ranges between 0.3 and 6 Sv (Tziperman and Speer, 1994; Krahmann, 1997; Castellari et al., 2000; Herrmann et al., 2008; Béranger et al., 2009; Beuvier et al., 2012; Pinardi

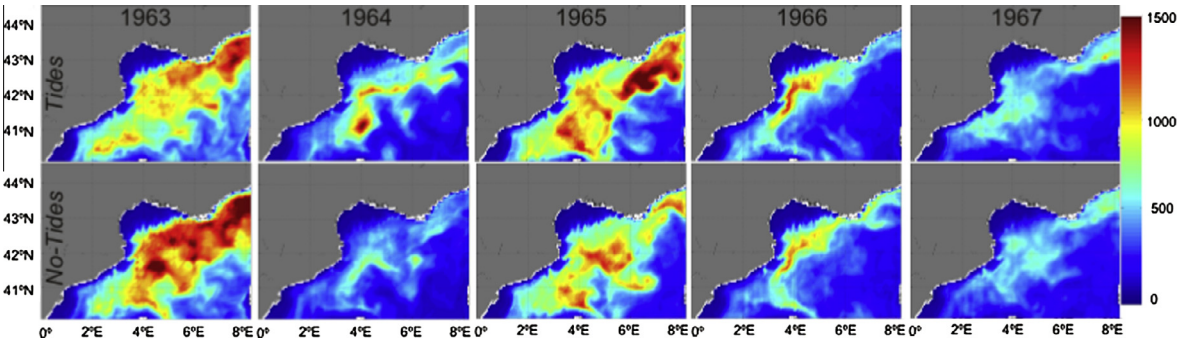

Fig. 6. Mixed layer depth in meters (color bar) in the Gulf of Lion area (see Fig. 1) computed using a threshold value for the vertical diffusion coefficient of 0.04 $m^2 s^{-2}$. Upper and lower rows correspond to tidal and non-tidal runs, respectively. The contours represent the January-to-April (both included) average. (For interpretation of the references to color in this figure legend, the reader is referred to the web version of this article.)

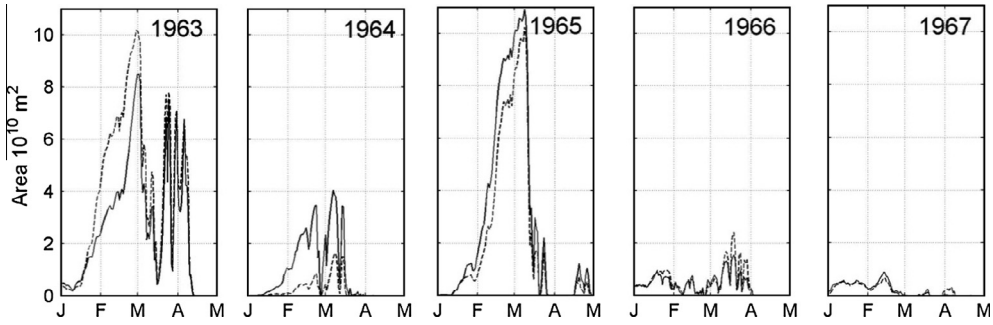

Fig. 7. Time evolution of the Deep Convection Area in the Gulf of Lion (see Fig. 1) from January to the end of April of every year. Solid and dashed lines represent the tidal and non-tidal runs respectively.

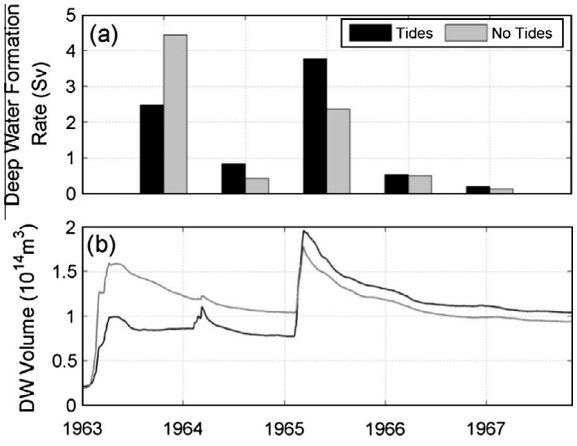

Fig. 8. (a) Deep water formation rate (in Sv) calculated as $(V_A - V_B)/T$, where V_A is the maximum volume in a particular year, V_B is the minimum volume before the convection event and $T = 1$ year $= 3.15 \times 10^7$ s (Lascaratos and Nittis, 1998). (b) Deep water volume measured in the volume control (Fig. 1). Black and gray colors correspond to the tidal and non-tidal run, respectively.

et al., 2013; Schott et al., 1994, 1996; Send et al., 1995; Schroeder et al., 2008; Durrieu de Madron et al., 2013).

Fig. 8b gives the time evolution of the estimated volume of deep water resident in the region of the Gulf of Lion as a function of time. The large formation rate in 1963 filled up the bottom layer, which started draining out once the winter formation processes had finished. The way it did is different for the tidal run, in which the volume decrease stopped after a very short time of drainage and remained constant thereinafter, and the non-tidal run that featured the exponential-like decay expected in this type of physical problem, where the rate of draining must be proportional to the volume of water that is being drained. Notice that, after this year, the drainage after the refilling of the basin predicted in the tidal run shapes an exponential curve reasonably well. We lack of a suitable explanation for the anomalous drainage in 1963, which could be the reason explaining the apparent paradox (according to our hypothesis) of why the non-tidal run predicts a higher rate of formation this year than the tidal run. The footprint of the winter of 1964 is the small cusp, more visible in the tidal run, while 1966 and 1967 with such small rates of deep water formation, hardly leave any signal in the curve. In contrast, 1965 doubled the volume of deep water stored in the Gulf of Lion due to the extraordinary rate of formation, much greater in the tidal run as seen in Fig. 8a.

Discussion and conclusion

This work examines the effect of tides in the SoG on several oceanographic processes whose spatial scales range from local to basin-wide. The most significant outcome is their contribution to increase the mean exchange that is described here, but there are other effects intuitively related to tidal forcing that have not been thoroughly addressed to our knowledge yet. Some of them are investigated in the different sections of this work by comparing the outputs of two numerical models which have been run with and without tidal forcing.

As expected, the model results confirm that the inclusion of tides generate eddy fluxes that increase the long-term exchange. Despite its very similar contribution in the different sections of the SoG (6–8%, see Table 1), the way the increment is achieved differs between sections. At the main CS section, eddy fluxes play a key role and represent a fundamental process to increase the long-term exchange, a result that agrees with previous findings (Bryden et al., 1994; Vargas et al., 2006). At the boundary sections of AC and ES the contribution of eddy fluxes is very small although the increment of the long-term flow due to tides is similar or even higher than at CS (8.5% at AC versus 6.4% at CS, see Table 1). A remarkable result that stems from the weakness of the eddy fluxes at the boundary sections is that the flows could be estimated satisfactorily there using only the slowly-varying term in Eq. (1). It is an interesting outcome for experimental studies because the computation of eddy fluxes from observations poses serious challenges. Actually, some experimental studies (Sanchez-Román et al., 2009; Garcia-Lafuente et al., 2000) have made already use of this flow property.

A second effect of the tides is the enhancement of the mixing between Mediterranean and Atlantic waters within the strait itself. The energy for mixing is mainly released in the various supercritical-to-subcritical flow transitions occurring in the Tangier basin (Sanchez-Garrido et al., 2011). The final outcome is the thickening and shoaling of the interfacial layer in the SoG, which is favored by the propagation of nonlinear internal waves and entrainment of MW by the Atlantic jet, an issue that has been recently addressed by Garcia-Lafuente et al. (2013). These processes are nearly inhibited in the absence of tides, a fact that is reflected by the very thin interfacial mixing layer in the non-tidal simulation (Fig. 3). In addition to the significant effect that the shoaling of the interface may have on biological communities, the tidally-induced mixing also makes the Atlantic jet saltier (0.47 units) and colder (0.37 °C). This water is finally advected to the Alborán Sea which therefore shows colder surface waters almost everywhere, although it is more visible along the mean path of the Atlantic jet and, particularly as it exits the SoG (Fig. 4). As shown recently by Sanchez-Garrido et al. (2013), the 4 °C colder surface water in this area obtained in the tidal simulation has its origin possibly in the advection of positive shear vorticity generated by the interaction of tidal currents with the solid northern boundary of the SoG. If so, this signature would be more related to the local doming of isotherms associated with the enhancement of the cyclonic circulation rather

than to the direct advection of colder water from the strait. The downstream temperature anomaly in the Alborán Sea would be a consequence of this process, at least partially, but it does not modify its tidal origin.

Of particular interest is the fact that the cold signature is still clearly visible in the Almería-Orán front and Algerian current, at the eastern exit of the Alborán Sea (dark blue strip over this area in Fig. 4). We hypothesize that the denser AW produced by mixing in the SoG in the tidal run facilitates the formation of WMDW in the Gulf of Lion. The comparison of two bulk variables, namely MLD and DCA, suggests that indeed, the tidal run tends to produce more volume of WMDW. However the first year of the hindcast does not behave so, as the non-tidal run produced more volume of WMDW (Fig. 8).

As mentioned in Section 'Basin scale processes, WMDW formation', we lack an explanation for this behavior, which is further confounded by the fact that this is the only year when the drainage of the WMDW out of the control volume in the tidal run does not follow an expected exponential decay with time (Fig. 7b).

Therefore, the results concerning 1963 must be interpreted with caution. What both models predict in a similar way is the marked year-to-year variability driven by the atmospheric forcing, a variability that has also been found in other studies (Herrmann et al., 2008; Pinardi et al., 2013).

The last issue addressed of whether or not tides favor the ventilation of the deep WMDW layer has a positive answer according to our results. Table 2 indicates that the outflow of WMDW (defined as the water colder than $\theta = 13$ °C in the neighborhood of the SoG) increases by nearly 30% in the tidal run. This percentage is greater than the 6–7% increment of the long-term outflow due to tides (column 5 in Table 1). The difference in percentages suggests that the drainage of WMDW is specially aided by tides and it is more favored than any of the other Mediterranean waters participating in the outflow. Table 2 also shows an interannual variability that is apparently related to the variability of the WMDW reservoir in the Gulf of Lion revealed in Fig. 8. For instance, the outflow of WMDW reaches its maximum in 1966, a year after the large WMDW formation that occurred in 1965. Taking into account the time the signal will take to travel from the Gulf of Lion to the SoG, this delay seems reasonable (Garcia-Lafuente et al., 2007, 2009). The trend of the WMDW stored in the control volume in the Gulf of Lion is to diminish after 1965 (Fig. 7a), a trend that seems to be followed by the outflow of WMDW with a year delay (Table 2).

In conclusion, our study has provided evidence that tides in the SoG has local (increase of the long-term exchange, noticeable tidally-driven mixing, eventually exported to the MS), regional or short-range (colder and saltier inflow, enhanced aspiration of WMDW) and long-range (influence in deep convection processes) influences. Of all them, the last one is more open to debate because a convincing conclusion requires much longer simulations that include tides in the forcing terms, which are computationally unaffordable at this moment.

Acknowledgments

This work is a contribution to the Spanish funded National Project INGRES 3 (CTM2010-21229) with partially financial support of Project P08-RNM-3738 from Plan Andaluz de Investigación. Cristina Naranjo acknowledges the fellowship BES-2011-043421 from the Ministry of Economy and Competitiveness – Spain. The Mediterranean tidal simulation has been carried out thanks to a CINECA ISCRA grant. The authors are also grateful to the Supercomputing and Bioinformatics (SCBI) Center of the University of Malaga and to CRESCO Supercomputing Facilities at ENEA (www.cresco.enea.it). This is the publication no. 62 from CEIMAR Publication Series.

References

Armi, L., Farmer, D., 1985. The internal hydraulics of the Strait of Gibraltar and associated sills and narrows. Oceanologica Acta 8, 37–46.

Armi, L., Farmer, D.M., 1986. Maximal two-layer exchange through a contraction with barotropic net flow. Journal of Fluid Mechanics 164, 27–51.

Artale, V., Calmanti, S., Carillo, A., Dell'Aquila, A., Herrmann, M., Pisacane, G., Ruti, P.M., Sannino, G., Struglia, M.V., Giorgi, F., Bi, X., Pal, J.S., Rauscher, S., The PROTHEUS Group, 2009. An atmosphere-ocean regional climate model for the Mediterranean area: assessment of a present climate simulation. Climate Dynamics 35, 721–740. http://dx.doi.org/10.1007/s00382-009-0691-8.

Baschek, B., Send, U., Garcia-Lafuente, J., Candela, J., 2001. Transport estimates in the Strait of Gibraltar with a tidal inverse model. Journal of Geophysical Research 106 (C12), 31033–31044. http://dx.doi.org/10.1029/2000JC000458.

Béranger, K., Testor, P., Crépon, M., 2009. Modelling water mass formation in the Gulf of Lion (Mediterranean Sea). In: Briand, F. (Ed.), Dynamics of Mediterranean Deep Waters, CIESM Workshop Monogr, vol. 38. Mediterr. Sci. Comm., Monaco, pp. 91–100.

Beuvier, J., Béranger, K., Lebeaupin-Brossier, C., Somot, S., Sevault, F., Drillet, Y., Bourdallé-Badie, R., Ferry, N., Lyard, F., 2012. Spreading of the Western Mediterranean Deep Water after winter 2005: time scales and deep cyclone transport. Journal of Geophysical Research 117, C07022. http://dx.doi.org/10.1029/2011JC007679.

Bray, N.A., Ochoa, J., Kinder, T.H., 1995. The role of the interface in exchange through the Strait of Gibraltar. Journal of Geophysical Research 100 (C6), 10755–10776. http://dx.doi.org/10.1029/95JC00381.

Bryden, H.L., Kinder, T.H., 1991. Steady two-layer exchange through the Strait of Gibraltar. Deep Sea Research Part A 38, S445–S463. http://dx.doi.org/10.1016/S0198-0149(12)80020-3.

Bryden, H.L., Stommel, H.M., 1982. Origin of the Mediterranean outflow. Journal of Marine Research 40, 55–71.

Bryden, H.L., Candela, J., Kinder, T.H., 1994. Exchange through the Strait of Gibraltar. Progress in Oceanography 33, 201–248. http://dx.doi.org/10.1016/0079-6611(94)90028-0.

Carrère, L., Lyard, F., 2003. Modeling the barotropic response of the global ocean to atmospheric wind and pressure forcing-comparisons with observations. Geophysical Research Letters 30, 1275. http://dx.doi.org/10.1029/2002GL016473.

Castellari, S., Pinardi, N., Leaman, K., 2000. Simulation of the water mass formation processes in the Mediterranean Sea: influence of the time frequency of the atmospheric forcing. Journal of Geophysical Research 105 (C10), 24157–24181. http://dx.doi.org/10.1029/2000JC900055.

Durrieu de Madron, X., Houpert, L., Puig, P., Sanchez-Vidal, A., Testor, P., Bosse, A., Estournel, C., Somot, S., Bourrin, F., Bouin, M.N., Beauverger, M., Beguery, L., Calafat, A., Canals, M., Cassou, C., Coppola, L., Dausse, D., D'Ortenzio, F., Font, J., Heussner, S., Kunesch, S., Lefevre, D., Le Goff, H., Martín, J., Mortier, L., Palanques, A., Raimbault, P., 2013. Interaction of dense shelf water cascading and open-sea convection in the northwestern Mediterranean during winter 2012. Geophysical Research Letters 40, 1379–1385. http://dx.doi.org/10.1002/grl.50331.

Farmer, D.M., Armi, L., 1986. Maximal 2-layer exchange over a sill and through the combination of a sill and contraction with barotropic flow. Journal of Fluid Mechanics 164, 53–76.

Farmer, D.M., Armi, L., 1988. The flow of Mediterranean Water through the Strait of Gibraltar. Progress in Oceanography 21 (1), 1–103.

Garcia-Lafuente, J., Vargas, J.M., Plaza, F., Sarhan, T., Candela, J., Bascheck, B., 2000. Tide at the eastern section of the Strait of Gibraltar. Journal of Geophysical Research 105 (C6), 14197–14213. http://dx.doi.org/10.1029/2000JC900007.

Garcia-Lafuente, J., Delgado, J., Vargas, J.M., Vargas, M., Plaza, F., Sarhan, T., 2002a. Low-frequency variability of the exchanged flows through the Strait of Gibraltar during CANIGO. Deep Sea Research Part II: Topical Studies in Oceanography 49 (19), 4051–4067. http://dx.doi.org/10.1016/S0967-0645(02)00142-X.

Garcia-Lafuente, J., Alvarez Fanjul, E., Vargas, J.M., Ratsimandresey, A.W., 2002b. Subinertial variability in the flow through the Strait of Gibraltar. Journal of Geophysical Research 107 (C10), 3168. http://dx.doi.org/10.1029/2001JC001104.

Garcia-Lafuente, J., Sanchez Roman, A., Díaz del Río, G., Sannino, G., Sanchez-Garrido, J.C., 2007. Recent observations of seasonal variability of the Mediterranean outflow in the Strait of Gibraltar. Journal of Geophysical Research 112, C10005. http://dx.doi.org/10.1029/2006JC003992.

Garcia-Lafuente, J., Delgado, J., Sanchez-Roman, A., Soto, J., Carracedo, L., Díaz-del-Río, G., 2009. Interannual variability of the Mediterranean outflow observed in Espartel sill, western Strait of Gibraltar. Journal of Geophysical Research 114, C10018. http://dx.doi.org/10.1029/2009JC005496.

Garcia-Lafuente, J., Sanchez-Roman, A., Naranjo, C., Sanchez-Garrido, J.C., 2011. The very first transformation of the Mediterranean outflow in the Strait of Gibraltar. Journal of Geophysical Research 116, C07010. http://dx.doi.org/10.1029/2011JC006967.

Garcia-Lafuente, J., Pozas, E.B., Sanchez-Garrido, J.C., Sannino, G., Sammartino, S., 2013. The interface mixing layer and the tidal dynamics at the eastern part of the Strait of Gibraltar. Journal of Marine Systems 117, 31–42. http://dx.doi.org/10.1016/j.jmarsys.2013.02.014.

Gascard, J.C., 1991. Open ocean convection and deep water formation revisited in the Mediterranean, Labrador, Greenland and Weddell Seas. In: Chu, P.C., Gascard, J.C. (Eds.), Deep Convection and Deep Water Formation in the Oceans.

Elsevier Oceanography Series, 57, Amsterdam, pp. 157–182, http://dx.doi.org/10.1016/s0422-9894(08)70066-7.
Gascard, J.C., Richez, C., 1985. Water masses and circulation in the western Alborán Sea and in the Straits of Gibraltar. Progress in Oceanography 15 (3), 157–216.
Helfrich, K.R., 1995. Time-dependent two-layer hydraulic exchange flows. Journal of Physical Oceanography 25 (3), 359–373.
Herrmann, M., Somot, S., Sevault, F., Estournel, C., Déqué, M., 2008. Modeling the deep convection in the northwestern Mediterranean Sea using an eddy-permitting and an eddy-resolving model: case study of winter 1986–1987. Journal of Geophysical Research 113, C04011. http://dx.doi.org/10.1029/2006JC003991.
Kinder, T.H., Bryden, H., 1990. Aspiration of deep waters through straits. In: Pratt, L.J. (Ed.), The Physical Oceanography of Sea Straits. Kluwer Acad., Norwell Mass., pp. 295–319, http://dx.doi.org/10.1007/978-94-009-0677-8_14.
Kinder, T.H., Parrilla, G., 1987. Yes, some of the Mediterranean outflow does come from great depth. Journal of Geophysical Research 92 (C3), 2901–2906.
Krahmann, G., 1997. Saisonale und zwischenjhrliche Variabiltim westlichen Mittelmeer-Analyse historischer Daten. Dissertation, Univ. Kiel, Kiel, Germany, 168 pp.
Lascaratos, A., Nittis, K., 1998. A high-resolution three-dimensional numerical study of intermediate water formation in the Levantine Sea. Journal of Geophysical Research 103 (C9), 18497–18511. http://dx.doi.org/10.1029/98JC01196.
Leith, C.E., 1968. Diffusion approximation for two-dimensional turbulence. Physics of Fluids 11, 671. http://dx.doi.org/10.1063/1.1691968.
Macías, D., Martin, A.P., Garcia-Lafuente, J., Garcia, C.M., Yool, A., Bruno, M., Echevarría, F., 2007. Analysis of mixing and biogeochemical effects induced by tides on the Atlantic–Mediterranean flow in the Strait of Gibraltar through a physical–biological coupled model. Progress in Oceanography 74 (2), 252–272. http://dx.doi.org/10.1016/j.ocean.2007.04.006.
Macías, D., Bruno, M., Echevarría, F., Vázquez, A., García, C.M., 2008. Meteorologically-induced mesoscale variability of the North-western Alboran Sea (southern Spain) and related biological patterns. Estuarine, Coastal and Shelf Science 78, 250–266. http://dx.doi.org/10.1016/j.ecss.2007.12.008.
Marshall, J., Schott, F., 1999. Open-ocean convection: observations, theory, and models. Reviews of Geophysics 37 (1), 1–64. http://dx.doi.org/10.1029/98RG02739.
Marshall, J., Hill, C., Perelman, L., Adcroft, A., 1997a. Hydrostatic, quasi-hydrostatic, and nonhydrostatic ocean modeling. Journal of Geophysical Research 102 (C3), 5733–5752. http://dx.doi.org/10.1029/96JC02776.
Marshall, J., Adcroft, A., Hill, C., Perelman, L., Heisey, C., 1997b. A finite-volume, incompressible Navier Stokes model for studies of the ocean on parallel computers. Journal of Geophysical Research 102, 5753–5766. http://dx.doi.org/10.1029/96JC02775.
MEDOC Group, 1969. Observations of formation of deep-water in the Mediterranean Sea. Nature 227, 1037–1040.
Mikolajewicz, U., 2011. Modeling Mediterranean Ocean climate of the last glacial maximum. Climate of the Past 7, 161–180. http://dx.doi.org/10.5194/cp-7-161-2011.
Naranjo, C., Garcia-Lafuente, J., Sanchez-Garrido, J.C., Sanchez-Roman, A., Delgado Cabello, J., 2012. The western Alborán gyre helps ventilate the western Mediterranean deep water through Gibraltar. Deep Sea Research Part I: Oceanographic Research Papers 63, 157–163. http://dx.doi.org/10.1016/j.dsr.2011.10.003.
Oddo, P., Adani, M., Pinardi, N., Fratianni, C., Tonani, M., Pettenuzzo, D., 2009. A nested Atlantic–Mediterranean Sea general circulation model for operational forecasting. Ocean Science Discussions 5 (461–473), 2009. http://dx.doi.org/10.5194/os-5-461-2009.
Pacanowski, R.C., Philander, S.G.H., 1981. Parameterization of vertical mixing in numerical models of tropical oceans. Journal of Physical Oceanography 11 (11), 1443–1451.
Pinardi, N., Zavatarelli, M., Adani, M., Coppini, G., Fratianni, C., Oddo, P., Bonaduce, A., 2013. Mediterranean Sea large-scale low-frequency ocean variability and water mass formation rates from 1987 to 2007: a retrospective analysis. Progress in Oceanography. http://dx.doi.org/10.1016/j.pocean.2013.11.003 (in press).
Sammartino, S., Garcia-Lafuente, J., Sanchez-Garrido, J.C., De los Santos, F.J., ÁlvarezFanjul, E., Naranjo, C., Bruno, M., Calero, C., 2014. A numerical model analysis of the tidal flows in the Bay of Algeciras, Strait of Gibraltar. Continental Shelf Research 72, 34–46. http://dx.doi.org/10.1016/j.csr.2013.11.002.
Sanchez-Garrido, J.C., Sannino, G., Liberti, L., Garcia-Lafuente, J., Pratt, L., 2011. Numerical modeling of three-dimensional stratified tidal flow over Camarinal Sill, Strait of Gibraltar. Journal of Geophysical Research 116, C12026. http://dx.doi.org/10.1029/2011JC007093.
Sanchez-Garrido, J.C., Garcia-Lafuente, J., Álvarez-Fanjul, E., Sotillo, M., de-los-Santos, F.J., 2013. What does cause the collapse of the Western Alborán Gyre? Results of an operational ocean model. Progress in Oceanography 116, 142–153. http://dx.doi.org/10.1016/j.pocean.2013.07.002.
Sanchez-Román, A., Sannino, G., Garcia-Lafuente, J., Carillo, A., Criado-Aldeanueva, F., 2009. Transport estimates at the western section of the Strait of Gibraltar: a combined experimental and numerical modeling study. Journal of Geophysical Research 114, C06002. http://dx.doi.org/10.1029/2008JC005023.
Sannino, G., Bargagli, A., Artale, V., 2004. Numerical modeling of the semidiurnal tidal exchange through the Strait of Gibraltar. Journal of Geophysical Research 109, C050115. http://dx.doi.org/10.1029/2003JC002057.
Sannino, G., Carillo, A., Artale, V., 2007. Three-layer view of transports and hydraulics in the Strait of Gibraltar: a three-dimensional model study. Journal of Geophysical Research 112, C03010. http://dx.doi.org/10.1029/2006JC003717.
Sannino, G., Sanchez Garrido, J.C., Liberti, L., Pratt, L., 2014. Exchange flow through the Strait of Gibraltar as simulated by a σ-coordinate hydrostatic model and a *z*-coordinate nonhydrostatic model. In: Borzelli, G.L.E., Gačić, M., Lionello, P., Malanotte-Rizzoli, P. (Eds.), The Mediterranean Sea: Temporal Variability and Spatial Patterns. John Wiley & Sons Inc., Oxford. http://dx.doi.org/10.1002/9781118847572.ch3.
Schott, F., Visbeck, M., Send, U., 1994. Open ocean deep convection, Mediterranean and Greenland Seas. In: Malanotte-Rizzoli, P., Robinson, A.R. (Eds.), Ocean Processes on Climate Dynamics: Global and Mediterranean Examples. Kluwer Acad., Norwell, Mass., pp. 203–225.
Schott, F., Visbeck, M., Send, U., Fischer, J., Stramma, L., Desaubies, Y., 1996. Observations of deep convection in the Gulf of Lions, northern Mediterranean, during the winter of 1991/92. Journal of Physical Oceanography 26 (4), 505–524. http://dx.doi.org/10.1175/1520-0485(1996) 026<0505:OODCIT>2.0.CO;2.
Schroeder, K., Ribotti, A., Borghini, M., Sorgente, R., Perilli, A., Gasparini, G.P., 2008. An extensive western Mediterranean deep water renewal between 2004 and 2006. Geophysical Research Letters 35, L18605. http://dx.doi.org/10.1029/2008GL035146.
Send, U., Schott, F., Gaillard, F., Desaubies, Y., 1995. Observation of a deep convection regime with acoustic tomography. Journal of Geophysical Research 100 (C4), 6927–6941. http://dx.doi.org/10.1029/94JC03311.
Smith, R.O., Bryden, H.L., Stansfield, K., 2008. Observations of new western Mediterranean deep water formation using Argo floats 2004–2006. Ocean Science 4 (2), 133–149.
Stommel, H., Bryden, H., Mangelsdorf, P., 1973. Does some of the Mediterranean outflow come from great depth? Pure and Applied Geophysics 105 (1), 879–889.
Tziperman, E., Speer, K., 1994. A study of water mass transformation in the Mediterranean Sea: analysis of climatological data and a simple three-box model. Dynamics of Atmospheres and Oceans 21, 53–82. http://dx.doi.org/10.1016/0377-0265(94)90004-3.
Vargas, J.M., Garcia-Lafuente, J., Candela, J., Sanchez, A.J., 2006. Fortnightly and monthly variability of the exchange through the Strait of Gibraltar. Progress in Oceanography 70 (2), 466–485. http://dx.doi.org/10.1016/j.pocean.2006.07.001.
Vázquez, A., Bruno, M., Izquierdo, A., Macías, D., Ruiz-Cañavate, A., 2008. Meteorologically forced subinertial flows and internal wave generation at the main sill of the Strait of Gibraltar. Deep Sea Research Part I: Oceanographic Research Papers 55 (10), 1277–1283. http://dx.doi.org/10.1016/j.dsr.2008.05.008.
Vázquez, A., Flecha, S., Bruno, M., Macías, D., Navarro, G., 2009. Internal waves and short-scale distribution patterns of chlorophyll in the Strait of Gibraltar and Alborán Sea. Geophysical Research Letters 36 (23), L23601. http://dx.doi.org/10.1029/2009GL040959.
Wang, D.P., 1993. The Strait of Gibraltar Model: internal tide, diurnal inequality and fortnightly modulation. Deep Sea Research Part I: Oceanographic Research Papers 40 (6), 1187–1203. http://dx.doi.org/10.1016/0967-0637(93)90133-N.
Wesson, J.C., Gregg, M.C., 1994. Mixing at Camarinal sill in the Strait of Gibraltar. Journal of Geophysical Research: Oceans 99 (5), 9847–9878. http://dx.doi.org/10.1029/94JC00256 (1978–2012).
Whitehead Jr., J.A., 1985. A laboratory study of gyres and uplift near the Strait of Gibraltar. Journal of Geophysical Research 90 (C4), 7045–7060. http://dx.doi.org/10.1029/JC090iC04p07045.

V. Modeling the impact of tidal flows on the biological productivity of the Alboran Sea

José C. Sánchez-Garrido[1], C. Naranjo,[1], D. Macías,[2], J. García-Lafuente[1], and T. Oguz[3]

Corresponding author: J. C. Sánchez-Garrido, Physical Oceanography Group, University of Málaga, ETSI Telecomunicación, 29071, Málaga, Spain. (jcsanchez@ctima.uma.es)

[1]Physical Oceanography Group, University of Málaga, Málaga, Spain.

[2]European Commission, Joint Research Center, Institute for Environment and Sustainability, Water Research Unit, Ispra, Italy.

[3]Institute of Marine Sciences Middle East Technical University, Erdemli, Turkey.

Abstract.

The control of phytoplankton production by tidal forcing in the Alboran Sea is investigated with a high-resolution ocean circulation model coupled to an ecosystem model. The aim of the modeling efforts was to elucidate the role of tides in sustaining the high biological productivity of the Alboran Sea, as compared with the rest of the Mediterranean sub-basins. It is shown that tidal forcing accounts for an increase of phytoplankton biomass and primary productivity in the basin of about 40% with respect to a non-tidal circulation, and about 60% in the western Alboran Sea alone. The tidal dynamics of the Strait of Gibraltar is shown to be the primary factor in determining the enhancement of productivity, pumping nutrients from depth to the photic zone in the Alboran Sea. Model results indicate that the biological implications of the propagating internal tides are small. These results imply that nutrient transports through the Strait of Gibraltar have to be parametrized in ocean models that do not resolve tides in order to properly represent the biochemical budgets of the Alboran Sea.

1. Introduction

The Alboran Sea (AS; Fig. 1a) is the first sub-basin that the jet of Atlantic Water (AW) entering through the Strait of Gibraltar (SoG) encounters in its way along the Mediterranean. Its surface circulation is fairly variable in both space and time, but its most typical and classically described configuration is that consisting of the Atlantic jet meandering around and feeding two mesoscale anticyclonic gyres, the so-called Western and Eastern Alboran Gyres (hereinafter WAG and EAG). Typical velocities along the jet are as large as 1-2 $\mathrm{m\,s^{-1}}$, and to a first approximation can be assumed to be geostrophically maintained by the strong density front between the relatively fresh incoming AW and the saltier ambient water (modified AW). As elsewhere in the ocean, such fronts feature a secondary cross-front ageostrophic circulation characterized by large vertical velocities and with potential to sustain high levels of biological productivity [e.g., *Spall*, 1995; *Nagai et al.*, 2008].

In biological terms, the AS is one of the most (if not the most) productive sub-basins of the Mediterranean [e.g., *Uitz et al.*, 2012], and there are a number of physical reasons for that. The most obvious one lies in its active frontal activity and, not surprisingly, field observations and ocean color images reveal enhanced levels of chlorophyll (chl) concentration along the jet [*Navarro et al.*, 2011]. The potential of the frontal jet ageostrophic circulation to sustain phytoplankton production has been further confirmed in the recent process-oriented model study by *Oguz et al.* [2014]. Another important factor is the wind-driven circulation, particularly that forced by westerlies that frequently drive strong

upwelling events with associated phytoplankton blooms along the northern shore of the basin [*Reul et al.*, 2005; *Macías et al.*, 2007a].

There are also several short-scale processes of tidal origin occurring in the SoG that have been put forward to be relevant for the the biology of the AS, although their actual impact has not been assessed yet. Of particularly concern is the assumed ability of tidal flows to fertilize the surface inflowing waters through the enhancement of vertical mixing, particularly at the west side of the Camarinal Sill (CS in Fig. 1b) where the flow undergoes a number of internal hydraulic transitions and high levels of turbulent energy dissipation rates have been measured during the flood tide (westwards tidal flow) [*Wesson and Gregg*, 1994; *Sánchez-Garrido et al.*, 2011]. *García-Lafuente et al.* [2013] estimated that as much as 30% of the pool of mixing water formed at the lee side of the sill (west side during the flood tide), a mixture of the nutrient-impoverished AW and the nutrient-rich underlying Mediterranean Water (MW), can overpass the sill with the tidal reversal and subsequently incorporate into the inflow. The likely important biological consequences of this fact was pointed out by these authors as the pool of water in question is rich in nutrients and eventually can reach the photic zone in its way to the AS, which makes it possible its utilization for photosynthesis. *Macías et al.* [2007b] drew attention to this tidal pumping of nutrients from the sill and analyzed its possible consequences for phytoplankton by applying a simple three-layer, one-dimensional (in the horizontal) model with physical domain restricted to the SoG. Despite the considerable input of nutrients, a very weak phytoplankton response was found, a fact that was attributed to the short residence time of the cells within the channel. The supply of nutrients provided by tides is therefore

expected to cause certain growth of phytoplankton further downstream, somewhere in the AS, although its implications for the biology of the basin is not clear.

It is also uncertain how the prominent internal tides generated at the sill [see, e.g., *Brandt et al.*, 1996; *Sánchez-Garrido et al.*, 2011] can affect productivity as they propagate in the AS. In a general context internal waves can stimulate phytoplankton growth by enhancing vertical diffusive fluxes of nutrients from the ocean interior into the surface mixed layer, especially in shallow areas where wave-breaking occurs [*Leichter et al.*, 1998; *Sangrà et al.*, 2001]. Another way in which waves can affect production is through vertical advection, periodically exposing phytoplankton to different levels of irradiance [*Holloway and Denman*, 1989]. The potential of this mechanism was explored by *Evans et al.* [2008] in a series of field experiments conducted in a lake where photosynthesis was light-limited, and reported differences of primary productivity (PP) ranging from a 15% reduction up to a 200% enhancement with respect to an unperturbed state, depending on surface irradiance. In the ocean, moderate increases of PP of $\approx 9-15\%$, driven by internal tides, have been reported [*Muacho et al.*, 2013; *Pan et al.*, 2012].

All these tidally driven processes were not captured by the model simulations conducted so far in the area devoted to investigate different aspects of the physical controls on PP, either by the inevitable coarse resolution applied in basin-scale models of the Mediterranean [*Lazzari et al.*, 2012], by the exclusion of tidal forcing [*Oguz et al.*, 2014], or both. The objective of the present paper is to fill this gap and clarify the role that tides play on the high productivity of the AS. For doing so we employ a circulation model coupled to an ecosystem model that is described in the following Section 2. Section 3 describes the experimental strategy that has been followed, Sections 4 and 5 present the model

results and analysis, respectively, whereas discussions and conclusions are finally drawn in Section 6.

2. Model description and initialization

2.1. Circulation model

The physical model used in this study is the Massachusetts Institute of Technology general circulation model [MITgcm, *Marshall et al.*, 1997a, b], which solves the Boussinesq form of the Navier-Stokes equations for an incompressible fluid on an staggered C-grid with level vertical coordinates and partial cell representation of the bottom topography. In the present work the model utilizes the hydrostatic approximation as well as an implicit linear free-surface formulation.

The model configuration is quite similar as in *Sánchez-Garrido et al.* [2013]. The domain is shown in Fig. 1a together with the model computational grid and bottom topography. The grid is curvilinear and has been squeezed in the AS and the SoG in order to increment the resolution in these areas. Horizontal resolution is approximately 0.5 km within the strait, which permits a quite good representation of small-scale topographic features and processes in consideration, namely, internal hydraulic jumps with the associated mixing and propagating internal waves. In the AS (specifically within the rectangle of Fig. 1a) cell sizes always lie between 1-4 km. Provided that the first baroclinic Rossby radius of deformation is approximately 20 km, the model is set to resolve an important wavenumber range of its submesoscale dynamic. In the vertical there are 46 z-levels with increasing cell size from the surface to the bottom.

Following previous model investigations of the flow through the SoG [*Vlasenko et al.*, 2009; *Sánchez-Garrido et al.*, 2013; *Sannino et al.*, 2014] the Richardson-number-

dependent scheme of *Pacanowski and Philander* [1981] is chosen for the parameterization of sub-grid scale vertical mixing:

$$\nu_z = \nu_b + \frac{\nu_0}{(1+\alpha \mathrm{Ri})^n}, \quad \kappa_z = \kappa_b + \frac{\nu_z}{(1+\alpha \mathrm{Ri})}.$$

Here ν_z and κ_z are vertical eddy viscosity and diffusivity coefficients, $\nu_b = \kappa_b = 10^{-5}$ $\mathrm{m^2\,s^{-1}}$ are their background values, and $\nu_0 = 1.5 \cdot 10^{-2}$ $\mathrm{m^2\,s^{-1}}$, $\alpha = 5$, and $n = 1$ are adjustable parameters. For the horizontal viscosity the model incorporates the biharmonic Smagorinsky-like closure scheme of *Griffies and Hallberg* [2000] with free parameter $C = 3$. Temperature, salinity, and the biochemical tracers described later are advected with a third-order direct-space-time scheme with flux limiting to avoid negative values in the solutions [*Hundsdorfer and Trompert*, 1994]. The scheme is stable and sufficiently diffusive without explicit horizontal diffusion. The integration time step is 12 s.

The model is laterally forced by daily temperature, salinity, and velocity fields extracted from MyOcean re-analysis products (`http://myocean.met.no/`). Initial conditions are obtained from the same data source. At the surface the model is driven by wind stress obtained from advanced scatterometer data (ASCAT), heat fluxes, and fresh water flux originating from precipitation, both obtained from NCEP/NCAR reanalysis [*Kalnay*, 1996]. Downward short wave and long wave radiation are directly prescribed, whereas sensitive and latent heat fluxes are interactively calculated by the model using standard bulk formulas. Tidal forcing has been incorporated by prescribing time-dependent barotropic velocities across the open boundaries associated with the main 8 tidal constituents. Non-slip conditions are applied at the solid boundaries together with a non-linear bottom drag at the sea floor.

The described model set-up produces a realistic mean circulation and variability that have been validated using different observational data sources, including satellite sea surface temperature images of the AS, ADCP measurements collected in the SoG, and a number of tide-gauge records. For the validation analysis the reader is referred to the paper by *Sánchez-Garrido et al.* [2013].

2.2. Ecosystem model

We consider the ecosystem model of *Follows et al.* [2007] coupled to the circulation model. The ecosystem model is of high complexity and was originally conceived to investigate the self-organization of stochastically generated phytoplankton communities. Our aim here is much simpler, thus a simplified configuration has been adopted in which the phytoplankton community consists of two fixed phytoplankton types. Additionally, only phosphate and the inorganic forms of nitrogen (nitrate, nitrite, and ammonium) are the nutrients of the system, which are limiting in the AS according to the literature [*Ramírez et al.*, 2005].

The model solves a system of partial differential equations determining the evolution of dissolved nutrients, phytoplankton, zooplankton, and detritus (particle and dissolved organic matters). The governing equation for any tracer B can be written as

$$\frac{\partial B}{\partial t} = -\mathbf{u} \cdot \nabla B + \nabla \cdot (\mathbf{k} \nabla B) - \frac{\partial (w^B B)}{\partial z} + R. \tag{1}$$

The local tendency of B is then the result of advection and diffusion determined by the circulation model ($\mathbf{u}$ is the flow velocity and $\mathbf{k}$ the eddy diffusivity coefficient), sinking of the tracer (at velocity w^B), and biochemical reactions denoted by R. For instance, for phytoplankton the term R includes mortality due to grazing by zooplankton, intrinsic

mortality, and a growth term depending upon environmental conditions (light, nutrients availability, and sea water temperature). Details regarding the paramatrization of the biochemical reactions and the specification of the parameters chosen for the experiments in this work are given in Appendix A; for an exhaustive description of the model the reader is referred to *Follows et al.* [2007] and *Dutkiewicz et al.* [2009].

For the initialization of the ecosystem model the same strategy as in *Losch et al.* [2014] has been followed. Initial and open boundary values for the tracers are prescribed distinctively depending upon the available information. For those for which there are enough observations to estimate a quasi-synoptic field, initial and boundary values have been readily derived. Nutrients are inside this category and they have been retrieved from the MEDAR/MEDATLAS data base [*Maillard*, 2002]. The rest of the variables, of which we have scarce information, are initialized from few observed vertical profiles or assumed small constant concentration. For this second class of variables we apply homogeneous Neumann boundary conditions (zero cross-boundary gradient).

Before presenting the model results two remarks are worth noting. First, the model uses phosphorous as currency for phytoplankton growth and biomass, although we have preferred to use carbon instead throughout the paper for conventionality. The conversion has been made with the Redfield ratio C:N:P = 106:16:1. Additionally, and for validation proposes satellite chlorophyll (chl) data has been used as a proxy of the surface phytoplankton biomass. To facilitate model-data comparisons the model phytoplankton biomass has been converted to chl concentration by applying a constant chl:C ratio of 1:50, in the range of the measured quantities in the zone [*Echevarría et al.*, 2009]. Note, however, that this ratio can vary substantially among species and is affected nonlinearly

by ambient nutrient, light, and temperatures [*Geider et al.*, 1997]. A perfect matching between model and remote sensing observations is not then to be expected, although general spatial patterns should be similar.

3. Experimental procedure

In a first experiment the model is run for three years without tidal forcing and with the rest of the forcing fields corresponding to the period 2011-2013. The first year of simulation (2011) is taken as spin-up time and is therefore excluded from the analysis. The aim of this run is to provide a basic circulation and ecosystem state on which later investigate the role of tides on the ecosystem. It will be referred as the reference experiment (REF). In a second run the model includes tides (TID experiment) and their biological implications are evaluated. This run covers only three months, a sub-period of the REF run. The reason to conduct a shorter run is largely motivated by the fact that tidal forcing makes the model substantially more expensive in computational terms. On the other hand, a period of three months that encompasses several spring-neap tidal cycles (this cycle is the main source of low-frequency tidal variability) is considered suitable to provide a good estimation of the effect of tides on biology.

4. Results

4.1. REF experiment

The results of the REF run are examined in order to assess the ability of the model to reproduce the general circulation and basic biological patterns of the AS. Likewise other regional models that do not incorporate tides nor explicitly resolve the exchange flow

through the SoG are successful in capturing such basic features [e.g. *Lazzari et al.*, 2012], thus great discrepancies between model and observations are not expected.

The mean sea surface height (SSH) of the simulation (black contours in Fig. 2a) reveals the presence of both gyres, the WAG and EAG. The WAG has larger size and features greater geostrophic currents than its eastern counterpart, as noted by the sharper cross-gyre SSH gradients. This result stems partially from the fact that the WAG is a rather permanent feature during the simulation, while the EAG exhibits more variability in both size and location (sometimes it is even absent). Figure 2a also displays the two-year climatology of the surface chl and reflects the oligotrophic nature of the gyres. As expected chl concentration is high in the vicinity of the jet that runs eastwards with its axis centered along the SSH=0 contour (thick solid line). This is particularly true for the cyclonic side of the frontal jet (to the north of the AS), a pattern that is consistent with a cross-front ageostrophic circulation causing downwelling at the anticyclonic side of the front, and upwelling in its cyclonic side. This creates an overall meridional gradient of chl with increasing concentration to the north of the basin. Additionally, there is a decrease of chl from west to east with the richest area being the northwestern region of the AS (NWAS), in agreement with field and remote sensing observations [see, e.g., *Sarhan et al.*, 2000; *Reul et al.*, 2005; *Macías et al.*, 2007a]. *Oguz et al.* [2014] attribute the eastwards decreasing pattern of chl to the gradual weakening of the density front, and thereby of its potential to fuel phytoplankton production, by accumulative mixing between incoming and ambient waters.

The spatial pattern of the surface chl in the REF run has been compared with remotely sensed chl obtained from the GlobColour Project (`http://www.globcolour.info/`).

They produce ocean color maps (Level-3) by merging data from the sensors SeaWiFS, MODIS and MERIS. The obtained chl is for case 1 waters where phytoplankton concentration prevails over inorganic particles and the applied algorithm is based on weighted averaging merging techniques. The spatial resolution of the downloaded composite images is 1/48° and consist of 8-day merged fields. The climatology computed during the analyzed period (Fig. 2b) displays the main features reproduced by the REF run, including the oligotrophic gyres and the biomass-rich NWAS, although with somewhat different characteristics. For instance, the chl-rich region of the NWAS is larger than in the model. Moreover, chl concentration in the WAG is considerably higher than in the EAG, both in its core and specially at the outer edges, and the west-to-east decreasing pattern of chl appears more marked than in the model. Another noticeable difference is observed over the continental shelf to the north west of the SoG, where the satellite image shows the greatest chl concentration of the domain (more than 1 $\mathrm{mg\,m^{-3}}$), whereas in the model this area is not particularly rich. These discrepancies are to a great extent due to tides, as we shall see later.

The time variability of the model and satellite chl has been also compared by computing spatial aggregate median values in the basin (Fig. 3). For the computation the model outputs were interpolated onto the satellite data grid and the cloud cover mask was applied to the interpolated chl for a more reliable comparison of the two data sets. Satellite chl (box-plot) exhibits a seasonal cycle with minimum values of chl by mid summer and maximum by the beginning of March and reflects the two regimes identified by *García-Gorriz and Carr* [1999], with a fall-to-spring bloom (November-March) and a non-bloom period (May-September). The model (red line) captures the timing and the duration of

these regimes, the agreement being better in year 2013. Less satisfactory is the agreement between the timing of wind-driven bloom events due to westerlies that induce coastal upwelling along the north coast of the AS. An example is the bloom occurring in the model by July 2012 (see zonal wind stress in Fig. 4b) that is not reflected in the observations. Conversely, there are some events of remarkably high chl concentration in the satellite records that are not captured by the model and could be associated with coastal upwelling as well, like the chl peak observed by the end of May 2013. There is then a mismatch in the timing of these blooms that could be ascribed to the coarse resolution of the forcing winds. Nonetheless, this is not of particular concern for the results discussed in this paper that focus on tidal processes.

Another noteworthy characteristic of the AS (and also of the rest of the Mediterranean) is the presence of a permanent deep chl maximum (DCM) with the possible exception of the late winter [*Siokou-Frangou et al.*, 2010]. Its mean depth is about 30 m and it is shallower than in the rest of the Mediterranean, presumably because of the higher productivity and hence lower seawater transparency of the AS. In the model the maximum concentration of phytoplankton biomass is found at $z = -34 \pm 25$ m (Fig. 4a), it deepens during summer, and shoals towards the late winter, which is in agreement with the mentioned behaviour of the DCM. The most dramatic vertical excursions of the DCM take place, however, during the mentioned upwelling events when, regardless the season the chl maximum reaches the very surface. According to the model this occurs by mid July 2012 and early September 2013 (Fig. 4a).

The last variable examined has been the depth-integrated PP (PP_{int}). In situ measurements reflects the great variability of the AS in both space and time with estimated PP_{int}

ranging in a broad interval, typically between 100-300 $g\,C\,m^{-2}\,y^{-1}$ [see *Siokou-Frangou et al.*, 2010, and the references therein]. Such variability has been largely attributed to the presence of the frontal jet in which a PP_{int} of up to 475 $g\,C\,m^{-2}\,y^{-1}$ has been reported [1300 $mg\,C\,m^{-2}\,d^{-1}$; *Lohrenz et al.*, 1988]. The basin-averaged PP_{int} in the REF run (136.1 ± 24.6 $g\,C\,m^{-2}\,y^{-1}$) is in the lower range of the reported values, and, as the DCM, exhibits both seasonal and wind-driven variability (Fig. 4b).

4.2. TID experiment

In the TID experiment the model was integrated with tidal forcing from February to June 2013 and starting from REF outputs as initial conditions. Approximately after one month of simulation the differences between the biochemical variables diagnosed in the REF and TID runs, including PP, remained stable over time, indicating that the ecosystem adjusted to the new hydrodynamic conditions after that period. The first 45 days of model outputs were then ruled out and so the final TID data set covered the last 2.5 months of the experiment (from mid March to the beginning of June).

It was found that tides increased the productivity of the AS by about 40%, from a mean value of 126.6 $g\,C\,m^{-2}\,y^{-1}$ in REF to 176.7 $g\,C\,m^{-2}\,y^{-1}$ in TID (Fig. 5a,b), this later value more in the range of reported estimates. The increase was not uniform over the basin, the ecosystem of its western half being particularly affected by tides. In the area between the SoG and 3°W, encompassing the NWAS and the WAG, the PP increment with respect to REF was 60% (from 141.4 $g\,C\,m^{-2}\,y^{-1}$ in REF to 226.1 $g\,C\,m^{-2}\,y^{-1}$ in TID) whereas in the eastern AS (east of 3°W) it was only 11% (from 111.1 to 124.1 $g\,C\,m^{-2}\,y^{-1}$). Zones that become particularly productive with tides are the NWAS, where PP_{int} locally exceeds 500 $g\,C\,m^{-2}\,y^{-1}$, and also a small area of the continental shelf northwest of the strait in which

the productivity is largely tidally driven (more than twice the REF value). Phytoplankton biomass increases approximately in the same proportion (Fig. 5c,d).

Regarding the spatial pattern of chl displayed in satellite images, the inclusion of tides in the TID run results in a spatial distribution that agrees with observations much better than the REF run. Of particular concern is the west-to-east decreasing pattern of remote sensing images (Fig. 6c) that is satisfactorily reproduced by the TID run (Fig. 6b) but not by the REF run (Fig. 6a). The TID run also gives rise to a localized spot of high chl concentration in the aforementioned region of the continental shelf northwest to the SoG (Fig. 6b), although it is still unable to reproduce the high chl signal along the Spanish coast displayed in the satellite image (Fig. 6c), a fact that we attribute to nutrient loads from the Guadalquivir river that were not prescribed in the model.

5. Analysis

Here we analyze the candidate physical processes for explaining the tidally driven increase of the AS productivity. First we assess the hypothesis that tidal flows in the SoG fertilize the Atlantic inflow. The tidal dynamic of the strait is examined and nutrient transports into the AS will be computed for both the REF and TID simulations. Attention will be also paid to other tidal processes with possible biological consequences such as propagating internal waves.

5.1. Tidal dynamics and nutrient transports through the SoG

The configuration of the flow through the SoG as simulated in the REF run is shown in Fig. 7, displaying salinity, velocity, and nutrient concentration (nitrate) along the strait. The flow consists of an undercurrent of nutrient-rich and salty MW (> 8 mmol NO_3 m^{-3};

$S > 37$) flowing westwards, and AW flowing to the AS ($S < 37$), which can be further partitioned into the nutrient-depleted Surface Atlantic Water (SAW; < 3 mmol $NO_3\,m^{-3}$) and the moderately nutrient-rich North Atlantic Central Water (NACW; $\approx 5-7$ mmol $NO_3\,m^{-3}$). The NACW is fresher but denser than the overlying SAW lies to the west of the Camarinal Sill at 150-200 m depth, with a salinity of $S \approx 36.2 - 36.4$. With this configuration the nutrient budget of the inflow is largely dependent upon the volume of NACW that can overpass the sill and participate in the inflow, as well as on the ability of the Atlantic current to entrain nutrients from the underlying MW. Figure 7 suggests that the second mechanism is at work 30 km to the east of the sill, in the so-called Tarifa Narrows (TN in inset of Fig. 1b), where the inflow accelerates in response to the constricted lateral boundaries.

The steady exchange in the REF run is notably modified in the TID run as it can be seen in the time evolution of the flow during a tidal cycle presented in Fig. 8. Figure 8a roughly corresponds to the time of maximum tidal flow towards the Atlantic (flood tide; see barotropic velocity over the sill in the bottom panel) and reflects important differences with respect to the steady flow configuration described above. The response of the flow to the tidal discharge is the expected for an hydraulically controlled sill flow exposed to a quasi-steady barotropic forcing [*Long*, 1954; *Lawrence*, 1993] both upstream (to the right) and downstream (left) of the bottom obstacle. In the upstream side the flow adjusts to the tidal forcing by raising the interface between Atlantic and Mediterranean Waters, in a clear manifestation of upstream influence exerted by the sill, whereas the most noticeable downstream effect is the enhancement of vertical mixing, as noted by the homogenization of both salinity and nutrient concentration over the water column. Such enhanced of

mixing is closely related to the increase of the internal Froude number at the downstream side of the sill [*Sánchez-Garrido et al.*, 2011].

The biological implications of the tides are revealed in the subsequent stages of the tidal cycle, when the tidal flow turns to the east (ebb tide; Fig. 8b,c). Tidal forcing is sufficiently strong to invert the direction of the Mediterranean current over the sill, temporally facilitating the eastwards advection of both NACW and MW, the later returning to the eastern flank of the sill with the tidal reversal (note positive velocities all over the sill crest in Fig. 8c). In fact, *García-Lafuente et al.* [2013] estimate that as much as 30% of the pool of mixed water formed west of the sill during the flood tide, a mixture of NACW and MW, can be subsequently pumped to the near surface in the eastern part of the strait, providing a nutrient supply to the AS. A second way in which tides can fertilize the inflowing waters is through the enhancement of diapycnal mixing to the east of the sill, driven in part by the eastwards propagation of the internal tidal bore generated at the sill (note it, for instance, at x=22 km in Fig. 8c).

The strong time dependence of the flow is transferred to the nutrient budget of the inflowing waters, as noticed in Fig. 9 that shows the time-space dependence of nitrate integrated in the uppermost 94 m of the water column. The maximum nutrient content is periodically reached in Camarinal Sill (x=0) around the end of the flood tide as a result of the shoaling of the interface (see Fig. 8a), and moves eastwards during the ebb tide at a velocity that can be estimated in 1.5 $\mathrm{m\,s^{-1}}$ from the slope of the contours in the time-space diagram of Fig. 9a. *García-Lafuente et al.* [2013] described a similar eastwards propagation pattern of the thickness of the interface mixing layer and ascribed it to the physical processes mentioned above, namely, advection of mixed water formed

west of the sill and enhanced entrainment of MW driven by the propagating baroclinic bore. The same processes are very likely involved in the eastward propagation of nutrients from the sill with tidal modulation. This behaviour differs from the REF run, in which the nutrient budget of the inflow hardly exhibits time dependence. It is from the Tarifa Narrows that it increases eastwards (Fig. 9b), due to the enhanced entrainment of MW driven by the spatial acceleration of the inflow in this location, as remarked earlier. Most importantly, the nutrient content of the inflow at the eastern mouth of the SoG (x=45 km) is greater in the TID experiment, oscillating between 350-550 mmol NO_3 m^{-2}, against the more constant value of 200-250 mmol NO_3 m^{-2} obtained in REF, which results in different nutrient transports into the AS in the two model simulations (Fig. 10).

The nitrate transport in TID (Fig. 10a; gray line) has a mean $\pm$ std value of 2.28 ± 1.28 kmol s^{-1}, nearly 75% greater than in REF (1.31 ± 0.28 kmol s^{-1}; black dashed line). The greater variability of the TID series is largely accounted for the M_2 tidal constituent, although a noticeable fortnightly signal can be also distinguished, with greater and smaller transports during spring and neap tides, respectively, as highlighted by the low-pass curve (tidal variability filtered out; black solid line). The same applies to phosphate, although differences between the two simulations are slightly more moderate (0.20 ± 0.10 and 0.15 ± 0.03 kmol s^{-1} in TID and REF, respectively; Fig. 10b). Note that these discrepancies are of particular concern because the input of nutrients provided by tides is within the photic zone and so can be utilized by phytoplankton. This becomes even more obvious by noting that the nutrients transport in TID are even greater with respect to those in REF when computed in the upper part of the photic zone ($-48 < z < 0$; Fig. 10c,d), where high levels of light can further stimulate phytoplankton growth. The tidal pumping

of nutrients from the sill is therefore a clear candidate to explain the increase of biomass and productivity obtained in the TID simulation.

5.2. Tides and tidal-related processes in the AS

It is also feasible that the different biological patterns of the TID and REF runs are accounted for, at least partially, by local tidal currents in the AS, rather than in the adjacent SoG. For instance, a distinctive feature of the tidal experiment is the internal tide that progresses eastwards through the SoG into the AS after being generated in the Camarinal Sill (Fig. 8). Such internal waves induce large vertical velocities (Fig. 11) that can potentially modify phytoplankton growth by exposing it to different levels of irradiance through vertical advection. Another tidal-related process that bears consideration refers to lateral boundary flows. *Sánchez-Garrido et al.* [2013] found that the back and forth motion of tides generate shear vorticity on the strait's lateral boundary layers (positive on the north, negative on the south) that can lead to a wake of coherent submesoscale eddies carried by the Atlantic jet [see also *La-Violette*, 1984]. The flow along the wake is quite ageostrophic and can stimulate productivity, much like observed in island wakes [*Hammer and Hauri*, 1981; *Hernández-León*, 1991; *Hasegawa et al.*, 2004].

In order to clarify whether these processes are biologically relevant, a third experiment has been conducted in which the physics is as in the REF run but with modified ecosystem equations so that biochemical tracers are nudged towards their TID values within the SoG. More especially, a Newtonian nudging term $\tau^{-1}(B - B_{tid})$ was added to the right hand side of eq. 1, where B_{tid} denotes the value of the biochemical tracer obtained in the tidal simulation (daily mean fields), and τ is the relaxation time scale. For a sufficiently small τ the nudging term acts more like a forcing rather than a relaxation term, forcing the

tracer to lie very close to B_{tid} during the calculations. The nudging term is only included within the SoG and a small relaxation time scale is set, $\tau = 2$ h. With this constraint nutrients concentration and the corresponding transports through the SoG in the new run are very similar to those obtained in TID, approximately following the low-pass curves of Fig. 10 (not shown). Note, however, that even if the transports are maintained as in TID, the circulation is non-tidal and therefore vertical fluxes driven by internal waves, eddies, or any other tidal-related process occurring in the AS are now inhibited. As such, this experimental strategy allows us to distinguish between biological effects resulting from (i) the increase of nutrient transport through the SoG and (ii) tidally driven flows in the AS itself.

The mean PP_{int} obtained in the nudging experiment is shown in Fig. 12. As tidal forcing is suppressed in these experiments the surface structures (suggested by the PP_{int} distribution) in the AS resemble those found in the REF run (compare Fig. 12 and Fig. 5a), but the PP_{int} values themselves are similar to the distribution obtained in the TID run (Fig. 5b), with PP_{int} exceeding 400 $\mathrm{g\,C\,m^{-2}y^{-1}}$ in the NWAS, 300-400 $\mathrm{g\,C\,m^{-2}y^{-1}}$ further east along the jet, and ≈ 150 $\mathrm{g\,C\,m^{-2}y^{-1}}$ in the center of the WAG. The same level of similarities is found in terms of integrated biomass (not shown). There are however some differences of PP_{int} distribution between Fig. 12 (Nudged run) and Fig. 5b (TID run). One of them is the extent of the plume of high productivity associated with the Atlantic jet, which reaches further east in the Nudging run (Fig. 12). This in turn leads to a slightly greater production in the eastern AS (compare Fig. 12 and Fig. 5b). Another small difference is found at the exit of the SoG in 5°W, where the TID run produces greater values of PP_{int} off the African coast. Both differences are ascribed to the absence of mixing

driven by tides in the nudging run, which in turn facilitates the lower residence of high nutrient concentration in the Atlantic plume. Despite these differences, the comparison of Fig. 12 and Fig. 5b strongly suggests that (i) is the prevailing mechanism for the tidally driven increase of biomass and productivity.

6. Discussion and conclusions

The results of this paper highlight the important role of tides for maintaining the high productivity of the AS, as compared with the rest of Mediterranean sub-basins. The tidal dynamics of the flow through the SoG, with the resulting pumping of nutrient-rich water from depth to the sunlit surface layer is the key process that explain the increase of biomass and productivity in the tidal simulation. The nutrient supply provided by tides does not cause, however, a substantial growth of phytoplankton within the strait itself (see Fig. 5d), a fact that agrees with the findings of *Macías et al.* [2007b] and that we ascribe to the short residence time of the cells within the channel. The distance from the Camarinal Sill to the eastern mouth of the SoG is 40 km and a typical along-strait velocity is 1.5 $\mathrm{m\,s^{-1}}$, which gives a residence time of $\approx$ 7.5 h, too short indeed for a noticeable increase of biomass (maximum phytoplankton growth rates are 1.4 and 2.5 $\mathrm{d^{-1}}$), initially scarce at the western side of the SoG except for a limited region of its north coast. It is not until the bulk of nutrients is carried into the AS that has an apparent impact on biochemistry, especially in the western half of the basin where it accounts for as much as a $\mathrm{PP_{int}}$ increase of 60%. By contrast, the eastern AS is barely affected by such nutrient supply which suggests that the input of nutrients coming from the SoG is consumed by phytoplankton in the western half of the basin. This is particularly true for the region of the NWAS where the maintenance of its nutrient-rich waters and elevated

biomass concentration has been so far attributed to its upwelling dynamic [*García-Gorriz and Carr*, 1999; *Sarhan et al.*, 2000].

By conducting an idealized experiment in which biochemical tracers (and transports) were locally restored to their tidal values within the SoG, local processes occurring in the AS have been ruled out from being responsible for the increase of biomass and productivity resulting in the tidal simulation. A prominent feature of the AS are the large internal tides that propagate in the basin, which however were found to play a negligible role on the ecosystem. While the model captures well the propagation of internal tides (of ≈ 50 km wavelength) in open waters and so also the associated vertical advection of biochemical tracers, smaller-scale features and processes such as short solitary waves evolving from the baroclinic bore generated in the strait's sill and their expected wave-breaking in shelf areas of the AS are not resolved in the simulation. It is then likely that internal waves can actually be more relevant over coastal regions that our model suggests.

A delicate point implicit in our results lies in the ability of the model to reproduce a realistic tidal dynamic and associated mixing in the SoG. The application of a high-resolution model configuration is necessary to achieve this but does not necessarily guarantees a satisfactory outcome. Of particular concern are the resulting nutrient transports that largely determine the biological response in the adjacent AS. The assessment of the validity of our results requires the comparison with estimates based on the scarce field observations collected in the area, like those included in the paper by *Huertas et al.* [2009]. These authors estimate a mean nitrate and phosphate transports of 2.59 $\mathrm{kmol\,s^{-1}}$ and 0.21 $\mathrm{kmol\,s^{-1}}$, respectively, which agree quite well with the values obtained in the TID simulation (2.28 $\mathrm{kmol\,s^{-1}}$ and 0.20 $\mathrm{kmol\,s^{-1}}$, see Fig. 10) and exceed those of REF. Regional ocean models

of the Mediterranean do not typically incorporate tidal forcing as it is generally assumed to have minor effects on the circulation and therefore also on biochemistry. This is not true for some locations and the AS is one example in light of the results presented herein. Attention need to be paid to the transports obtained in these model as the simulated inflowing waters are expected to result more oligotrophic than actually are.

The last remark concerns implications of our results for the future in which a decline of marine PP is expected for the low- and mid-latitude ocean, including the Mediterranean [*Steinacher et al.*, 2010]. The decline is related to enhanced stratification and reduced mixed layer depth by the end of the 21st century, which limits vertical fluxes of nutrients into the euphotic zone. In such scenario dynamical regions with strong energy sources such those originating from tides are expected to be less vulnerable, as it can be the case of the AS.

Appendix A: Ecosystem model

We use a two-species configuration of the ecosystem model developed by *Follows et al.* [2007] with the modifications introduced by *Dutkiewicz et al.* [2009]. The reader is referred to these papers for an exhaustive description of the model theoretical background, equations, and parametrizations; here we only outline the basic features and details of our set up.

In our configuration the inorganic forms of nitrogen and phosphorus nourish two phytoplankton species (iron and silica chemistry are switched off) which in turn are grazed by two zooplankton types. Mortality of and excretion from the plankton community as well as sloppy feeding by zooplankton contribute to a sinking particulate and dissolved organic matter that eventually transform into inorganic forms by remineralization.

The two classes of phytoplankton consist of an "opportunist" species with the ability to rapidly develop in situations of abundant nutrient supply and a "gleaner" class better adapted to low-nutrient conditions. The opportunistic class is characterized by a larger size, larger sinking speed, and greater intrinsic growth rate, among other distinctive parameters described below. There are also a large and a small zooplankton that preferentially graze on the large and the small phytoplankton, respectively, although can also graze on the other. Two maximum grazing rates are therefore defined and their given values will be specified later.

The local tendency for each phytoplankton depends upon advection and diffusion determined by the circulation model, grazing, intrinsic mortality rate, sinking speed, and a growth term depending upon environmental conditions. The latter is written as

$$\mu_j = \mu_{max_j} \gamma_j^T \gamma_j^I \gamma_j^N,$$

where μ_{max_j} is the maximum growth rate and γ_j^T, γ_j^I, γ_j^N are non-dimensional factors that modify μ_{max_j} due to ambient temperature, light, and nutrient availability, respectively. Subscript j refers to the phytoplankton type, with $j = 1$ for the opportunistic species and $j = 2$ for the gleaner. Primary productivity is $\sum_j \mu_j P_j$, where P denotes phytoplankton concentration.

The temperature modification of the growth rate is

$$\gamma_j^T = \frac{1}{\tau_1}(A^T - \tau_2),$$

where T is the local ocean temperature, coefficient A regulates the shape of the curve, and τ_1 and τ_2 normalize the maximum value of the modification function.

Light modification is parametrized as

$$\gamma_j^I = \frac{1}{F_{max}}(1 - e^{-k_{par_j} I})e^{-k_{inhib_j} I},$$

where I is the local vertical flux of photosynthetically active radiation (PAR). The parameter k_{par_j} defines the increase of growth rate with light at low levels of irradiation while k_{inhib_j} regulates the rapidity of the decline of growth efficiency due to photo-inhibition. The coefficient F_{max} is chosen to normalize the maximum value of γ_j^I to unity. Nutrient limitation is determined by the most limiting nutrient:

$$\gamma_j^N = \min(N_{PO_4}^{lim}, N_N^{lim}),$$

where N_{PO_4},N_N denote nutrient phosphate and dissolved inorganic nitrogen. The effect of phosphate concentration on phytoplankton growth rate is represented by a Michaelis-Menten function

$$N_{PO_4}^{lim} = \frac{N_{PO_4}}{N_{PO_4} + \kappa_{PO4_j}},$$

with κ_{PO4} the half-saturation constant for phytoplankton type j with respect to the ambient concentration of phosphate. The model resolves three potential sources of inorganic nitrogen (ammonium, nitrite, and nitrate) and in our configuration phytoplankton is able to assimilate all of them. The effect of nitrogen concentration on the grow rate is modified as follows in order to reflect the inhibition of nitrate and nitrite uptake due to ammonium

$$N_N^{lim} = \frac{NO_3 + NO_2}{NO_3 + NO_2 + \kappa_{IN}} e^{-\psi NH_4} + \frac{NH_4}{NH_4 + \kappa_{NH4}},$$

where ψ introduces the mentioned inhibition and κ_{IN} is the half-saturation constant of $NO_3 + NO_2$.

Table 1 displays the values given to all described parameters together with the most relevant ones involved in zooplankton and detritus equations; further details can be found in the referred papers.

Acknowledgments. The data of this work are available upon request to the corresponding author (jcsanchez@ctima.uma.es). This study was funded by Consejería de Economía, Innovación, Ciencia y Empleo (Junta de Andalucía, Spain) under the Research Project MOCBASE (RNM-1540). JCSG was supported by a Juan de la Cierva Postdoctoral Grant (JCI-2012-13451) from the Spanish Ministry of Economy and Competitiveness. CN acknowledges a postgraduate fellowship (BES-2011-043421) from the same Ministry. The model calculations were conducted in the facilities of the Supercomputing and Bioinnovation Center of the University of Málaga. We thank the ESA for distributing the GlobColour data used in this paper. NCEP Reanalysis data were provided by the NOAA/OAR/ESRLPSD, Boulder, Colorado, USA. ASCAT data were obtained from the Centre de Recherche et d'Exploitation Satellitaire (CERSAT), at IFREMER, Plouzané (France).

References

Brandt, P., W. Alpers, and J. O. Backhaus (1996), Study of the generation and propagation of internal waves in the strait of gibraltar using a numerical model and synthetic aperture radar images of the european ers 1 satellite, *J. Geophys. Res.*, *101*(C6), 14,237–14,252.

Dutkiewicz, S., M. J. Follows, and J. G. Bragg (2009), Modeling the coupling of ocean ecology and biogeochemistry, *Global Biogeochem. Cycles*, *23*(4), n/a–n/a, doi:

10.1029/2008GB003405.

Echevarría, F., L. Zabala, A. Corzo, G. N. L. Prieto, and D. Macías (2009), Spatial distribution of autotrophic picoplankton in relation to physical forcings: the gulf of Cádiz, Strait of Gibraltar and Alborán Sea case study, *J. Plankton Res.*, *31*(11), 1339–1351.

Evans, M. A., S. MacIntyre, and G. W. Kling (2008), "internal wave effects on photosynthesis: Experiments, theory, and modeling ", *Limnol. Oceanogr.*, *53*(1), 339–353.

Follows, M. J., S. Dutkiewicz, S. Grant, and S. W. Chisholm (2007), Emergent biogeography of microbial communities in a model ocean, *Science*, *315*(5820), 1843–1846, doi:10.1126/science.1138544.

García-Gorriz, E., and M.-E. Carr (1999), The climatological annual cycle of satellite-derived phytoplankton pigments in the Alboran Sea, *Geophys. Res. Lett.*, *26*(19), 2985–2988, doi:10.1029/1999GL900529.

García-Lafuente, J., E. Bruque, J. C. Sánchez-Garrido, G. Sannino, and S. Sammartino (2013), The interface mixing layer and the tidal dynamics at the eastern part of the Strait of Gibraltar, *J. Marine Syst.*, *117-118*(0), 31–42, doi: http://dx.doi.org/10.1016/j.jmarsys.2013.02.014.

Geider, R. J., H. L. McIntyre, and T. M. Kana (1997), Dynamic model of phytoplankton growth and acclimation: responses of the balanced growth rate and the chlorophyll a: carbon ratio to light, nutrient-limitation and temperature, *Mar. Ecol. Prog. Ser.*, *148*, 187–200.

Griffies, S. M., and R. W. Hallberg (2000), Biharmonic friction with a smagorinsky-like viscosity for use in large-scale eddy-permitting ocean models, *Mon. Wea. Rev.*, *128*,

2935–2946.

Hammer, W. M., and I. R. Hauri (1981), Effects of island mass: Water flow and plankton pattern around a reef in the great barrier reef lagoon, Australia, *Limnol. Oceanogr.*, *26*, 1084–1102.

Hasegawa, D., H. Yamazaki, R. G. Lueck, and L. Seuront (2004), How islands stir and fertilize the upper ocean, *Geophys. Res. Lett.*, *31*(16), n/a–n/a, doi: 10.1029/2004GL020143.

Hernández-León, S. (1991), Accumulation of mesozooplankton in a wake area as a causative mechanism of the island-mass effect, *Mar. Biol.*, *109*(1), 141–147, doi: 10.1007/BF01320241.

Holloway, G., and K. Denman (1989), Influence of internal waves on primary production, *J. Plankton Res.*, *11*(2), 409–413.

Huertas, I. E., A. F. Ríos, J. García-Lafuente, A. Makaoui, S. Rodríguez-Gálvez, A. Sánchez-Román, A. Orbi, J. Ruíz, and F. F. Pérez (2009), Anthropogenic and natural co_2 exchange through the Strait of Gibraltar, *Biogeosciences*, *6*(4), 647–662, doi:10.5194/bg-6-647-2009.

Hundsdorfer, W., and R. A. Trompert (1994), Method of lines and direct discretization: A comparison for linear advection, *Appl. Numer. Math.*, *13*(6), 469–490, doi: http://dx.doi.org/10.1016/0168-9274(94)90009-4.

Kalnay (1996), The NCEP/NCAR 40-year reanalysis project, *Bull. Amer. Meteor. Soc.*, *77*, 437–470.

La-Violette, P. E. (1984), The advection of submesoscale thermal features in the Alboran Sea Gyre, *J. Phys. Oceanogr.*, *14*, 550–565.

Lawrence, G. A. (1993), The hydraulics of steady two-layer flow over a fixed obstacle, *J. Fluid Mech.*, *254*, 605–633.

Lazzari, P., C. Solidoro, V. Ibello, S. Salon, A. Teruzzi, K. Béranger, S. Colella, and A. Crise (2012), Seasonal and inter-annual variability of plankton chlorophyll and primary production in the Mediterranean Sea: a modelling approach, *Biogeosciences*, *9*(1), 217–233, doi:10.5194/bgd-8-5379-2011.

Leichter, J. J., G. Shellenbarger, S. J. Genovese, and S. R. Wing (1998), Breaking internal waves on a Florida (USA) coral reef: A plankton pump at work?, *Mar. Ecol. Prog. Ser.*, *166*, 83–97.

Lohrenz, S. E., D. A. Wiesenburg, I. P. DePalma, K. S. Johnson, and D. E. Gustafson (1988), Interrelationships among primary production, chlorophyll, and environmental conditions in frontal regions of the western Mediterranean Sea, *Deep-Sea Res. Oceanogr., A*, *35*(5), 793 – 810, doi:http://dx.doi.org/10.1016/0198-0149(88)90031-3.

Long, R. R. (1954), Some aspects of the flow of stratified fluids. ii. experiments with a two-fluid system, *J. Fluid Mech.*, *6*, 97–115.

Losch, M., V. Strass, B. Cisewski, C. Klaas, and R. G. Bellerby (2014), Ocean state estimation from hydrography and velocity observations during eifex with a regional biogeochemical ocean circulation model, *J. Marine Syst.*, *129*(0), 437–451, doi: http://dx.doi.org/10.1016/j.jmarsys.2013.09.003.

Macías, D., G. Navarro, F. Echevarría, C. M. García, and J. L. Cueto (2007a), Phytoplankton pigment distribution in the northwestern Alboran Sea and meteorological forcing: A remote sensing study, *J. Mar. Res.*, *65*(4), 523–543, doi: doi:10.1357/002224007782689085.

Macías, D., A. Martin, J. Garciá-Lafuente, C. García, A. Yool, M. Bruno, A. Vázquez-Escobar, A. Izquierdo, D. Sein, and F. Echevarría (2007b), Analysis of mixing and biogeochemical effects induced by tides on the AtlanticMediterranean flow in the Strait of Gibraltar through a physicalbiological coupled model, *Prog. Ocenogr.*, *74*(2-3), 252 – 272.

Maillard, C. (2002), *MEDAR/MEDATLAS: a database for Mediterranean and Black Sea projects*, 16, 115-117 pp., CIESM, IFREMER/SISMER, Centre de Brest, B.P.70, 29280 Plouzane France.

Marshall, J., C. Hill, L. Perelman, and A. Adcroft (1997a), Hydrostatic, quasi-hydrostatic, and nonhydrostatic ocean modeling, *J. Geophys. Res.*, *102*(C3), 5733–5752, doi: 10.1029/96JC02776.

Marshall, J., A. Adcroft, C. Hill, L. Perelman, and C. Heisey (1997b), A finite-volume, incompressible Navier Stokes model for studies of the ocean on parallel computers, *J. Geophys. Res.*, *102*(C3), 5753–5766, doi:10.1029/96JC02775.

Muacho, S., J. da Silva, V. Brotas, and P. Oliveira (2013), Effect of internal waves on near-surface chlorophyll concentration and primary production in the nazar canyon (west of the iberian peninsula), *Deep Sea Research Part I: Oceanographic Research Papers*, *81*(0), 89–96.

Nagai, T., A. Tandon, N. Gruber, and J. C. McWilliams (2008), Biological and physical impacts of ageostrophic frontal circulations driven by confluent flow and vertical mixing, *Dyn. Atmos. Oceans.*, *45*(3-4), 229 – 251.

Navarro, G., A. Vázquez, D. Macías, M. Bruno, and J. Ruíz (2011), Understanding the patterns of biological response to physical forcing in the Alboran Sea (western Mediter-

ranean), *Geophys. Res. Lett.*, *38*(23), n/a–n/a, doi:10.1029/2011GL049708.

Oguz, T., D. Macías, J. García-Lafuente, A. Pascual, and J. Tintoré (2014), Fueling plankton production by the meandering frontal jet in the Alboran Sea (Western Mediterranean), *PloS ONE*, *9*(11), e111,482.

Pacanowski, R. C., and S. G. H. Philander (1981), Parameterization of vertical mixing in numerical models of tropical oceans, *J. Phys. Oceanogr.*, *11*, 1443–1451.

Pan, X., G. Wong, F.-K. Shiah, and T.-Y. Ho (2012), Enhancement of biological productivity by internal waves: observations in the summertime in the northern south china sea, *Journal of Oceanography*, *68*(3), 427–437.

Ramírez, T., D. Cortés, J. Mercado, M. Vargas-Yaez, M. Sebastián, and E. Liger (2005), Seasonal dynamics of inorganic nutrients and phytoplankton biomass in the {NW} alboran sea, *Est. Coast. Shelf Sci.*, *65*(4), 654–670.

Reul, A., V. Rodríguez, F. Jiménez-Gómez, J. Blanco, B. Bautista, T. Sarhan, F. Guerrero, J. Ruíz, and J. García-Lafuente (2005), Variability in the spatio-temporal distribution and size-structure of phytoplankton across an upwelling area in the NW-Alboran Sea, (W-Mediterranean), *Cont. Shelf Res.*, *25*(5-6), 589 – 608, doi: http://dx.doi.org/10.1016/j.csr.2004.09.016.

Sánchez-Garrido, J. C., G. Sannino, L. Liberti, J. García Lafuente, and L. Pratt (2011), Numerical modeling of three-dimensional stratified tidal flow over Camarinal Sill, Strait of Gibraltar, *J. Geophys. Res.*, *116*(C12), n/a–n/a, doi:10.1029/2011JC007093.

Sánchez-Garrido, J. C., J. García-Lafuente, E. Álvarez-Fanjul, M. García-Sotillo, and F. J. de los Santos (2013), What does cause the collapse of the Western Alboran Gyre? Results of an operational ocean model, *Prog. Ocenogr.*, *116*(0), 142–153, doi:

http://dx.doi.org/10.1016/j.pocean.2013.07.002.

Sangrà, P., G. Basterretxea, J. L. Pelegrí, and J. Arístegui (2001), Chlorophyll increase due to internal waves in the shelf-break of Gran Canaria Island (Canary Islands), *Sci. Mar.*, *65*, 89–97.

Sannino, G., J. C. Sánchez Garrido, L. Liberti, and L. Pratt (2014), Exchange flow through the Strait of Gibraltar as simulated by a sigma-coordinate hydrostatic model and a z-coordinate non-hydrostatic model, in *The Mediterranean Sea: Temporal Variability and Spatial Patterns*, pp. 25–50, John Wiley and Sons, Inc., doi:10.1002/9781118847572.ch3.

Sarhan, T., J. García-Lafuente, M. Vargas, J. M. Vargas, and F. Plaza (2000), Upwelling mechanisms in the northwestern Alboran Sea, *J. Marine Syst.*, *23*(4), 317–331, doi: http://dx.doi.org/10.1016/S0924-7963(99)00068-8.

Siokou-Frangou, I., U. Christaki, M. G. Mazzocchi, M. Montresor, M. Ribera d'Alcalá, D. Vaqué, and A. Zingone (2010), Plankton in the open Mediterranean Sea: a review, *Biogeosciences*, *7*(5), 1543–1586, doi:10.5194/bg-7-1543-2010.

Spall, M. A. (1995), Frontogenesis, subduction, and cross-front exchange at upper ocean fronts, *J. Geophys. Res.*, *100*(C2), 2543–2557.

Steinacher, M., F. Joos, T. L. Frölicher, L. Bopp, P. Cadule, V. Cocco, S. C. Doney, M. Gehlen, K. Lindsay, J. K. Moore, B. Schneider, and J. Segschneider (2010), Projected 21st century decrease in marine productivity: a multi-model analysis, *Biogeosciences*, *7*(3), 979–1005, doi:10.5194/bg-7-979-2010.

Uitz, J., D. Stramski, B. Gentili, F. D'Ortenzio, and H. Claustre (2012), Estimates of phytoplankton class-specific and total primary production in the Mediterranean Sea from satellite ocean color observations, *Global Biogeochem. Cycles*, *26*(2), n/a–n/a,

doi:10.1029/2011GB004055.

Vlasenko, V., J. C. Sánchez-Garrido, N. Stashchuk, J. García-Lafuente, and M. Losada (2009), Three-dimensional evolution of large-amplitude internal waves in the Strait of Gibraltar, *J. Phys. Oceanogr.*, *39*, 2230–2246.

Wesson, J. C., and M. C. Gregg (1994), Mixing at Camarinal Sill in the Strait of Gibraltar, *J. Geophys. Res.*, *99*(C5), 9847–9878, doi:10.1029/94JC00256.

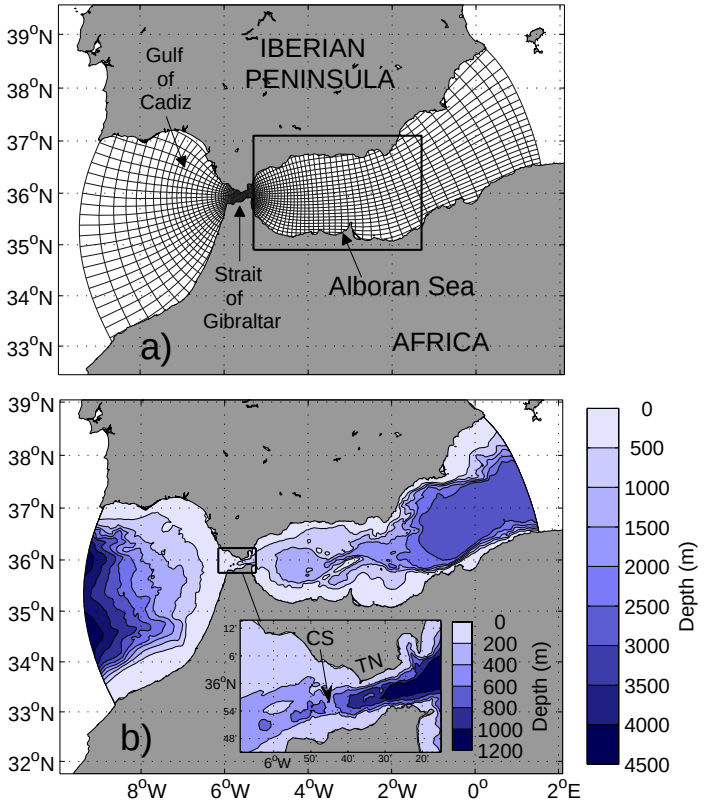

Figure 1. a) Model domain and computational grid. For the sake of clarity only one third of the total grid lines are shown. The rectangle encloses the Alboran Sea, the selected area in which some variables have been spatially averaged (see text for details). b) Model bathymetry with a zoom area of the Strait of Gibraltar displayed in the inset. Two relevant bathymetric features have been labelled: Camarinal Sill (CS), and Tarifa Narrows (TN).

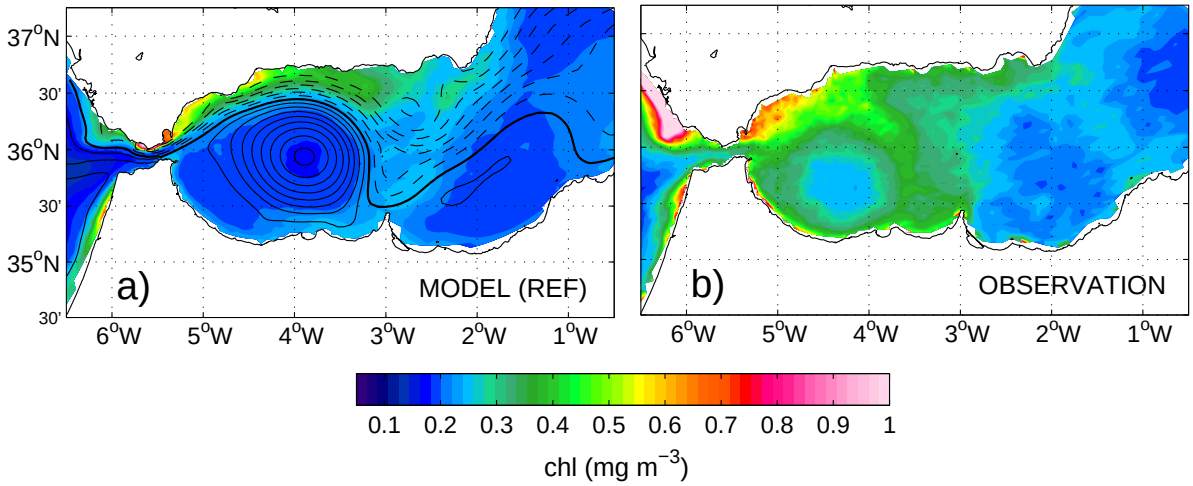

Figure 2. a) Model derived climatology of surface chl for the period 2012-2013 (REF experiment; median values). Black contours display the model mean SSH. The contour interval is 1.5 cm, with solid and dashed lines corresponding to positive and negative values, respectively. The thick solid line corresponds to SSH=0. b) Surface chl climatology derived from remote sensing images corresponding to the period 2012-2013 (median values are shown). In the computation of the climatologies, satellite data were interpolated onto the model grid and its cloud mask was applied to the model outputs for a better comparison of the two data sets.

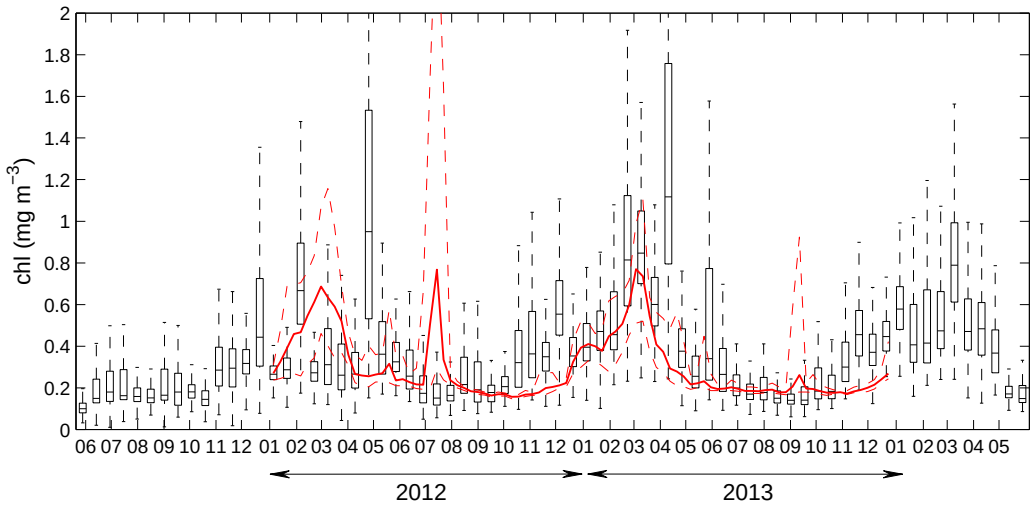

Figure 3. a) Surface chl time variability as simulated in REF. The solid red line shows the median chl value in the basin while the dashed lines are the first and third percentiles. The box-plot corresponds to satellite data described in the text. For the computation the model outputs have been interpolated onto the regular satellite grid and the corresponding cloud mask has been applied in order to make the two data sets comparable.

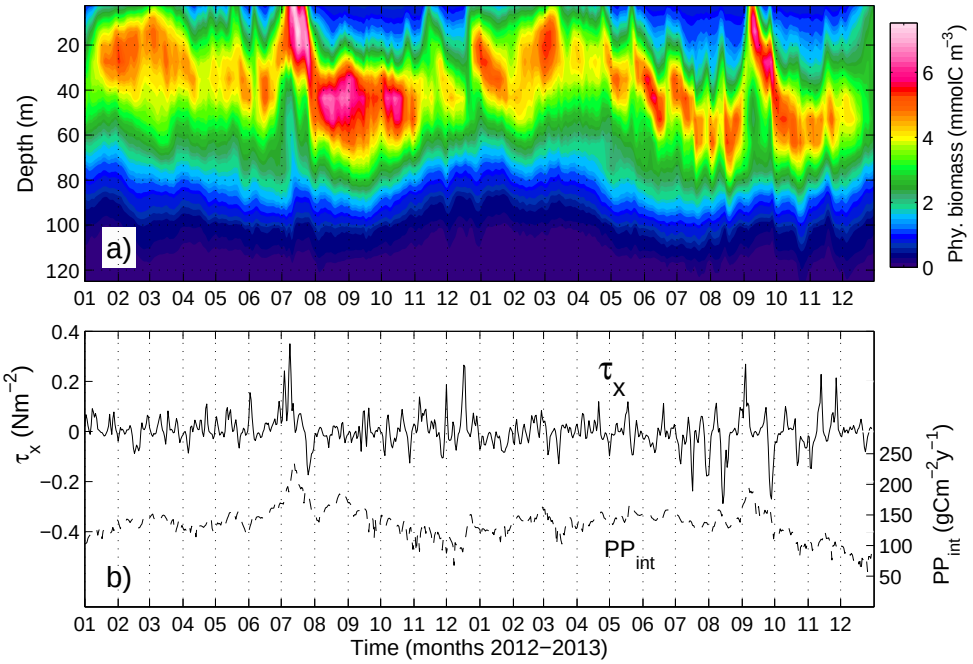

Figure 4. a) Time-depth diagram of phytoplankton biomass horizontally averaged in the Alboran Sea (REF run; see specific domain in Fig. 1). b) Spatial mean of the zonal component of wind stress (solid line; left axis) and depth-integrated primary productivity (dashed line; right axis).

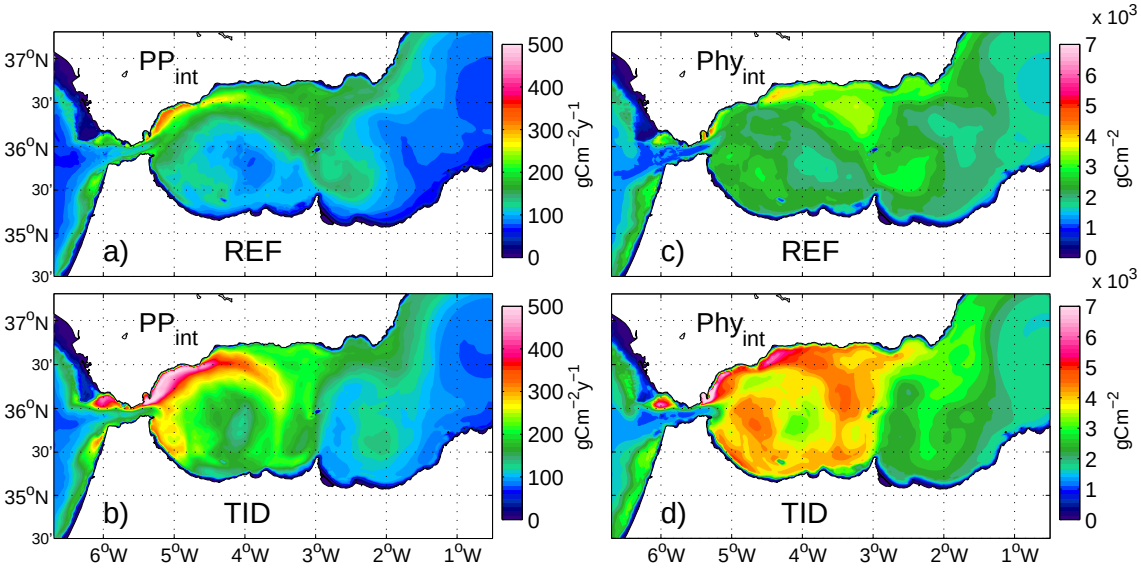

Figure 5. Mean depth-integrated primary productivity obtained in the REF (a) and TID (b) simulations (period March 15-June 1, 2013). Panels c) and d) are the depth-integrated phytoplankton biomass. The integration interval is in both cases from the sea surface to the bottom.

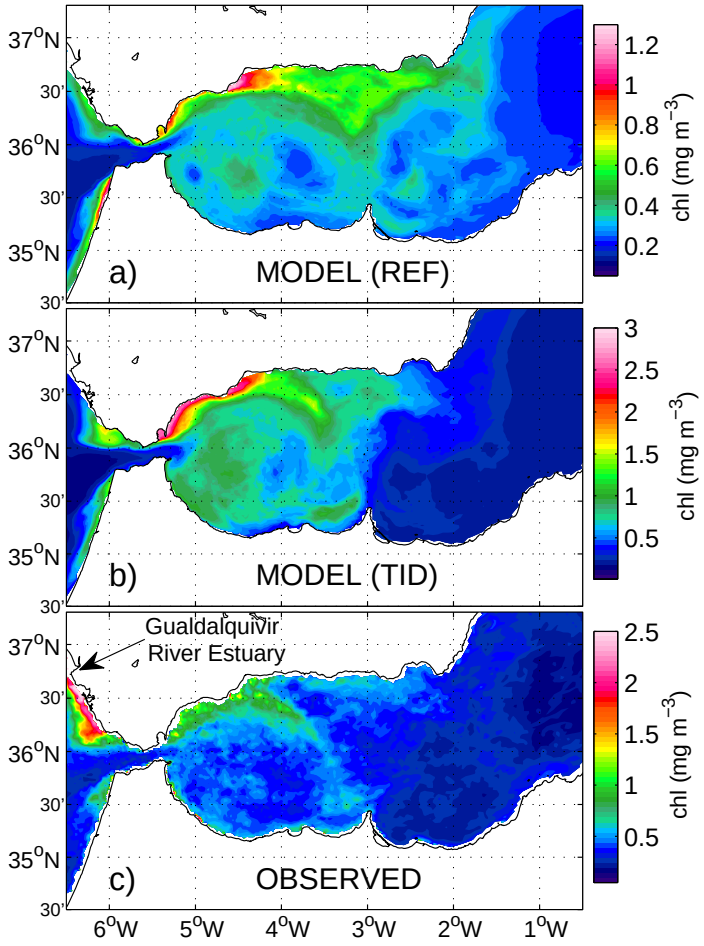

Figure 6. Median surface chl obtained in the REF (a) and TID (a) experiments for the overlapping period March 15-June 1, 2013. c) Same as a)-b) for satellite data.

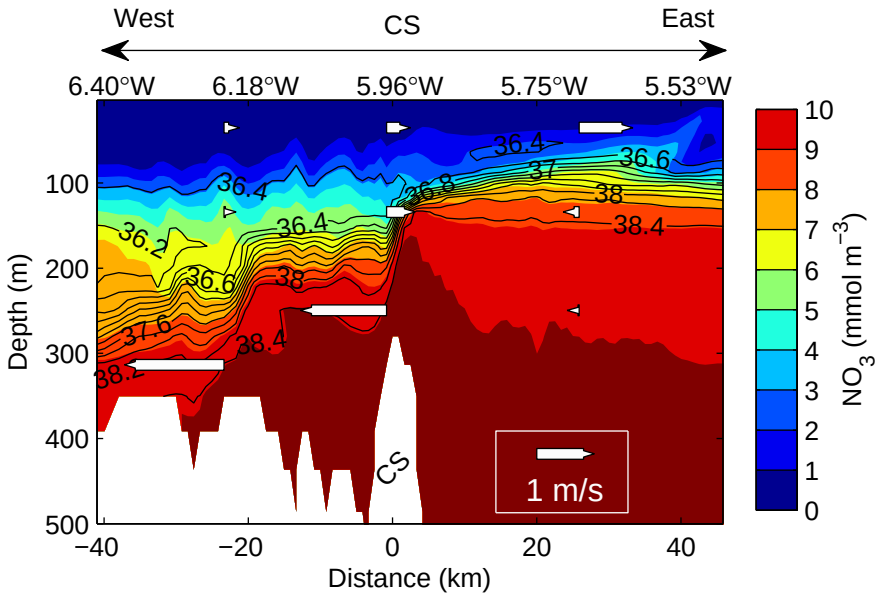

Figure 7. Vertical cross section of nitrate (color contours), salinity (line contours; contour interval is 0.2), and zonal velocity (arrows) along the central axis of Strait of Gibraltar. The fields correspond to a snapshot of the REF experiment. The bottom x-axis indicate distance from the Camarinal Sill (CS), with positive (negative) values towards the east (west) of the sill. The top x-axis indicates longitude.

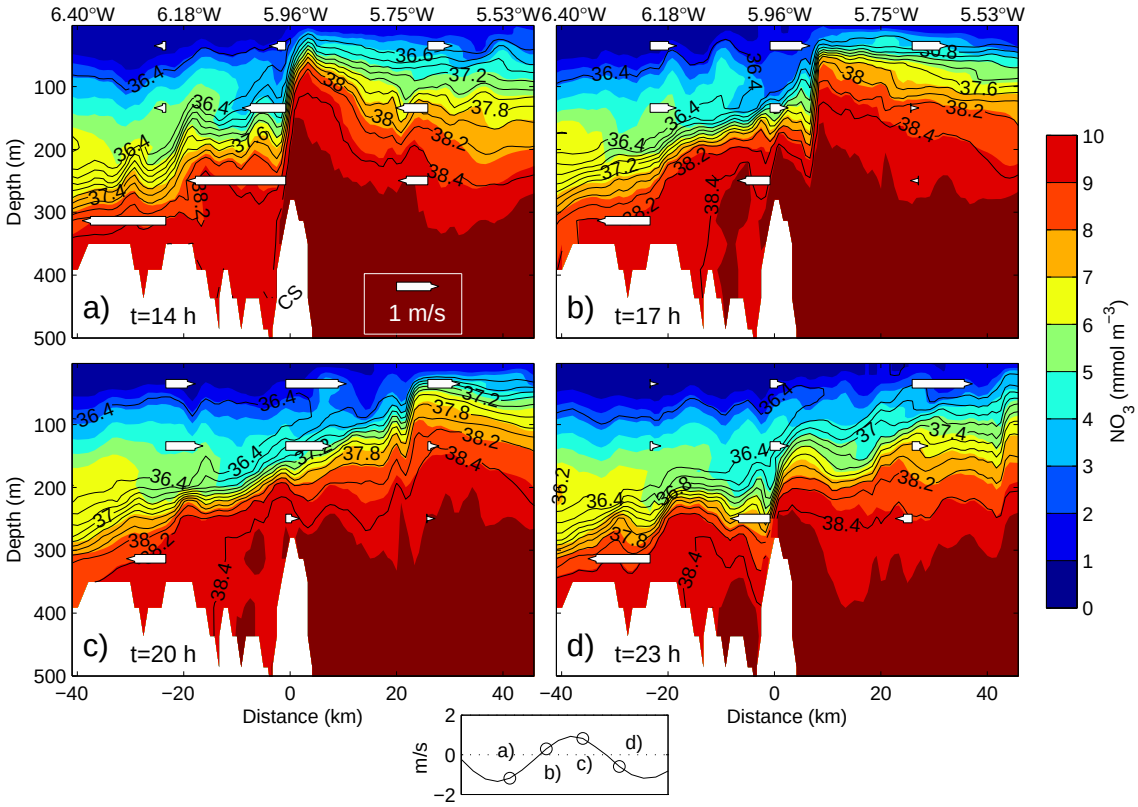

Figure 8. Same as Fig. 7 for a tidal cycle of the TID simulation. Time increases from panels a) to d) with a time interval of 3 hours. Time is given in hours from March 15th 2013. The bottom axis displays the batrotropic (depth-integrated) velocity over the Camarinal Sill.

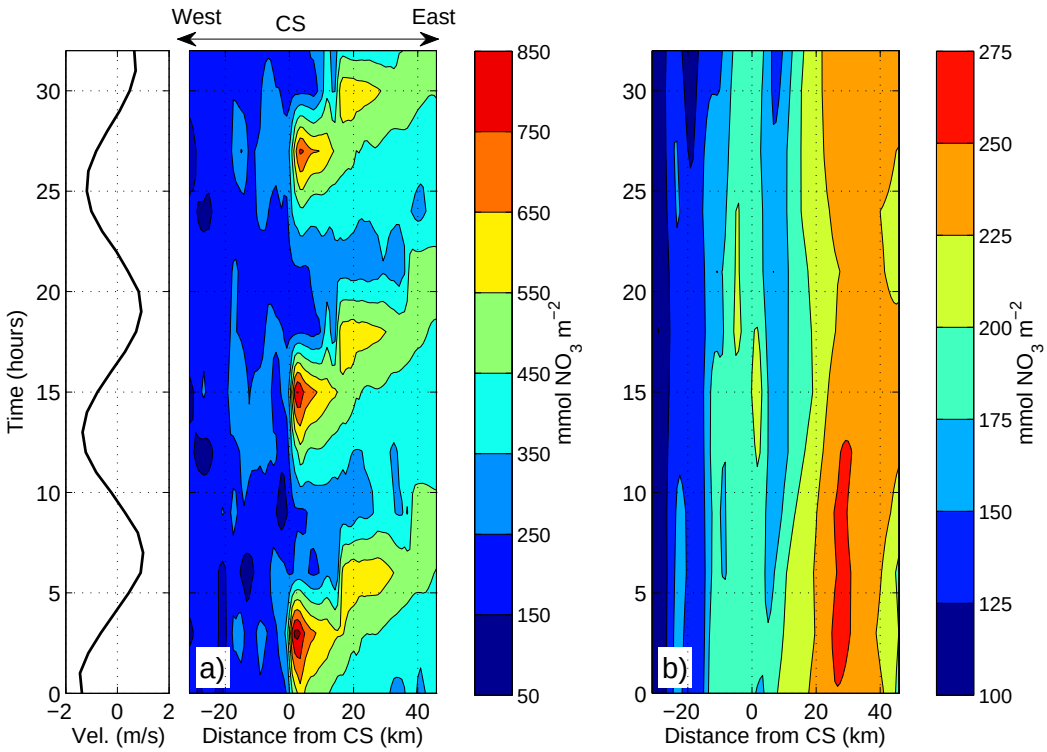

Figure 9. Temporal and spatial dependence of the depth-integrated nitrate along the central axis of the Strait of Gibraltar. Nitrate concentration is integrated from z=-94 to z=0, $\int_{-94}^{0} \mathrm{NO_3}\, dz$. Panel a) corresponds to the TID run, with the leftmost axis showing the batrotropic (depth-integrated) velocity over the Camarinal Sill, while b) corresponds to the REF run. Time is given in hours from March 15th 2013.

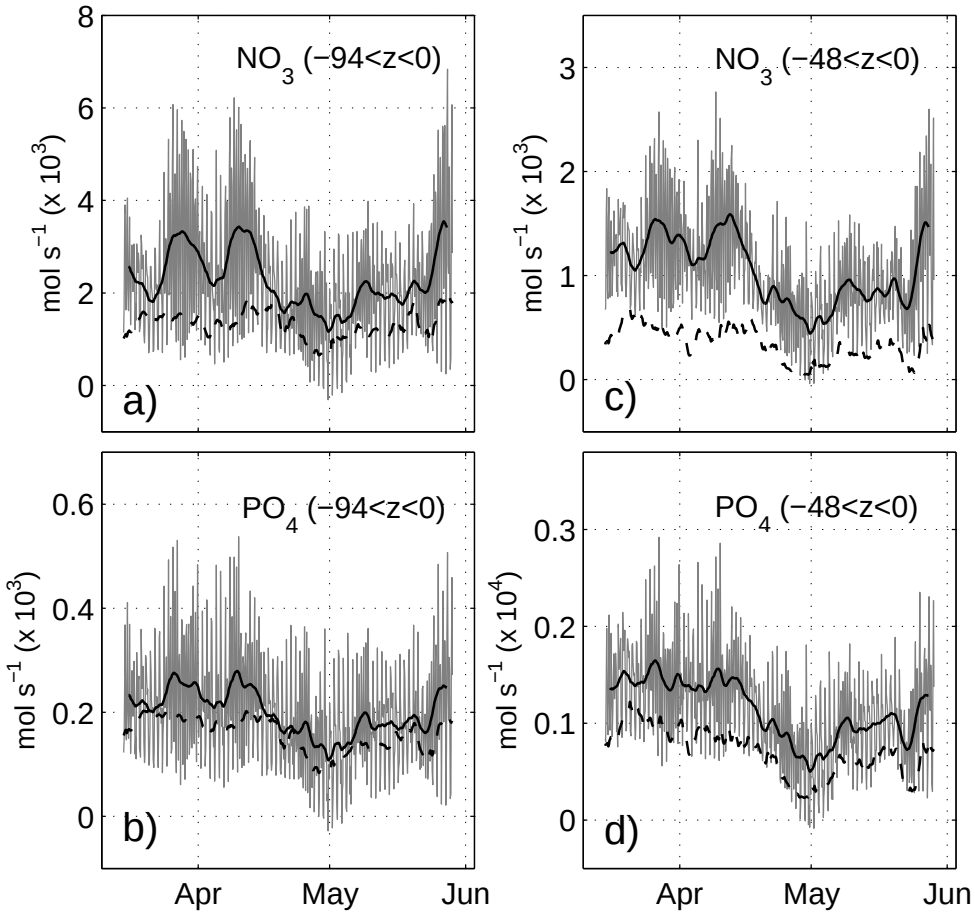

Figure 10. a) Nitrate transport at the eastern end of the Strait of Gibraltar ($x = 40$ km in Fig.7) as simulated in the TID (gray line; 3-hourly data) and REF (black dashed line) runs. The black solid line if the low-pass TID series (tidal variability removed). The transport is computed in the first 94 m of the water column, roughly encompassing the inflowing Atlantic layer. b) same as a) but with the transport computed in the first 48 m of the water column. c) and d) and as a) and b) but for phosphate.

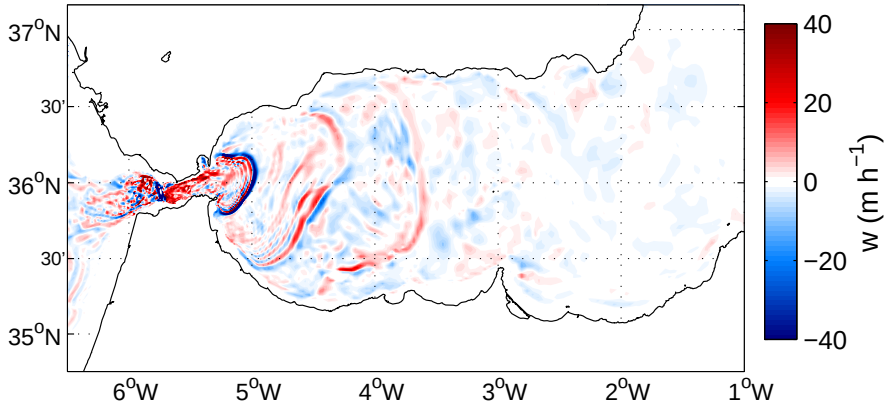

Figure 11. a) Synoptic field of vertical velocity at $z = -88.5$m, as simulated in the TID experiment.

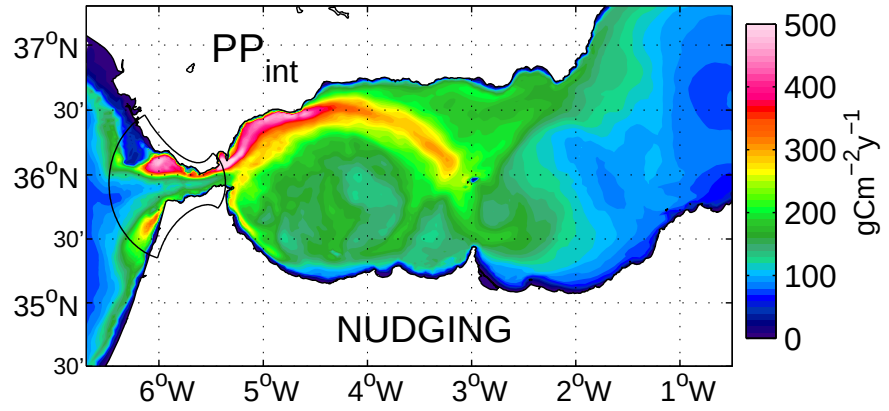

Figure 12. Mean depth-integrated primary production obtained in the nudging experiment. The polygon around the Strait of Gibraltar encloses the area where the nudging term described in the text has been applied.

Parameter	Symbol	Value	Units
Maximum growth rates	μ_{max_1}, μ_{max_2}	2.5, 1.4	d^{-1}
Phytoplankton mortality rates	m_1^p, m_2^p	$0.1, 0.1$	d^{-1}
Phytoplankton sinking rates	w_1^p, w_2^p	$0.5, 0$	$\mathrm{m\,d}^{-1}$
Phosphate half-saturation const.	$\kappa_{PO4_1}, \kappa_{PO4_2}$	$3.5 \cdot 10^{-2}, 1.5 \cdot 10^{-2}$	μM P
Nitrate+Nitrite half-saturation const.	$\kappa_{IN_1}, \kappa_{IN_2}$	$0.56, 0.24$	μM N
Ammonium half-saturation const.	$\kappa_{NH4_1}, \kappa_{NH4_2}$	$0.28, 0.12$	μM N
Ammonium inhibition	ψ	4.6	$(\mu\mathrm{M\ N})^{-1}$
PAR saturation coeff.	k_{par_1}, k_{par_2}	$1.2 \cdot 10^{-2}, 1.2 \cdot 10^{-2}$	$(\mu\mathrm{Ein\ m}^{-2}\mathrm{s}^{-1})^{-1}$
PAR inhibition coeff.	k_{inhib_1}, k_{inhib_2}	$10^{-3}, 6 \cdot 10^{-3}$	$(\mu\mathrm{Ein\ m}^{-2}\mathrm{s}^{-1})^{-1}$
Temperature curve coeff.	A	1.04	
Temperature normalization coeff.	τ_1, τ_2	3, 0.3	
Zooplankton mortality rate	m^z	$3.3 \cdot 10^{-2}$	d^{-1}
Maximum grazing rates	g_{max_a}, g_{max_b}	$0.2, 3.3 \cdot 10^{-2}$	d^{-1}
Grazing half-saturation const.	K^p	0.1	μM P
DOM remineralization rates	r_{DOP}, r_{DON}	$10^{-2}, 10^{-2}$	d^{-1}
POM remineralization rates	r_{POP}, r_{PON}	$2 \cdot 10^{-2}, 2 \cdot 10^{-2}$	d^{-1}
POM sinking rate	w_{POM}	10	$\mathrm{m\,d}^{-1}$

Table 1. Ecosystem model parameters and given values. Subscripts 1 and 2 refers to different phytoplankton species.

VI. Mediterranean waters along and across the Strait of Gibraltar, characterization and zonal modification.

Cristina Naranjo[(1)], Simone Sammartino[(1)], Jesús García-Lafuente[(1)], María J. Bellanco[(2)], Isabelle Taupier-Letage[(3)].

[(1)] Grupo de Oceanografía Física, Universidad de Málaga, 29071 Málaga, Spain

[(2)] Centro Oceanográfico de Cádiz, Instituto Español de Oceanografía (IEO), 11006 Cádiz, Spain.

[(3)] Aix Marseille Université, CNRS, Université de Toulon, IRD, MIO UM 110, Antenne de la Seyne, 83507 La Seyne, France

Abstract

Hydrological data collected in the Strait of Gibraltar have been used to examine the distribution and spatial-temporal evolution of the water masses in the area. The spatial variability has been addressed by means of a clustering method that determines the affinity of a collection of Temperature-Salinity samples to one of the water masses involved in the exchange. The method, which has been applied to a nearly-synoptic data set, highlights the clear evolution of the Mediterranean Waters as they flow westward through the Strait. While up to four different Mediterranean Waters are spatially distinguishable east of the main sill of Camarinal in the Strait, most of their differentiating characteristics are eroded after flowing over this restrictive topography due to mixing. West of the sill, therefore, speaking of a unique Mediterranean Water seems more appropriate. The same applies to the North Atlantic Central Water flowing in the opposite direction, which is noticeably modified along its path to the Mediterranean Sea, most of its transformation taking place in the Camarinal sill surroundings. A series of repeated transects carried out in the eastern and western sides of the Strait, provided a temporal analysis of the water masses evolution: the temporal variability manifests seasonality in the surface waters, while interannual signal is mainly detected in the deeper water masses. It is worth remarking the statistically significant positive trend of Western Mediterranean Deep Water (0.009ºC/year) and Winter Intermediate Water (0.03ºC/year), with the latter showing also intermittent occurrence in the Strait.

Keywords:

Strait of Gibraltar, Mediterranean outflow, water masses, cluster analysis.

1. Introduction

In the Mediterranean Sea (MedS, hereinafter) the Atlantic Water (AW) that flows in through the Strait of Gibraltar (SoG) is modified by evaporation and transformed into Mediterranean water, saltier and denser, which ends up flowing out through the SoG to the Atlantic Ocean. A simplified Mediterranean basin is schematized by an eastern and a western basins connected by the Strait of Sicily. In the eastern basin, Levantine Intermediate Water (LIW) is formed through open-sea convection. In the western basin, more specifically in the Gulf of Lion, Western Mediterranean Deep Water (WMDW) is formed by deep convection. It was known since long ago that the LIW was a permanent contributor to the outflow. However, the possibility that the WMDW was participating significantly in the outflow was first presented by Stommel et al. (1973), who attributed its presence to the Bernouilli aspiration of this water from great depth in the MedS over the main sill of Camarinal in the SoG. Subsequently, other authors have revisited the topic and stressed this thought [*Bryden and Stommel*, 1982; *Gascard and Richez*, 1985; *Whitehead*, 1985; *Kinder and Parrilla*, 1987; *Kinder and Bryden*, 1990; *Millot and Taupier-Letage*, 2005; *J. García Lafuente et al.*, 2007; *Naranjo et al.*, 2012; *Naranjo et al.*, 2014] At present, it is accepted that this deep water is a permanent part of the outflow.

Studies dealing with the outflow within and nearby the SoG used to focus on the two main Mediterranean Waters (MWs hereinafter), the LIW and the WMDW [*Pettigrew*, 1989; *Bray et al.*, 1995; *J. García Lafuente et al.*, 2007], which are easily identified by the maximum and minimum potential temperature, respectively, in the densest part of the θ-S diagram [*Gascard and Richez*, 1985]. Recent efforts made to clarify the hydrological characteristics of the water masses leaving the MedS through the SoG have suggested the presence of other Mediterranean water masses, more specifically, the Tyrrhenian Dense Water (TDW) and the Winter Intermediate Water (WIW) [*Rhein et al.*, 1999; *Millot et al.*, 2006; *Millot*, 2009, 2014b, a]. The first is formed by the mixing of old WMDW residing in the Tyrrhenian Sea with newly entered LIW flowing into the western MedS through the Strait of Sicily [*Rhein et al.*, 1999; *Millot et al.*, 2006]. The WIW is seasonally formed by convection of cooled modified Atlantic Water under severe winter condition along the continental shelf of the Liguro-Provençal sub-basin and Catalan Sea [*Conan and Millot*, 1995; *Vargas-Yáñez et al.*, 2012]. At its source, it is the coolest water in the Western MedS [*Salat and*

Font, 1987; *Lopez Jurado et al.*, 1995; *Millot*, 1999] and it is easily detected in any θ-S diagram by a minimum of potential temperature between potential density anomaly σ_θ=28.0 and σ_θ=29.0 [*Millot*, 2014a]. The volume of formed WIW has been reported to show marked interannual fluctuations [*Pinot et al.*, 2002; *Monserrat et al.*, 2008], the case of no formation being non-discardable [*Pinot et al.*, 2002; *Ribó et al.*, 2015].

These MWs are rather well differentiated (when present) at the eastern side of the SoG [*Fuda et al.*, 2000; *Millot*, 2009], but the question remains as whether or not they are still distinguishable at the western part of the SoG once the Mediterranean outflow has crossed the Camarinal sill. The reason behind this noticeably different spatial distribution of the water masses in both halfs of the SoG (East-West) is the outstanding tidal dynamics in the area [*Candela et al.*, 1990; *Bryden et al.*, 1994; *García-Lafuente et al.*, 2000; *J. García Lafuente et al.*, 2007], which is strongly enhanced in the surrondings of Camarinal sill and westwards of it [*Wesson and Gregg*, 1994; *J. C. Sánchez Garrido et al.*, 2008; *J.C. Sánchez Garrido et al.*, 2011].The barotropic tidal currents interact with the SoG's topography, mainly with Camarinal sill, to produce a remarkable internal tide [*Candela et al.*, 1990; *Bryden et al.*, 1994; *García-Lafuente et al.*, 2000] that in turn gives rise to dissipation rates that are amongst the highest found in the world ocean [*Wesson and Gregg*, 1994]. The supercritical-to-subcritical flow transitions at the different critical (in hydraulic sense) sections, that happen not only in Camarinal sill but also oceanwards of it at specific times of the tidal cycle, drive that enhanced mixing [*J.C. Sánchez Garrido et al.*, 2011; *Jesús García Lafuente et al.*, 2013], which is the responsible for the fading out of the water masses identities in the western half of the SoG.

On the other hand, *Millot* [2014a], using schematic mixing lines in the Mediterranean zone of a θ-S diagram, has proposed that the four MWs can be still detected as far as at 6º 15' W to the West of the main sill and, even, traced along the Gulf of Cadiz in the Atlantic Ocean. This stand point differs from the widespread view of a Mediterranean Water that exits the SoG as a rather well mixed plume with typical properties of θ~13ºC and S~38.4 [*M Baringer*, 1993; *M O N Baringer and Price*, 1997] in which the different MWs water masses are not discernable.

With the aim of provide a clear and standardized method to classify the water masses in the SoG, this work proposes a statistical method to automatically classify every water mass involved in the exchange. Two sets of data, described in Section 2, were specifically collected in the SoG area

to address the topic. The first dataset was acquired during the Gibraltar International Campaign (GIC, Section 2.1) and the second one throughout the lifespan of the INGRES projects (Section 2.2) funded by the Spanish Government. Section 3 describes the data processing, paying special attention to the description of the proposed method of analysis (Section 3.2). The hydrological information contained in these two sets of data has been exploited in different ways in this study. GIC data were collected during a very short period and allow us to make a quasi-synoptic description of the water masses distribution in the SoG. On the contrary, INGRES data gather samples spanning a rather long period of time and have the potential of addressing the time variability and evolution of the water masses. Section 4 discusses both topics in Subsections 4.1 (GIC) and 4.2 (INGRES) respectively. Finally, Section 5 summarizes the findings and conclusions of the study.

2. Data

2.1. CTD and MVP data from Gibraltar International Campaign

In the framework of the international Hydrochanges programme sponsored by the Commission Internationale pour l'Exploration Scientifique de la Méditerranée (Mediterranean Science Commission, CIESM) and supported by the HyMeX programme, the French *Mediterranean Institute of Oceanography* carried out the *Gibraltar International Campaign* on board the R/V Tethys II from the 4th to the 6th July 2012. The cruise was aimed at obtaining high resolution Conductivity-Temperature-Depth (CTD) profiles along the transects showed in Figure 1 in order to give an accurate water mass characterization and distribution of Mediterranean waters within the SoG. Except for section R5, a Moving Vessel Profiler (MVP) was employed; this instrument allows semi-autonomous sampling of the water column with very high spatial resolution (horizontal averaged resolution is 500m while vertically resolution is 1m). A drawback of the MVP is its limited range depth (~350m). Transect R5 and a repetition of transect R2 were sampled with a CTD probe (SBE 911plus CTD, sampling frequency of 24Hz) that reached the seafloor. The CTD vertical profiles in these transects, however, are substantially further apart than MVP profiles (typical distance between casts ranging from 1 to 3 Km).

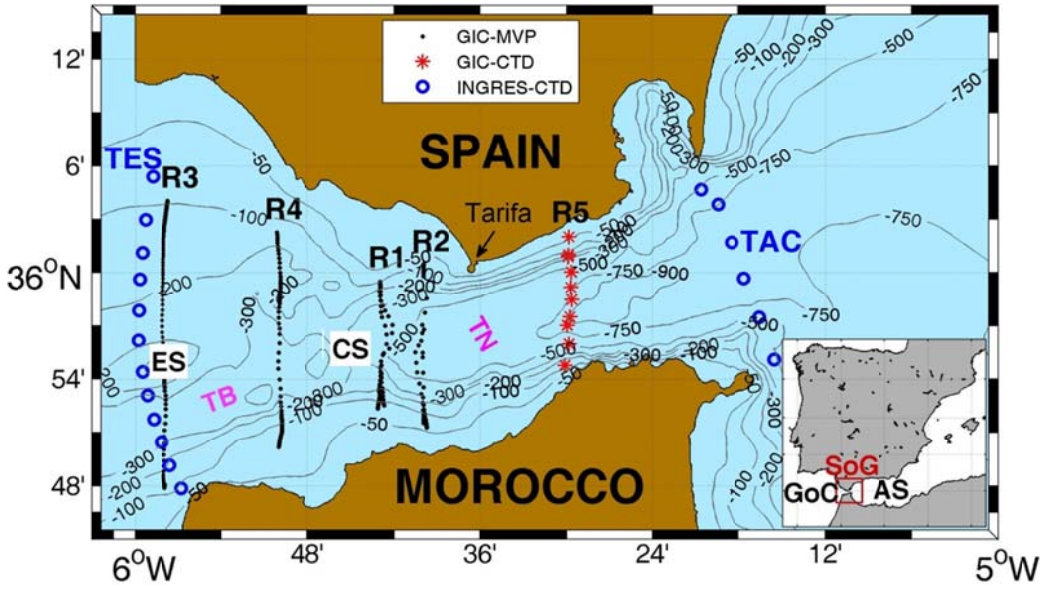

Figure 1. Map of the Strait of Gibraltar showing bathymetric contours, in meters. The black dots and red asterisks indicate the location of the vertical profiles along the 5 sampled sections for MVP and CTD data in GIC campaign (R1-R5), respectively. Blue circles represent the two CTD sections regularly repeated in the INGRES project (TAC and TES). The main sills of Espartel (ES) and Camarinal (CS), the small Tangier Basin (TB) between them and the Tarifa Narrows (TN) are also indicated. The inset shows the location of the Strait (SoG) between the Alboran Sea (AS), the westernmost basin of the Mediterranean Sea, and the Gulf of Cadiz (GoC) in the Atlantic Ocean.

2.2. Historical CTD data from INGRES project

The INGRES projects were initiated in 2004 with the objective of monitoring the Mediterranean outflow and its variability in response to subinertial and longer-term forcing as well as the hydrological properties of the densest and, hence, deepest Mediterranean water leaving the MedS. At the time of this study the monitoring, which is planned to be kept on position *sine die*, is still in progress. Whenever the station was serviced (every 4 or 6 months) and weather permitting, CTD transects were accomplished. Among them, transects labeled TES and TAC in Figure 1 have been repeatedly sampled during the lifespan of INGRES projects. They make up an unevenly distributed time series since the meteorological conditions often prevented the accomplishment of one or both transects. Overall, TES was sampled 15 times and TAC 12 times (details about the dates when these transects were collected are shown in Table 1).

TAC, located at the eastern entrance of the SoG, is the last MedS transect where the MWs may be found as unmixed as in the interior of the Alboran Sea, the westernmost basin of the MedS. Further west, the enhanced turbulence associated with the tidal dynamics and the very hydrodynamics of the exchange [*Wesson and Gregg*, 1994; *J.C. Sánchez Garrido et al.*,

2011] favours the mixing and erodes the specific θ-S characteristics of the different MWs participating in the outflow. The TES transect on the other hand lays along the western boundary of the SoG and represents its last gateway for the MWs before they plunge down into the Gulf of Cádiz and the Atlantic Ocean.

INGRES DATA																
TES	2005	2007	2008		2011			2012		2013		2014				
	Feb	*Oct*	*Mar*		*Mar*	*Ago*	*Sep*	*Ago*	*Oct*	*Jun*	*Sep*	Mar	Jun	Oct	Dec	
TAC		2009	2010		2011			2012		2013		2014				
		Jun	*Jul*	*Nov*	*Ago*		*Nov*	*Ago*	*Nov*	*Jun*	*Sep*	*Apr*		*Oct*		

Table 1. Data from the INGRES project were collected unevenly spaced in time, this table summarizes the details of the dates when each transect presented in this work was carried out.

3. Methodology

3.1. Definition of Water masses in the Strait of Gibraltar.

Beside the four MWs that can be detected in the outflow (LIW, WIW, TDW and WMDW), two AWs, the Surface Atlantic Water (SAW) and North Atlantic Central Water (NACW) shape the inflow. Therefore, a total of six water masses may be involved in the exchange. In order to provide the necessary inputs for the cluster analysis (Section 3.2), all of them have to be defined by certain hydrological characteristics that locate them in the θ-S diagram. This identification is a necessary step to quantify their influence, importance, and distribution in the SoG.

There is no general agreement about the values characterizing each water mass. Table 2 summarizes the information coming from different sources, which differs slightly from one another due to the marked spatial and time variability in the SoG. Along with this information, Table 1 shows the θ-S characteristics assigned to each of the six water masses in this study. These reference values have been selected specifically for the data set analysed in this work, after the observation of the θ-S diagram of the whole GIC and INGRES casts (Figure 2). Despite being inside the range mentioned in the literature, the chosen values are subjective. However, the important issue for our study is to maintain unaltered these values when analysing the different CTD transects in order to have the outputs of the analysis comparable.

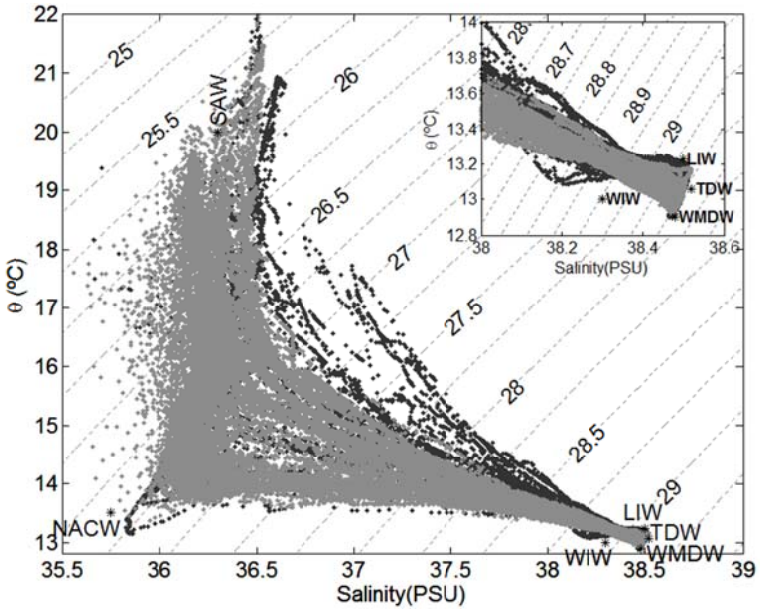

Figure 2. *θ-S* diagram of the whole data set (*GIC* data in grey, *INGRES* data in black). The locations of the water masses defined by the thermohaline properties showed in Table 1 are marked by stars, with their acronyms aside. The inset is a zoom of the Mediterranean Water zone of the diagram.

The noticeable seasonality of the SAW [*Bray et al.*, 1995] caused by the heat exchange with the atmosphere coerced us to define two different θ values for this water mass, depending on when the measurements were collected (see Table 1). In summer months, the potential temperature representing this water was set to 19.7ºC. If the maximum temperature found in the sampling exceeded 19.7 ºC, this maximum replaced the θ=19.7ºC reported in Table 1.

Water mass	Author		θ (°C)	Salinity (PSU)
SAW	[*Bray et al.*, 1995]		15.9 – 22.7	36.2 - 36.5
	[*Criado-Aldeanueva et al.*, 2006]		16	36.4
	GIC&INGRES	*March to June*	17	36.3
		July to November	19.7	36.3
NACW	[*Bray et al.*, 1995]		12.7 - 13.3	35.7 – 35.8
	[*Criado-Aldeanueva et al.*, 2006]		11-17	35.6 - 36.5
	GIC&INGRES		13.5	35.75
LIW	[*Smith et al.*, 2008]		> 13.2	38.45 - 38.75
	[*Font*, 1987]		13.3	38.5
	[*Parrilla and Kinder*, 1987]		13.15 - 13.25	38.47 - 38.51
	[*Millot*, 1999]		13.2 - 14.0	38.5 - 38.7
	[*J. García Lafuente et al.*, 2007]		13.22	38.56
	GIC&INGRES		13.23	38.50
WMDW	[*Bray et al.*, 1995]		12.8 – 12.9	38.4 – 38.5
	[*Salat and Font*, 1987]		12.75 - 12.9	38.4 - 38.48
	[*Parrilla et al.*, 1986]		13.15 - 13.25	38.47 - 38.51
	[*Fuda et al.*, 2000]		12.70 - 13.03	38.40 - 38.50
	[*J. García Lafuente et al.*, 2007]		12.80	38.45
	GIC&INGRES		12.90	38.48
WIW	[*Vargas-Yáñez et al.*, 2002]		12.5 – 13.0	38.1 - 38.3
	[*Smith et al.*, 2008]		12.821	37.9 - 38.1
	[*Salat and Font*, 1987]		12.5 - 13.0	38.1 - 38.3
	[*Ben Ismail et al.*, 2014]		<13.8	39.9 - 38.2
	[*Ribó et al.*, 2015]		12.7	38.1
	GIC&INGRES		13	38.3
TDW	[*Millot*, 2009]		13.0 - 13.1	38.48 - 38.51
	[*Santinelli et al.*, 2008]		12.8–13.1	38.44-38.58
	GIC&INGRES		13.06	38.52

Table 2. Historical values of the hydrological characteristics of the six water masses involved in the exchange through the SoG. Shaded rows highlight the pair of values used in this work.

3.2. Classification of the water masses: cluster analysis.

3.2.1 The cluster analysis

The cluster analysis is a mathematical tool used in this work to assess the presence and prevalence of each of the water masses in the different transects sampled in GIC and INGRES datasets. The cluster analysis is a multivariate method that aims at classifying samples on the basis of a set of measured variables. The method separates the dataset into groups, called clusters, each cluster including samples that are more similar to each other than to the items located into another cluster, according to a given criterion.

After an initial classification of the samples (a first guess, defined by the user in the present case), the inter-cluster and intra-cluster variance is calculated, and a new distribution of the samples is proposed, which has to maximize (minimize) a certain metric that define the similarity (dissimilarity) within (between) the clusters. The algorithm iterates until it converges. The technique has been widely used to classify hydrographical datasets [*Kim et al.*, 1991; *Hur et al.*, 1999; *Warn-Varnas et al.*, 2005]. Classical clustering tends to give clusters with similar shape [*Yan*, 2005] and the method is especially appropriate to discriminate water masses with similar salinity and temperature variance. Unfortunately, this is not the case in the SoG, where MWs range much more in temperature than in salinity and AWs are largely variable in temperature, as was already remarked regarding the SAW. This drawback has been overcome by including the potential density anomaly (σ_θ) in the hydrological properties of each water mass, which is computed directly from the sea water state equation. The addition of this new variable makes the model more robust, since a water particle with the same θ-S distance to the centroid of two clusters will finally be linked to the one with more similar σ_θ, which is of concern for the isopycnal mixing taking place between the different MWs whose densities are almost the same. This inclusion hardly affects the prevailing diapycnal mixing between MWs and the overlying AWs.

Shaded rows in Table 2 and symbols in Figure 2 give the θ-S pairs for each of the six defined water masses, which are the centroids of the clusters. While NACW, LIW, WMDW, WIW and TDW have fixed θ-S and, hence, σ_θ values, the θ of the SAW changes depending on the time of the year. Another remark concerns the WIW: due to its intermittency, this water mass may or may not be detected in the SoG. For instance and according to the zoom in the inset of Figure 2, no traces of WIW were detected during the GIC campaign since the θ-S dots do not deviate towards the WIW centroid. In these cases, WIW must not be included in the cluster analysis. Thus, previously to carry out the analysis, each CTD cast is carefully inspected to detect the WIW and in case that a convincing evidence of its presence is not found, this water mass is excluded from the analysis of the cast in order to avoid the distortion of the results.

The metric employed to calculate the similarity between the observation and the cluster is the squared Euclidean distance

$$D_{o,c} = \sum_{i=1}^{n} \left(\vec{P}_n(i) - \vec{P}_c(i) \right)^2 \qquad [1]$$

$$P_n(i) = \frac{P_o(i) - \overline{P_o(i)}}{P_{max}(i) - P_{min}(i)} \qquad [2]$$

where $D_{o,c}$ is the distance between a sample at a given longitude, latitude and depth, denoted by the vector $\vec{P}_n(\theta, S, \sigma_\theta)$, and a cluster centroid, denoted by the vector $\vec{P}_c(\theta_c, S_c, \sigma_{\theta c})$, which represents a certain water mass. The θ-S-σ_θ variables and the cluster centroid have been previously normalized following [2]. Sub-index "o" denotes the observed value, while "n" designate the normalized variable. "P_{max}" and "P_{min}" are the maximum and minimum observed value of the i variable. Index i stands for the i-th variable of the sample (or cluster vector), thus $n = 3$ in eq. [1].

The fraction of a given water mass in a given sample "o", F_{o,c_j}, is determined by

$$F_{o,c_j} = \frac{D_{o,c_j}^{-1}}{\sum_{j=1}^{m} D_{o,c_j}^{-1}} \qquad [3]$$

using the distance D_{o,c_j} of the sample to the centroid of cluster j ($j = 1, \ldots, m$). Distances have been normalized ($\sum_{j=1}^{m} D_{o,c_j} = 1$) to have all them lying between 0 and 1. Index *m* is the number of cluster in the analysis, which can be 6 or 5 depending on whether or not WIW is included.

3.2.2 Sensitivity of the method

As long as the method to classify the samples in clusters depends on the cluster centroids, and so, on the definition of the water masses, its sensitivity must be tested. This will be achieved by computing the percentage of samples (measurements) that change from one cluster to another when the centroid is slightly modified.

Table 3 shows the sensitivity analysis for transect R2 (see Figure 1) when the θ of the LIW was modified between 13.196-13.264 ºC, a 20% of the maximum difference for the TDW potential temperature, which is its nearest water mass.

The number of samples that were removed from their initial cluster does not reach the 5% in the worst case, which corresponds to θ_{LIW} decreasing by 0.034 ºC (first row in Table 2). In this case, LIW cluster increases at the expense of WMDW and TDW, thus removing samples near equally. On the contrary, when θ_{LIW} is raised from its chosen reference, nearly all samples leaving LIW go to WMDW cluster while a smaller proportion moves toward the TDW cluster, and a negligible portion moves from NACW to LIW. Overall, Table 3 supports the robustness of the method, as no significant changes occur if the centroids are moved within a realistic range. Similar tests have been carried out by moving other centroids with the same results.

$\Delta\theta_{LIW}$	Samples modified (%)	WMDW to LIW (%)	TDW to LIW (%)	LIW to TDW (%)	LIW to WMDW (%)	NACW to LIW (%)
-0.034	4.77	2.14	2.63	0	0	0
-0.019	2.44	1.44	1	0	0	0
-0.004	0.64	0.46	0.18	0	0	0
+0.011	1.40	0	0	0.37	1	0.03
+0.026	2.17	0	0	0.46	1.68	0.03

Table 3. Sensitivity analysis of the clustering algorithm when the θ assigned to the LIW centroid is slightly changed. The variation of θ corresponds to 20% of the difference between θ_{LIW} and the nearest water mass to LIW, θ_{TDW}. The first column shows the variation of LIW temperature over its assigned value of θ=13.23ºC. The second column shows the percentage of samples that changed membership from one cluster to another. Columns third to seventh specify the implied clusters in the new distribution. The sum of these four columns has to coincide with column two.

Regardless of the accuracy of the θ-S pairs defining each cluster centroid and as long as the paper is comparing data collected in the same region with the aim of investigating the spatial-temporal variability of the water masses, the key issue is to maintain the same centroids throughout the analysis. Even when the exact proportions of the involved water masses depend slightly on the centroids choice, their relative variations from place to place and/or from time to time will be representative of the investigated variability.

4. Results

4.1. GIC dataset

The tidal variability in the SoG, subdued by semidiurnal frequencies, makes the water masses pattern be dependent on the time of the tidal cycle when the transect was accomplished [*J. García Lafuente et al.*, 2007] and the tidal phase during which the sampling was carried out must be specified for each transect. This information is provided by the sea level oscillation in Tarifa (see Figure 1). In this regard, it is interesting to remind that the barotropic semidiurnal tide in the SoG behaves like a standing wave [*García-Lafuente et al.*, 2000; *J. García Lafuente et al.*, 2007] and that the tidal flow goes westwards during the rising tide (low to high water, or flood tide) and eastwards during the falling tide (high to low water, or ebb tide). On the other hand, the GIC sampling was accomplished during a relatively short period of time (4th to 6th of July, 2012). In some sense, the observations are synoptic for lower frequency fluctuations (subinertial or seasonal/interannual variability) and they should reflect the water mass composition in the SoG during that period of time, despite the tidal variability.

The results of the analysis of the GIC transects are presented from east to west in Figure 3 and Figure 4. During this survey, no traces of WIW were observed and the cluster analysis identifies only five water masses: WMDW, TDW, LIW, NACW and SAW.

Figure 3 corresponds to the easternmost transect, R5, where the less mixed MWs that enter the SoG from the MedS are expected to be found. The transect was carried out from south to north with a CTD probe during the ebb tide, the last station being completed shortly after the slack tide of low water (Figure 3a). The θ-S values of the densest water sample were 12.92ºC-38.48, which corresponds to WMDW (Figure 3c). Figure 3d shows that this water stacks up in the south while the LIW layer is thicker in the north, a spatial pattern that agrees with *Parrilla et al.* [1986] and *Naranjo et al.* [2012]. *Millot* [2014b] pointed out that LIW (and also TDW to some extent) flows counterclockwise and is pushed to the north due to the Coriolis force, while the WMDW is compelled to flow attached to the southern shore preferably, where the incoming AWs, NACW in particular, are accumulated due to the Coriolis effect (Figure 3d). Such a distribution facilitates the mixing of WMDW with AWs in the south part, a fact reflected by the mixing lines of the southernmost stations of the transect, which head

directly towards the AWs region from the vicinity of the WMDW centroid (Figure 3c). This is not so for the sations located further north in the transect where the mixing lines bend towards the LIW centroid before heading towards the AWs, showing that it is mainly the LIW and not the WMDW nor the TDW that mixes with the AWs.

The remaining transects discussed below were sampled with the MVP. The way the instrument samples the water column results in shorter times to complete a transect and higher spatial resolution (Figure 4). However, the maximum sampled depth is less than the one reached by CTD.

Next transect to the west is R2 (panels in column I of Figure 4). It is located to the east of CS so that the water masses have not been exposed yet to the strong mixing happening in the sill area [*Wesson and Gregg*, 1994; *J.C. Sánchez Garrido et al.*, 2011]. Moreover, it is not far from R5 and no significant differences are thus expected. That is the case for AWs, which depict a similar pattern (Figure 4-I-d). However, R2 transect was sampled during the rising tide and near the high tide (Figure 4-I-a). At this moment of the tide, the WMDW and TDW are allowed to reach shallower depths due to the interface rising associated with the internal tide [*Bryden et al.*, 1994; *Sánchez Román et al.*, 2012]. The situation is just the opposite of R5 sampling. The most interesting feature, however, is the spatial differentiation of the MWs (Figure 4-I-c,d) with WMDW occupying the southern part and TDW and LIW the northern area, although the latter is found at intermediate depths all over the transect.

The following transect R1 is still east, although near, of CS (R1, Figure 4-II). It is also close to R2 so a certain similarity between them is expected. But differences are apparent in the south due to the inversion of the tidal flow. R2 was accomplished from south to north and the southern stations were sampled ~1h before the high tide during the flood tide (Figure 4-I-a), while R1 was accomplished from north to south with the stations in the south done during the ebb tide, ~1h after the high tide (Figure 4-II-a). During the ebb phase the interface between AWs and MWs sinks nearby CS [*Sánchez Román et al.*, 2008], giving rise to a considerably thicker AWs layer (Figure 4-II-d). The northern half of both sections were sampled under similar tidal conditions near the high water, when the interface is at its shallowest position [*Sánchez Román et al.*, 2012], and show similar accumulation of LIW and TDW and a very thin layer of AWs. The spatial differentiation showed in Figure 4-I-c for R2 is easily recognisable in Figure 4-II-c for transect R1 as well, which is another remarkable similarity.

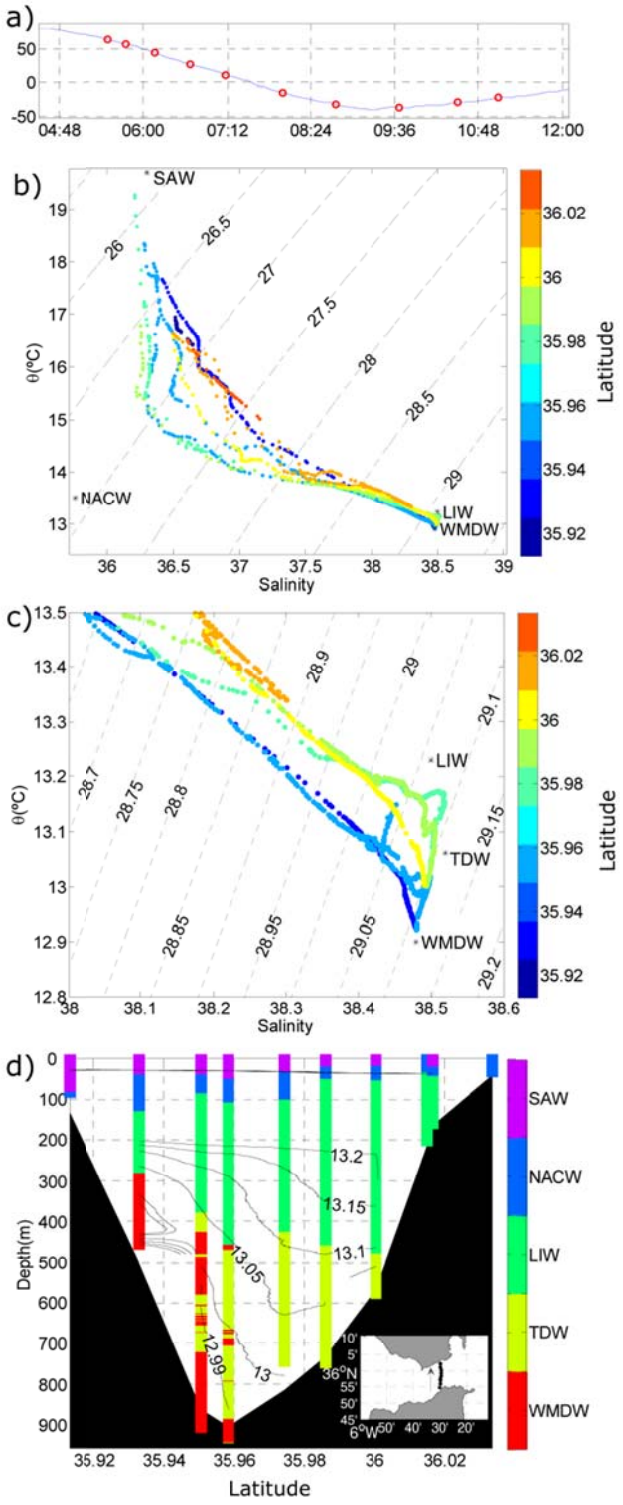

Figure 3. (a) Tidal oscillation at Tarifa displaying the time of the CTD casts (red dots) in the R5 transect, which was accomplished from south to north. (b) θ-S diagram showing the CTD data of the R5 transect, contours lines indicate potential density anomaly. The centroids of the different water masses are marked with asterisks and the colour scale on the right identify the different casts by their latitude. (c) Zoom of the MWs area of the θ-S diagram. (d) Results of the cluster analysis where each colour represents the cluster associated with a water mass according to the legend on the right.

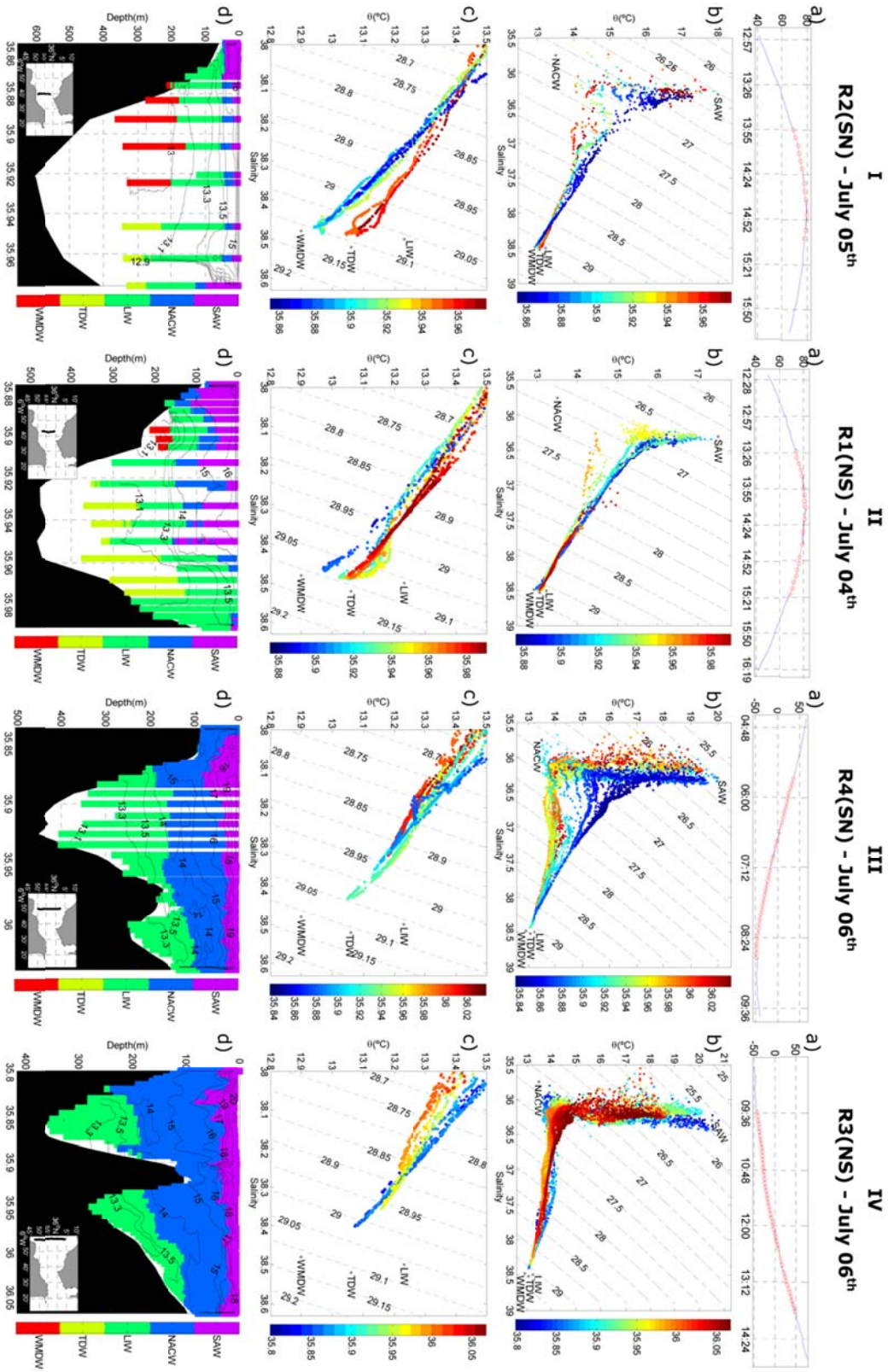

Figure 4. Zonal evolution, from East to West, of the thermohaline properties for the different water masses involved in the exchange at the SoG. The figure is divided in four columns named I, II, III and IV and each of them is subdivided in rows. The upper row, (a), shows the sea level during the sampling of each transect, with the red circles indicating the time of the different casts. The second row, (b), displays the θ-S diagram of the whole section. The names and locations of the defined water masses are indicated. The third row, (c), is a zoom of the θ-S diagram that focuses on the MWs, contours lines are σ_θ. Finally, the last row, (d), shows the classification of the water masses in the section provided by the cluster analysis.

Next transect to the west is R4 (Figure 4-III), which is already west of CS. The θ-S diagram shows two noticeable differences with regard to the three previous transects. Firstly, the θ-S curves bend towards the NACW centroid, implying a much greater impact of this water mass that now spreads downwards to 200m depth in the south (Figure 4-III-d). Secondly, the spatial differentiation of the MWs has disappeared and now they nearly lay along a single mixing line. This is an obvious outcome of the strong mixing in the Tangier basin [*J.C. Sánchez Garrido et al.*, 2011] which makes the MWs lose their specific identity to a great extent. The cluster algorithm only returns one kind of MWs in this transect, LIW in this case, which is somewhat misleading in view of the θ-S diagram in Figure 4-III-c. Therefore, it requires clarification. The algorithm situates the water samples in a cluster, which is the one with the greater percentage of the water mass defined by the corresponding centroid. According to the chosen metrics (Eq. 1 and 2), the deep water samples in this transect (and also in the next one, R3, commented below) have similar proportions of the three MWs but a slightly higher proportion of LIW (Figure 5[1]). Should we have displaced any of the centroids of the MWs by a tiny distance, the algorithm would have possibly returned a different prevailing cluster. The reasonable conclusion is that the MWs are hardly distinguishable once the Mediterranean outflow has passed CS and that the sensible option is to speak of a unique "Mediterranean water".

On the other hand, it is noteworthy here the effect of adding σ_θ to the metrics. Should it not be included, all the deep water would have been classified as TDW with an overwhelming percentage, as can be easily deduced from Figure 4-III-c. Its inclusion in the metrics makes the algorithm work more realistically in the sense that the actual sampled water is more likely to be the result of local mixing between LIW and WMDW (and TDW as well) than the outcome of the individual contribution of TDW.

[1] Figures like Figure 5 are helpful in order to supplement the information displayed in Figures like Figure 4 or 7. However, and in order to keep the length of the manuscript within a reasonable limit, such Figures are not included in the text, but they are offered as supplementary material.

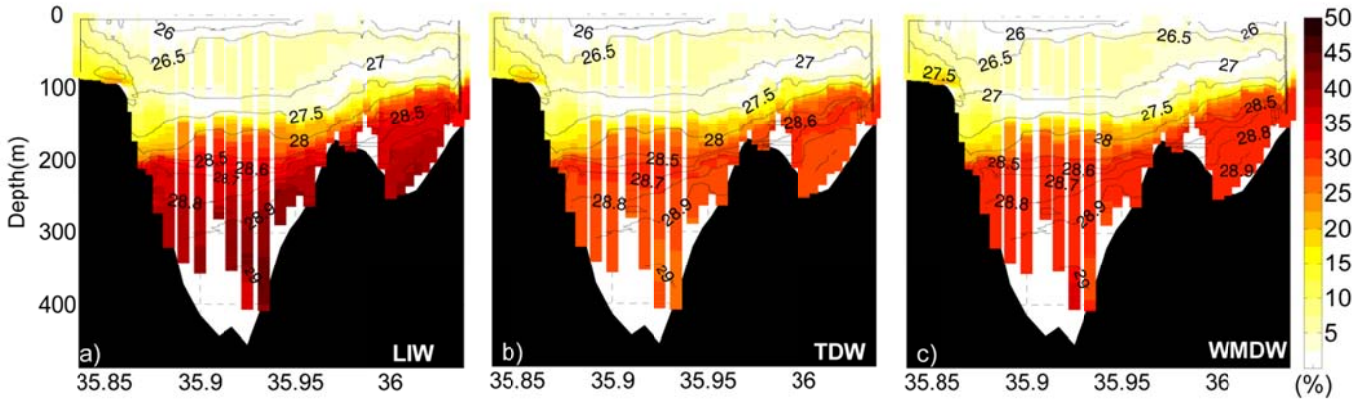

Figure 5. Percentage of the MWs in transect R4 (Figure 4, column III). The sum of the three contributions gives the 100% in the Mediterranean layer. The colour scales go from 0 to 50% for the sake of clarity. Contours represent the σ_θ.

The westernmost section R3, located in the western exit of the SoG, shows large similarity with the previous one. The fading out of the spatial differentiation of the MWs already detected in R4 is now more evident (Figure 4-IV-c), and so it is the prevalence of the NACW in the Atlantic layer (Figure 4-IV-d). Mixing lines are organised along two well-depicted directions, from MWs to NACW, and from NACW to SAW (Figure 4-IV-b), indicating that direct mixing of MWs with SAW does not happen any longer. Notice that this mixing can be partially detected in the previous transect R4 (Figure 4-III-b), this feature being almost the only difference among the two westernmost transects. The commentaries about the outputs of the cluster algorithm regarding the MWs made for R4 still apply in this transect.

The previous discussion has focussed on the spatial evolution of the different water masses as they flow through the SoG. Table 4 presents the θ-S values of the coldest water sampled in every transect, which is taken as a proxi of the MWs, in order to illustrate their transformation along its path to the Atlantic Ocean. To this regard, two remarks are noteworthy. The first one is about the density of the MWs: all the coldest samples are the densest samples too, except for section R1 where the densest sample has σ_θ=29.090 while the coldest sample has σ_θ=29.087 (see also Figure 4-IIc). The second and more important remark is that the MVP does not reach the bottom so that the values reported in Table 4 should not be identified with the coldest/densest water in the section, which might not have been sampled. Even so, the regular east-west spatial trend of temperature is quite suggestive of the erosion the MWs undergo along the SoG. Table 4 also displays the coldest sample with salinity lower than 36.5, which is the best example representing NACW at each transect, in order to show the alteration of this water in its way towards the MedS. None of the former

concerns apply to this water mass which has been correctly sampled by the MVP.

In the case of the MWs, θ increases and S decreases towards the west, the greatest jumps occurring between the transects R1 and R4 that surround CS, thus stressing the importance of this area as a source of turbulence [*Wesson and Gregg*, 1994; *J.C. Sánchez Garrido et al.*, 2011]. The same applies to the North Atlantic Central Water flowing in the opposite direction, since both θ and S tend to increase as the water flows eastward. Once again the main changes happen in the surroundings of CS, although the rising of θ and, in particular, of S still continues from R2 to R5.

		R5 (east)	R2	R1	R4	R3 (west)
MWs	θ (ºC)	12.92	12.94	12.97	13.05	13.07
	S (psu)	38.48	38.47	38.46	38.43	38.40
NACW	θ (ºC)	14.72	14.03	14.45	13.37	13.64
	S (psu)	36.48	36.15	36.24	35.95	36.03

Table 4. The two first rows show the potential temperature and salinity, respectively, of the coldest MW sample observed in the transect (MWs block). Third and fourth rows show the potential temperature and salinity of the coldest sample with salinity less than 36.5 (NACW block). The different columns correspond to the different transects, which have been organised from east (R5) to west (R3), see Figure 1 for details.

4.2. INGRES

Transects TES and TAC (see Figure 1) have been sampled repeatedly since 2004 and they are more regularly accomplished since 2011. Figure 6 presents the θ-S diagrams of both transects confirming the already mentioned evolution of the water masses as they progress through the SoG: the fading of the spatial differentiation between MWs from TAC (east) to TES (west) and the erosion of the NACW signal from TES (west) to TAC (east). In particular, the reddish colours in the inset of Figure 6b illustrates the fact that LIW, WIW and TDW flow preferably across the northern half of the SoG while the WMDW flows attached to the southern slope. The inset of Figure 6a shows how the former pattern is lost at TES.

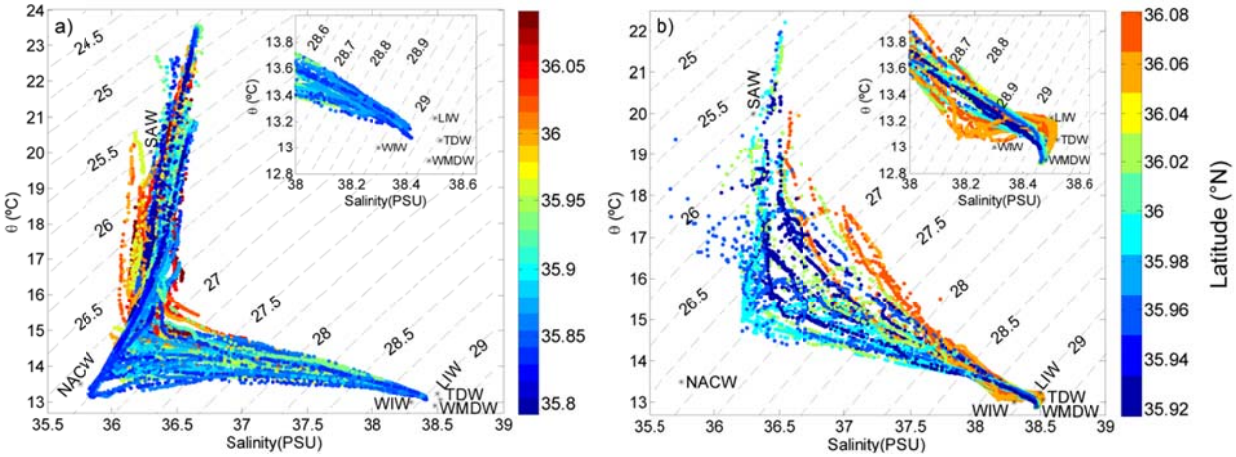

Figure 6. θ–S diagram showing the CTD data collected at TES (a) and TAC (b) transects during the INGRES project from 2004 up to the present. The colour scale indicates latitude and the contour lines shows σ_θ . Black stars mark the θ–S pairs of the water masses involved in the exchange (see Table 2). The insets zoom in the Mediterranean water zone of the diagram.

4.2.1. Spatial distribution

Figure 7a-b show the mean potential temperature and salinity distributions at TES and TAC sections, respectively, which have been obtained by averaging all the transects collected within INGRES. Figure 7c-d show the results of applying the cluster analysis to the same sets of data.

The cluster analysis at TAC transect shows the averaged spatial distribution of the six water masses involved in the exchange (Figure 7d). Contrary to GIC, INGRES data recorded WIW, which now is identified flowing attached to the north shore just below a very thin layer of NACW. The remaining MWs display the same spatial pattern as in GIC: the WMDW, easily identified by θ<13ºC in Figure 7d, resides in the deepest layer and preferably stacked up in the southern half of the transect; the TDW and LIW, which appear as a salty wedge encircled by the isohaline 38.485 (grey line in Figure 7b), occupy an intermediate layer that thickens to the north. Any of these MWs is saltier (S>38.4, see Figure 7b) than the rather mixed MW at TES (Figure 7a), a result that can only be explained by the entrainment of AW by the Mediterranean outflow west of Camarinal Sill, as discussed in *Jesús García Lafuente et al.* [2011]. The two AWs are at the top of the water column in a layer that thickens from ~100m in the north to ~150m in the south. The presence of NACW is appreciably reduced as it experiences a marked mixing with respect to the TES transect (compare Figure 7c and Figure 7d). The blue colour identifying NACW in Figure 7d must be then interpreted as the sample being closer to NACW than to any other water mass and not as if it were aside the point marking the pure NACW.

At TES, the cluster analysis only detects three water masses (Figure 7c), in agreement with the results obtained from the GIC data in this area. The bottom layer is occupied by the MWs, which the cluster analysis identifies as LIW (the same cautionary comments on the identification of MWs as LIW made for R4 transect in the previous Section apply here). These MWs, whose averaged salinity is ~38.2 with maxima of 38.4, flow mainly through the southern channel below 250 meters, the volume flowing through the northern channel being much smaller. NACW is the prevailing water mass, occupying a layer from 50 to 250 meters in the southern channel (Figure 7c). Obviously not all this layer is NACW. It includes its mixture with the overlying (SAW) and underlying (LIW) waters, with the NACW entering in greater proportion than the others. Actually, Figure 7a shows a core of minimum salinity around 150-200m depth in the southern channel, which would be the depth where the purest NACW is flowing.

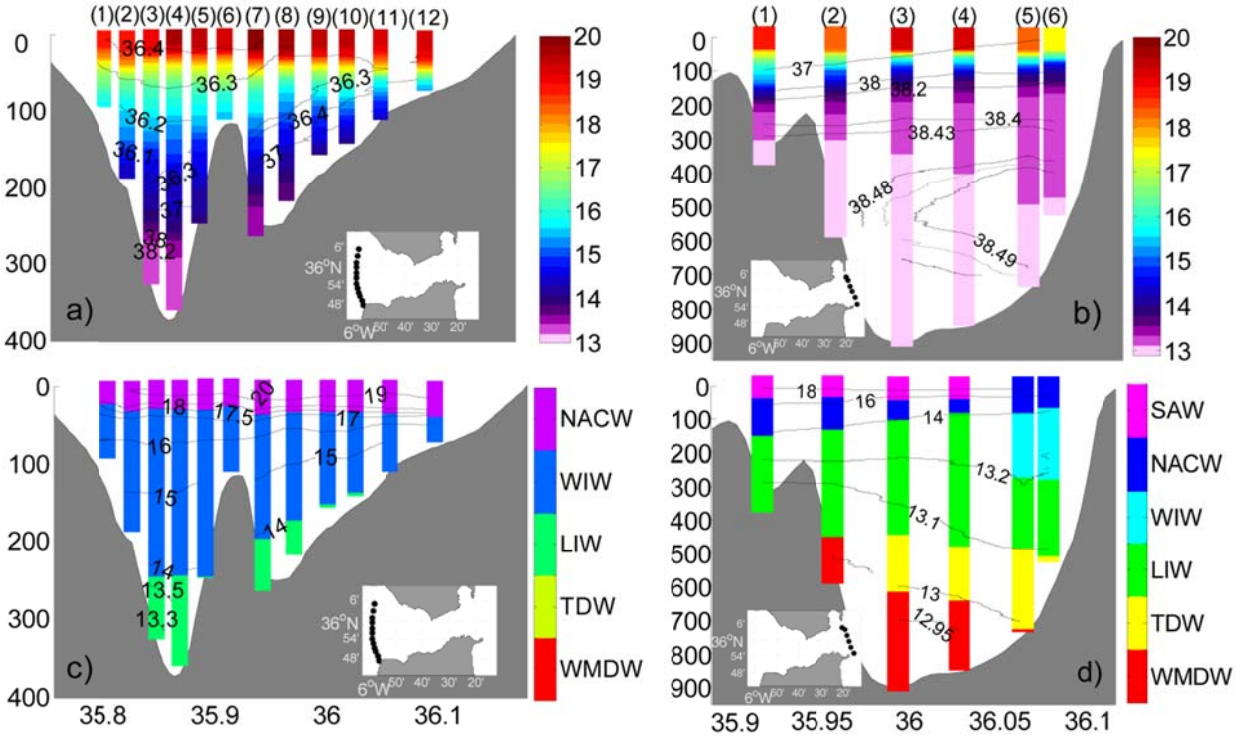

Figure 7. Averaged potential temperature (colour scale) and salinity (labelled contours) of the whole dataset collected at TES (a) and TAC (b). Panels (c) and (d) show the distribution of water masses in these transects provided by the cluster analysis. Contours display the potential temperature. Insets show the location of the cast in each transect.

4.2.2. Temporal fluctuations in the core of the water masses

This section addresses the time variability of the thermohaline characteristics found in INGRES data. To this aim, we have selected representative samples of each water mass with the same criterion for a given transect, although the criterion may change slightly from the west (TES) to the east (TAC) transect, as explained below.

At TAC the criterion to define each water mass must be selected carefully, as the four MWs detected in this transect have only very small thermohaline differences. The SAW is selected as the warmest sample. The most appropriate criterion for the NACW will be to take the freshest sample, but NACW has been widely altered by mixing and the freshest water criterion may be not applicable at TAC (which however is pretty suitable in the TES section, see θ-S diagram of Figure 6b). Even more, the mixing could have been so important that speaking of NACW makes no clear sense. Thus, we only admit the presence of NACW if a clear minimum of salinity with respect to the overlying SAW is observed in the vertical profile, otherwise we ignore this water mass, even if temperature/salinity dots in the θ-S diagram bend gently towards the mark representing the NACW. Regarding the MWs, WMDW is determined as the coldest sample, TDW as the saltiest one, and LIW as the warmest whenever its salinity exceeds 38.4. As for the WIW, it is identified as the coldest sample between σ_θ=28.0 and σ_θ=29.0 (Millot, 2014), provided that it is visually detected in the θ-S diagram previously (that is, whenever the relative minimum around the WIW position in the diagram is positively identified, see inset in Figure 6b).

Figure 8 shows the series of these representative samples at TAC transect, which are displayed along with the depth where the sample was found (in brackets) and the location of the profile (see labels on top of Figure 7). The seasonality of SAW is recognisable at TAC despite being more intense in the TES section (compare Figure 8a with Figure 9a). As for the NACW, it was positively identified only 4 out of 11 times (Figure 8b). In all these occasions its core mass was always found in the southern casts (cast 2 or 3) at depths between 20 and 85m, quite shallower than at TES, where the NACW core was between 150 and 200m (Figure 7a).

Regarding MWs, except for 2012 when WIW was not observed, the four water masses were positively identified during all cruises. The lightest one is the WIW, which is at the top of the Mediterranean layer between 150 and 260m and it is detected in casts near the northern shore, in agreement with

Figure 7d. April 2014 was the exception as the WIW sample was detected deeper (293m) and shifted to the south (cast 3), a situation that apparently extended until October 2014. LIW layer is beneath the WIW. Despite being spread out through the whole transect (Figure 7d), its core is found in the northern part, usually at the position of cast number 5 (Figure 8d) at depths between 260 and 300m. April and October 2014 were again the exception, the LIW core was allways noticeably deeper. Curiously, warmer and fresher LIW was detected in 2012, coincidentally with the absence of WIW in the SoG. TDW is observed beneath the LIW between 370 and 550m with preference to be detected close to the northern coast (casts 4 and 5), according to Figure 8e. Once again April 2014 shows an anomalously large depth of the TDW core (567m). Finally, the densest WMDW occupies the deepest layer with its core showing up close to the southern shore (casts 2 to 4) and always deeper than ~700m except for November 2011, when it was detected at 566m in cast number 2 (Figure 8f). An absolute minimum of θ and S is observed in June 2009.

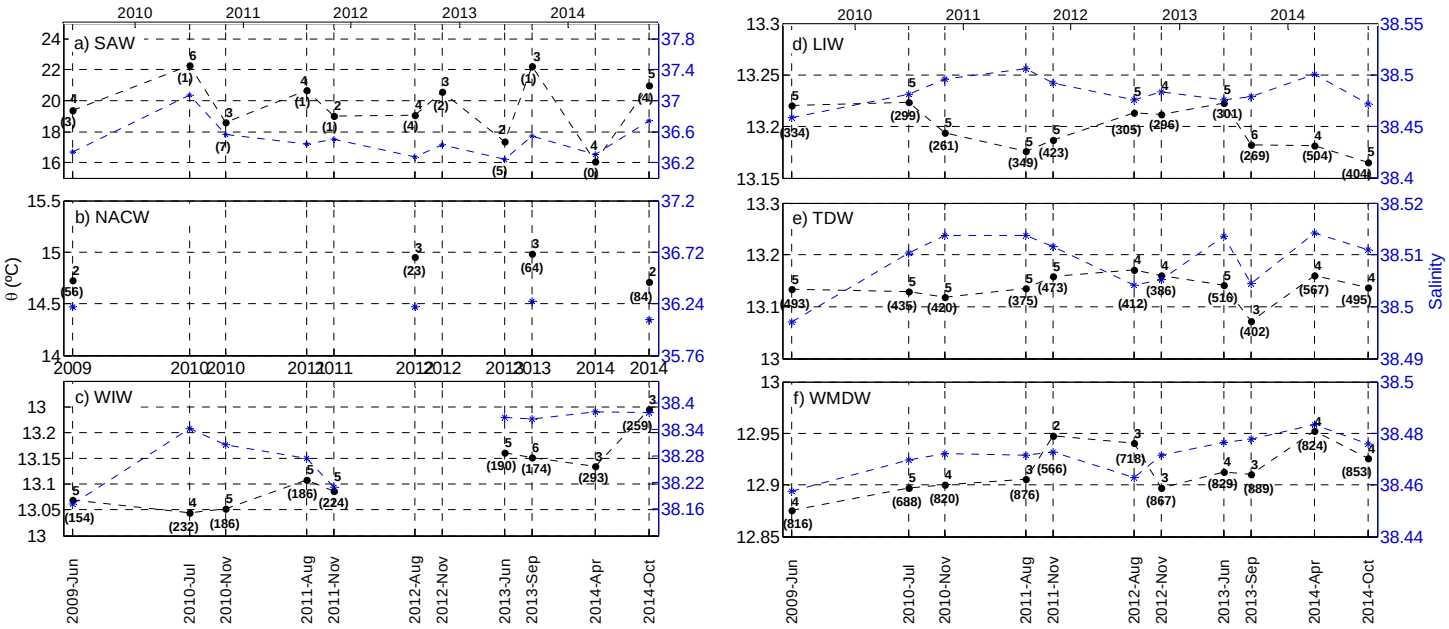

Figure 8. Potential temperature (left axes, black dots) and salinity (right axes, blue asterisks) of the water samples representing each water masses at the TAC transect (see text for details). Numbers 1 to 6 aside the symbols indicate the cast were the samples were detected, according to the labels on top of Figure 7. Numbers within brackets display the depth of the sample (in meters from the surface). Ticks in the x-axes at the top of the figures indicate January the 1st of each year.

A similar analysis has been conducted at TES, taking into account only three water masses: SAW, NACW and what we shall refer to as MW_{TES}, a mixing of all the MWs that are no longer distinguishable. The representative sample of SAW and of NACW were the warmest and freshest ones, respectively,

while MW_{TES} was represented by the saltiest sample. Figure 9 displays the selected points for each cruise. As expected, seasonal fluctuations is the obvious characteristic of SAW (Figure 9a), with warmer and also saltier water during the summer and early-autumn months. It is the most variable water mass, as can be deduced from Table 4 as well. The NACW (Figure 9b) shows some seasonality, which consists in a diminution of θ in summer months. It would be associated with the upwelling-favourable winds in the Gulf of Cádiz, which uplift deeper and, hence, colder NACW, making it available for the inflow during the upwelling season [*Folkard et al.*, 1997; *Criado-Aldeanueva et al.*, 2006]. A positive salinity trend is visible in Figure 9b, only interrupted during the second part of 2014. The MW_{TES} (Figure 9c) is the least variable water mass in this transect. Temperature and salinity display a rather specular pattern, suggesting that colder (warmer) water is simultaneously saltier (fresher), giving thus rise to enhanced fluctuations of density. MW_{TES} does not show a clear seasonality, neither a short-term trend, although from 2012 onwards the salinity is greater than the mean of the series (38.34, see Table 4).

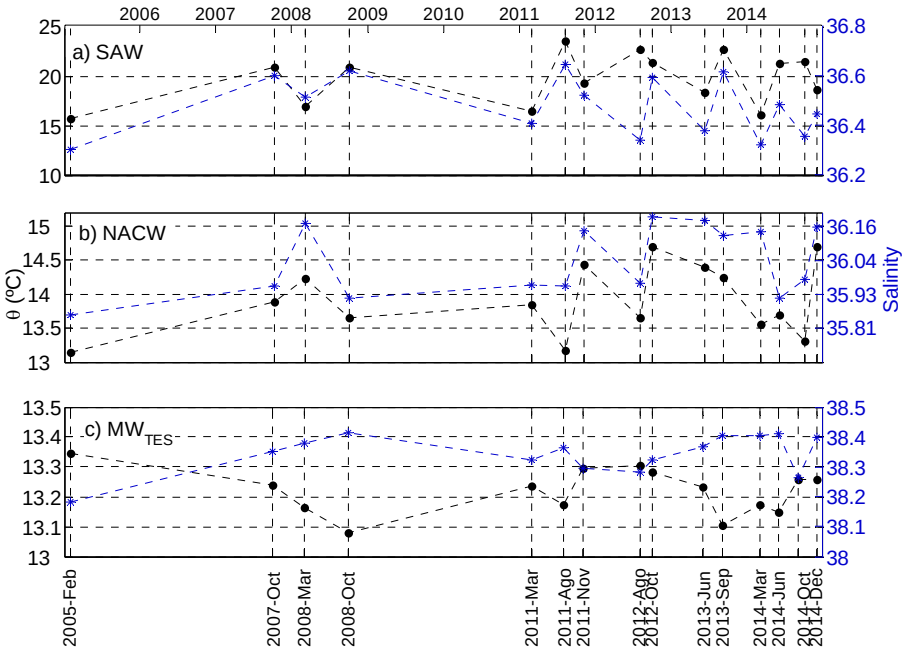

Figure 9. Potential temperature (left axis, black points) and salinity (right axis, blue stars) of the water masses addressed in TES: Panel (a) is for SAW, panel (b) is for NACW, and panel (c) is for MW_{TES}. See text for details. Ticks in the x-axes at the top of the figure indicate January the 1st of each year.

	TES		TAC		TES		TAC	
	$\overline{\theta} \pm \sigma$ (°C)	Trend (°C/year)	$\overline{\theta} \pm \sigma$ (°C)	Trend (°C/year)	$\overline{S} \pm \sigma$ (psu)	Trend (psu/year)	$\overline{S} \pm \sigma$ (psu)	Trend (psu/year)
SAW	19.76±2.60	*0.28*	19.74±1.80	*0.18*	36.47±0.12	*0.0047*	37.15±0.08	*0.026*
NACW	13.91±0.51	*0.05*	14.84±0.14	-	36.03±0.12	*0.017*	36.19±0.07	-
WIW	-	-	13.11±0.06	**0.030**	-	-	38.31±0.07	**0.031**
MW_{TES}/LIW	13.22±0.07	*0.0035*	13.20±0.02	*-0.0064*	38.34±0.06	*0.0087*	38.48±0.01	*$9x10^{-4}$*
TDW	-	-	13.13±0.03	*$9.3x10^{-4}$*	-	-	38.51±0.005	*0.001*
WMDW	-	-	12.91±0.02	**0.0089**	-	-	38.47±0.07	**0.003**

Table 5. Mean values with standard deviation and trends of the potential temperature and salinity data displayed in Figure 8 and Figure 9. TES (shaded columns) correspond to the western exit of the Strait where MWs are not distinguishable and, therefore, a unique MW, denoted MW_{TES}, is specified (see text for details). Trend values in bold indicate that the trend is significant at the 95% significance level, while values in italics mean a non-significant trend at this level. Trends for NACW at TAC have not been computed since only four points were available.

5. Discussion and conclusions

The present study had the twofold objective of depicting the spatial distribution of the water masses participating in the exchange through the SoG and investigating the time variability of this pattern during the last years. An intensive oceanographic survey carried out in summer 2012 (GIC data) allowed us to address the first objective and the rather systematic CTD monitoring of two specific transects at both ends of the SoG (INGRES data) made it possible the analysis of the time variability.

5.1. Spatial variability

A cluster analysis was performed on GIC data to classify the water samples. Of all water masses reported in Table 1, the WIW was not detected and therefore it was excluded from the analysis. Also, after examining the five GIC transects and scrutinizing the zoomed θ-S diagrams of Figure 3 and Figure 4, it is questionable the inclusion of the TDW in the algorithm. If it is included the outcome of the analysis for the transects located east of CS provides a pattern with the LIW and TDW occupying preferably the northern part and the WMDW attached to the south (Figure 3d and Figure 4-I-II panels d). It is in good agreement with the previous study by *Millot* [2014b], who put forward that TDW flowing over the bottom piled up

against the northern half of the SoG. Indeed, if we remove TDW from our analysis the samples which will correspond with TDW are divided between WMDW and LIW, with the samples incorporated to the LIW (WMDW) being located to the centre-north (centre-south) of the transect, without modifying heavily the distribution of Figure 7 (not shown).

West of CS, the AWs are well differentiated but the MWs are not, according to the cluster analysis, which outputs LIW in all cases. This result is somewhat misleading as the proportion of all the MWs in the samples is very alike (Figure 5). It is just because the proportion of LIW is slightly greater that the analysis ascribes the samples to the LIW cluster. Our interpretation, however, is that the intense tidal mixing undergone by the MWs flowing west over CS blurs out their specific characteristics, leaving a rather mixed water that we have denoted by MW_{TES}, whose characteristics depend on the tide to some extent. This would be the water making up the different veins of the Mediterranean outflow in studies dealing with the Gulf of Cadiz and Eastern North Atlantic Ocean circulation.

It should be remarked that there is not full consensus with this description. Millot (2014) put forward an organised structure of the Mediterranean outflow along the Iberian slope of the Gulf of Cadiz in four veins, each of them having its origin in one of the four MWs discussed so far. While our dataset does not allow for addressing this point in the Iberian slope west of the SoG, our observations in Espartel sill do not support such differentiation, especially regarding the vein supposedly ascribed to the WIW, which was absent during the GIC survey. The strong mixing reflected in the CTD transects west of Camarinal sill (Figures 4b and 4c), which is further revealed by the cluster analysis (Figure 4d), suggests that such a downstream organisation of the Mediterranean veins is quite improbable at the time of the GIC survey, if not impossible. Overall, the most significant result of the analysis of these data is the pronounced west-to-east erosion observed in the NACW, and of the MWs in the opposite way (Figures 4b and 4c), which lose their specific identities. Both outcomes are a consequence of the outstanding mixing driven by tides that takes place in the Camarinal sill and its surroundings (Sánchez Garrido et al., 2011; Wesson and Gregg, 1994).

5.2. *Temporal variability*

The same cluster analysis has been performed on the whole set of INGRES data at TES and TAC transects (Figure 7) with similar results. The main

difference is the presence of WIW among the MWs in the eastern transect in 9 out of 11 cruises, which shows up embedded between the LIW and the AWs flowing close to the northern shore. Nevertheless, the goal of the INGRES data analysis is the investigation of the time variability, for which we have devised a criterion to identify the most representative samples of each of the water masses involved in the exchange during every cruise (Figure 8 and Figure 9). Mean values and trends during the period covered by the observations are summarized in Table 4. Mean values at the different transects merely inform about spatial variations and reflect the already discussed changes suffered by the NACW in its path to the MedS as well as the important mixing undertaken by the MWs after passing Camarinal sill. Interestingly the mean value of MW_{TES} potential temperature at the western transect (TES) is greater than any of the MWs mean values at the eastern transect (TAC), which implies that a small proportion of NACW must be involved in the MW_{TES} mixing. Salinity mean values also require the participation of NACW in the mixing [*J. García Lafuente et al.*, 2007].

The marked seasonality of the SAW, and the NACW to some extent, along with the intermittent sampling of the transects make the trends reported in Table 4 to be very uncertain for the AWs (notice that trends for NACW are not computed at TAC due to the very small number of samples available). Apparently, NACW shows a tendency to increase its salinity from 2011 onwards at TES (Figure 9b), although the drop by the summer of 2014 would deny this conclusion. Actually, the trend reported in Table 4 for this water is non-significant at the 95% confidence level. On the other hand, the fact that the seasonal expected drop of salinity during the previous summer (June 2013 cruise, Figure 9b) had not taken place supports the salinity increase scenario, which otherwise would not be so apparent.

Trends in MWs are better investigated at the TAC transect. Six-year observations are obviously insufficient to speak of long-term trends, but some of the short-term trends that are drawn from our reduced dataset may be related to trends already mentioned in the literature [*Borghini et al.*, 2014]. During the studied period, neither the LIW nor the TDW show significant trends (Table 4), whereas both WIW and WMDW exhibit positive temperature and salinity trends, which are more pronounced for the former (Table 4). While the seasonality, intermittency, relatively small volume, and intermediate nature of the WIW formed in the northwest area of the Western MedS raise questions about the reaching and consequences of their estimated trends, the trends found for the WMDW will have more profound

implications as they would be linked to similar trends in the interior of the MedS, which have been traced back up to several decades [*Bethoux et al.*, 1990; *Leaman and Schott*, 1991; *Rohling and Bryden*, 1992; *Krahmann and Schott*, 1998]. Recently, *Borghini et al.* [2014] have concluded that the MedS is becoming saltier, in which case the trend of WMDW in Table 4 would be nothing more than the mere reflection of this salinification. It is remarkable, however, that this trend is not observed in the MW_{TES} at TES section. A likely explanation would be that the WMDW is diluted with the rest of the MWs along the SoG, none of the later showing a significant trend, with the consequence that the WMDW trend at TAC fades out at TES.

The intermittency of WIW is illustrated in Figure 8c. Traces of this water were not found either during the INGRES cruises carried out in August and November of 2012, or during the intensive GIC survey in July the same year (inset of Figure 2). It suggests that WIW was not produced this year or, if so, the volume formed was quite small. Moored-based observations collected in the Gulf of Valencia near the area of WIW formation by *Ribó et al.* [2015] identify WIW passing by the mooring line in early spring of 2011, but not during late winter of 2012. Although the authors do not discard the possibility of WIW flowing above the moored instrumentation, the lack of WIW, or its fainter signal, in early 2012 would be connected with the absence of WIW in the SoG later on that year.

Almost coincidentally with this lack of WIW, the WMDW shows a relative potential temperature maximum in TAC (Figure 8f) while MW_{TES} does the same at TEC (Figure 9c). It would be the reflection of a rather mild 2010-11 winter, as discussed in *Severin et al.* [2014]. Figure 8f shows that the minimum WMDW potential temperature of all the period was reached in 2009, which could be related with the exceptional WMDW formation in the Gulf of Lion mentioned by [*Salat et al.*, 2010]. There are no data available at TES this year to support the observations at TAC transect, but it is noteworthy that similar strong events of WMDW formation left a recognisable footprint in the SoG.

Acknowledgement

This work is a Spanish contribution funded by the National Project INGRES 3 (CTM2010-21229), a French contribution to the HyMeX and MOOSE programmes funded by MISTRALS, and to the CIESM HYDROCHANGES Programme (ciesm.org/marine/programs/hydrochanges.htm). Cristina Naranjo acknowledges the fellowship BES-2011-043421 from the Ministry of Economy and Competitiveness - Spain, and M. Jesús Bellanco acknowledges the pre-doc fellowship IEO-FPI 2011/10. We are also grateful to the crews of the R/V Angeles Alvariño and the R/V TETHYS II, and to G. Rougier (MIO) and Deny Malengros (SAM/MIO) who operated the MVP. The MVP has been funded through the CETSM project.

References

Baringer, M. (1993), Mixing and dynamics of the Mediterranean outflow(Ph. D. Thesis).

Baringer, M. O. N., and J. F. Price (1997), Mixing and Spreading of the Mediterranean Outflow, *Journal of Physical Oceanography*, *27*(8), 1654-1677, doi:10.1175/1520-0485(1997)027<1654:MASOTM>2.0.CO;2.

Ben Ismail, S., K. Schroeder, C. Sammari, G. P. Gasparini, M. Borghini, and L. Aleya (2014), Interannual variability of water mass properties in the Tunisia–Sicily Channel, *Journal of Marine Systems*, *135*(0), 14-28, doi:http://dx.doi.org/10.1016/j.jmarsys.2013.06.010.

Bethoux, J. P., B. Gentili, J. Raunet, and D. Tailliez (1990), Warming trend in the western Mediterranean deep water, *Nature*, *347*(6294), 660-662.

Borghini, M., H. Bryden, K. Schroeder, S. Sparnocchia, and A. Vetrano (2014), The Mediterranean is becoming saltier, *Ocean Sci.*, *10*(4), 693-700, doi:10.5194/os-10-693-2014.

Bray, N. A., J. Ochoa, and T. H. Kinder (1995), The role of the interface in exchange through the Strait of Gibraltar, *Journal of Geophysical Research: Oceans*, *100*(C6), 10755-10776, doi:10.1029/95JC00381.

Bryden, H. L., J. Candela, and T. H. Kinder (1994), Exchange through the Strait of Gibraltar, *Progress in Oceanography*, *33*(3), 201-248, doi:http://dx.doi.org/10.1016/0079-6611(94)90028-0.

Bryden, H. L., and H. M. Stommel (1982), Origin of the Mediterranean Outflow, *Journal of Marine Research*, *40*, 55-71.

Candela, J., C. Winant, and A. Ruiz (1990), Tides in the Strait of Gibraltar, *Journal of Geophysical Research: Oceans*, *95*(C5), 7313-7335, doi:http://dx.doi.org/10.1029/JC095iC05p07313.

Conan, P., and C. Millot (1995), Variability of the northern current off marseilles, western mediterranean-sea, from february to june 1992, *Oceanologica acta*, *18*(2), 193-205.

Criado-Aldeanueva, F., J. García-Lafuente, J. M. Vargas, J. Del Río, A. Vázquez, A. Reul, and A. Sánchez (2006), Distribution and circulation of water masses in the Gulf of Cadiz from in situ observations, *Deep Sea Research Part II: Topical Studies in Oceanography*, *53*(11–13), 1144-1160, doi:http://dx.doi.org/10.1016/j.dsr2.2006.04.012.

Folkard, A. M., P. A. Davies, A. F. G. Fiúza, and I. Ambar (1997), Remotely sensed sea surface thermal patterns in the Gulf of Cadiz and the Strait of Gibraltar: Variability, correlations, and relationships with the surface wind field, *Journal of Geophysical Research: Oceans*, *102*(C3), 5669-5683, doi:10.1029/96JC02505.

Font, J. (1987), The path of the Levantine intermediate water to the Alboran sea, *Deep Sea Research Part A. Oceanographic Research Papers*, *34*(10), 1745-1755, doi:http://dx.doi.org/10.1016/0198-0149(87)90022-7.

Fuda, J. L., C. Millot, I. Taupier-Letage, U. Send, and J. M. Bocognano (2000), XBT monitoring of a meridian section across the western Mediterranean Sea, *Deep Sea Research Part I: Oceanographic Research Papers*, *47*(11), 2191-2218, doi:http://dx.doi.org/10.1016/S0967-0637(00)00018-2.

García-Lafuente, J., J. M. Vargas, F. Plaza, T. Sarhan, J. Candela, and B. Bascheck (2000), Tide at the eastern section of the Strait of Gibraltar, *Journal of Geophysical Research: Oceans*, *105*(C6), 14197-14213, doi:http://dx.doi.org/10.1029/2000JC900007.

García Lafuente, J., E. Bruque Pozas, J. C. Sánchez Garrido, G. Sannino, and S. Sammartino (2013), The interface mixing layer and the tidal dynamics at the eastern part of the Strait of Gibraltar, *Journal of Marine Systems*, *117–118*(0), 31-42, doi:http://dx.doi.org/10.1016/j.jmarsys.2013.02.014.

García Lafuente, J., A. Sánchez Román, G. Díaz del Río, G. Sannino, and J. C. Sánchez Garrido (2007), Recent observations of seasonal variability of the Mediterranean outflow in the Strait of Gibraltar, *Journal of Geophysical Research: Oceans*, *112*(C10), C10005, doi:http://dx.doi.org/10.1029/2006JC003992.

García Lafuente, J., A. Sánchez Román, C. Naranjo, and J. C. Sánchez Garrido (2011), The very first transformation of the Mediterranean outflow in the Strait of Gibraltar, *Journal of Geophysical Research: Oceans*, *116*(C7), C07010, doi:http://dx.doi.org/10.1029/2011JC006967.

Gascard, J. C., and C. Richez (1985), Water masses and circulation in the Western Alboran sea and in the Straits of Gibraltar, *Progress in Oceanography*, *15*(3), 157-216, doi:http://dx.doi.org/10.1016/0079-6611(85)90031-X.

Hur, H. B., G. A. Jacobs, and W. J. Teague (1999), Monthly Variations of Water Masses in the Yellow and East China Seas, November 6, 1998, *Journal of Oceanography*, *55*(2), 171-184, doi:10.1023/A:1007885828278.

Kim, K., K. R. Kim, T. S. Rhee, H. K. Rho, R. Limeburner, and R. C. Beardsley (1991), Identification of Water Masses in the Yellow Sea and the East China Sea by Cluster Analysis, in *Elsevier Oceanography Series*, edited

by K. Takano, pp. 253-267, Elsevier, doi:http://dx.doi.org/10.1016/S0422-9894(08)70100-4.

Kinder, T. H., and H. L. Bryden (1990), Aspiration of Deep Waters through Straits, in *The Physical Oceanography of Sea Straits*, edited by L. J. Pratt, pp. 295-319, Springer Netherlands, doi:10.1007/978-94-009-0677-8_14.

Kinder, T. H., and G. Parrilla (1987), Yes, some of the Mediterranean outflow does come from great depth, *Journal of Geophysical Research: Oceans*, *92*(C3), 2901-2906, doi:10.1029/JC092iC03p02901.

Krahmann, G., and F. Schott (1998), Longterm increases in western Mediterranean salinities and temperatures: Anthropogenic and climatic sources, *Geophysical Research Letters*, *25*(22), 4209-4212, doi:10.1029/1998GL900143.

Leaman, K. D., and F. A. Schott (1991), Hydrographic Structure of the Convection Regime in the Gulf of Lions: Winter 1987, *Journal of Physical Oceanography*, *21*(4), 575-598, doi:10.1175/1520-0485(1991)021<0575:HSOTCR>2.0.CO;2.

Lopez Jurado, J. L., J. García Lafuente, and N. Cano Lucaya (1995), Hydrographic conditions of the Ibiza channel during November 1990, March 1991 and July 1992, *Oceanologica acta*, *18*(2), 235-243, doi:http://archimer.ifremer.fr/doc/00097/20868/.

Millot, C. (1999), Circulation in the Western Mediterranean Sea, *Journal of Marine Systems*, *20*(1–4), 423-442, doi:http://dx.doi.org/10.1016/S0924-7963(98)00078-5.

Millot, C. (2009), Another description of the Mediterranean Sea outflow, *Progress in Oceanography*, *82*(2), 101-124, doi:http://dx.doi.org/10.1016/j.pocean.2009.04.016.

Millot, C. (2014a), Heterogeneities of in- and out-flows in the Mediterranean Sea, *Progress in Oceanography*, *120*(0), 254-278, doi:http://dx.doi.org/10.1016/j.pocean.2013.09.007.

Millot, C. (2014b), Levantine Intermediate Water characteristics: an astounding general misunderstanding!, *Scientia Marina*, *78*(2), 165-171, doi:doi: 10.3989/scimar.04045.30H.

Millot, C., J. Candela, J.-L. Fuda, and Y. Tber (2006), Large warming and salinification of the Mediterranean outflow due to changes in its composition, *Deep Sea Research Part I: Oceanographic Research Papers*, *53*(4), 656-666, doi:http://dx.doi.org/10.1016/j.dsr.2005.12.017.

Millot, C., and I. Taupier-Letage (2005), Circulation in the Mediterranean Sea, in *The Mediterranean Sea*, edited by A. Saliot, pp. 29-66, Springer Berlin Heidelberg, doi:10.1007/b107143.

Monserrat, S., J. L. López-Jurado, and M. Marcos (2008), A mesoscale index to describe the regional circulation around the Balearic Islands, *Journal of Marine Systems*, *71*(3–4), 413-420, doi:http://dx.doi.org/10.1016/j.jmarsys.2006.11.012.

Naranjo, C., J. García-Lafuente, J. C. Sánchez-Garrido, A. Sánchez-Román, and J. Delgado-Cabello (2012), The Western Alboran Gyre helps ventilate

the Western Mediterranean Deep Water through Gibraltar, *Deep Sea Research Part I: Oceanographic Research Papers*, *63*(0), 157-163, doi:http://dx.doi.org/10.1016/j.dsr.2011.10.003.

Naranjo, C., J. Garcia-Lafuente, G. Sannino, and J. C. Sanchez-Garrido (2014), How much do tides affect the circulation of the Mediterranean Sea? From local processes in the Strait of Gibraltar to basin-scale effects, *Progress in Oceanography*(0), doi:http://dx.doi.org/10.1016/j.pocean.2014.06.005.

Parrilla, G., and T. H. Kinder (1987), The Physical Oceanography of the Alboran Sea*Rep.*, DTIC Document.

Parrilla, G., T. H. Kinder, and R. H. Preller (1986), Deep and intermediate mediterranean water in the western Alboran Sea, *Deep Sea Research Part A. Oceanographic Research Papers*, *33*(1), 55-88, doi:http://dx.doi.org/10.1016/0198-0149(86)90108-1.

Pettigrew, N. R. (1989), Direct measurements of the flow of western Mediterranean deep water over the Gibraltar sill, *Journal of Geophysical Research: Oceans*, *94*(C12), 18089-18093, doi:10.1029/JC094iC12p18089.

Pinot, J. M., J. L. López-Jurado, and M. Riera (2002), The CANALES experiment (1996-1998). Interannual, seasonal, and mesoscale variability of the circulation in the Balearic Channels, *Progress in Oceanography*, *55*(3–4), 335-370, doi:http://dx.doi.org/10.1016/S0079-6611(02)00139-8.

Rhein, M., U. Send, B. Klein, and G. Krahmann (1999), Interbasin deep water exchange in the western Mediterranean, *Journal of Geophysical Research-Oceans*, *104*, 23495-23508, doi:10.1029/1999jc900162.

Ribó, M., P. Puig, and H. van Haren (2015), Hydrodynamics over the Gulf of Valencia continental slope and their role in sediment transport, *Deep Sea Research Part I: Oceanographic Research Papers*, *95*(0), 54-66, doi:http://dx.doi.org/10.1016/j.dsr.2014.10.004.

Rohling, E. J., and H. L. Bryden (1992), Man-induced salinity and temperature increases in western Mediterranean deep water, *Journal of Geophysical Research: Oceans*, *97*(C7), 11191-11198, doi:10.1029/92JC00767.

Salat, J., and J. Font (1987), Water mass structure near and offshore the Catalan coast during the winters of 1982 and 1983, *Annales Geophysicae, Series B*, *5 B*(1), 49-54.

Salat, J., P. Puig, and M. Latasa (2010), Violent storms within the Sea: dense water formation episodes in the NW Mediterranean, *Adv. Geosci.*, *26*, 53-59, doi:10.5194/adgeo-26-53-2010.

Sánchez Garrido, J. C., J. García Lafuente, F. Criado Aldeanueva, A. Baquerizo, and G. Sannino (2008), Time-spatial variability observed in velocity of propagation of the internal bore in the Strait of Gibraltar, *Journal of Geophysical Research: Oceans*, *113*(C7), n/a-n/a, doi:10.1029/2007JC004624.

Sánchez Garrido, J. C., G. Sannino, L. Liberti, J. García Lafuente, and L. Pratt (2011), Numerical modeling of three-dimensional stratified tidal flow

over Camarinal Sill, Strait of Gibraltar, *Journal of Geophysical Research: Oceans*, *116*(C12), C12026, doi:http://dx.doi.org/10.1029/2011JC007093.

Sánchez Román, A., F. Criado Aldeanueva, J. García Lafuente, and J. C. Sánchez Garrido (2008), Vertical structure of tidal currents over Espartel and Camarinal sills, Strait of Gibraltar, *Journal of Marine Systems*, *74*(1–2), 120-133, doi:http://dx.doi.org/10.1016/j.jmarsys.2007.11.007.

Sánchez Román, A., J. García Lafuente, J. Delgado, J. C. Sánchez Garrido, and C. Naranjo (2012), Spatial and temporal variability of tidal flow in the Strait of Gibraltar, *Journal of Marine Systems*, *98–99*(0), 9-17, doi:http://dx.doi.org/10.1016/j.jmarsys.2012.02.011.

Santinelli, C., A. Ribotti, R. Sorgente, G. P. Gasparini, L. Nannicini, S. Vignudelli, and A. Seritti (2008), Coastal dynamics and dissolved organic carbon in the western Sardinian shelf (Western Mediterranean), *Journal of Marine Systems*, *74*(1–2), 167-188, doi:http://dx.doi.org/10.1016/j.jmarsys.2007.12.005.

Severin, T., P. Conan, X. Durrieu de Madron, L. Houpert, M. J. Oliver, L. Oriol, J. Caparros, J. F. Ghiglione, and M. Pujo-Pay (2014), Impact of open-ocean convection on nutrients, phytoplankton biomass and activity, *Deep Sea Research Part I: Oceanographic Research Papers*, *94*(0), 62-71, doi:http://dx.doi.org/10.1016/j.dsr.2014.07.015.

Smith, R. O., H. L. Bryden, and K. Stansfield (2008), Observations of new western Mediterranean deep water formation using Argo floats 2004–2006, *Ocean Sci.*, *4*(2), 133-149, doi:10.5194/os-4-133-2008.

Vargas-Yáñez, M., F. Plaza, J. García-Lafuente, T. Sarhan, J. M. Vargas, and P. Vélez-Belchi (2002), About the seasonal variability of the Alboran Sea circulation, *Journal of Marine Systems*, *35*(3–4), 229-248, doi:http://dx.doi.org/10.1016/S0924-7963(02)00128-8.

Vargas-Yáñez, M., P. Zunino, K. Schroeder, J. L. López-Jurado, F. Plaza, M. Serra, C. Castro, M. C. García-Martínez, F. Moya, and J. Salat (2012), Extreme Western Intermediate Water formation in winter 2010, *Journal of Marine Systems*, *105–108*(0), 52-59, doi:http://dx.doi.org/10.1016/j.jmarsys.2012.05.010.

Warn-Varnas, A., A. Gangopadhyay, J. A. Hawkins, and A. R. Robinson (2005), Wilkinson Basin area water masses: a revisit with EOFs, *Continental Shelf Research*, *25*(2), 277-296, doi:http://dx.doi.org/10.1016/j.csr.2004.09.005.

Wesson, J. C., and M. C. Gregg (1994), Mixing at Camarinal Sill in the Strait of Gibraltar, *Journal of Geophysical Research: Oceans*, *99*(C5), 9847-9878, doi:10.1029/94JC00256.

Whitehead, J. A. (1985), A laboratory study of gyres and uplift near the Strait of Gibraltar, *Journal of Geophysical Research: Oceans*, *90*(C4), 7045-7060, doi:10.1029/JC090iC04p07045.

Yan, M. (2005), Methods of Determining the Number of Clusters in a Data Set and a New Clustering Criterion, Virginia, Blacksburg.

VII. GENERAL DISCUSSION

Briefly summarized, the research of this dissertation has been carried out as follows: The starting point was the study of the influence of regional-scale structures on the drainage of deep Mediterranean water toward the Atlantic, which was completed by the evaluation of the consequences that tidal forcing in the Strait produces both, on the ventilation of the deep/bottom layers of the Alboran Sea and in the formation of deep water in the Gulf of Lion. The next step clarified the role of the dynamics of the Strait in fueling the productivity of the surface waters of the Alboran Sea, particularly in its northwestern sector. Finally, an exhaustive characterization of the water masses involved in the exchange was presented. Overall, this research provides satisfactory answers to questions like how and from where the deep water is uplifted, what is the tidal contribution, how it affects at the physical-ecological system and which are the water masses participating in the deep water ventilation. A more detailed discussion of the main results is presented below.

Chapter III studied the role of the WAG in uplifting deep water and elucidated whether or not the gyre facilitates its drainage toward the Atlantic Ocean. As commented in section II.d, the experimental support to this study was provided by a time series of θ obtained by a CT probe placed near the sea bed in ES that sampled the densest water flowing out the Mediterranean. Simultaneous altimetry data were employed to devise an index of the WAG intensity, which was compared with the θ series. The comparison reveals that they are highly correlated with θ lagging by two weeks the WAG index. This result strongly suggests that the WAG helps to raise the WMDW pool residing in the deep layer of the western Alboran Sea.

The depth from which this water is aspirated was also addressed. *García Lafuente et al.* [2011] showed that the averaged minimum θ observed in ES corresponds to θ=12.98°C in CS. This isotherm is found between 300 and 600 m depth in the eastern boundary of the Strait and, according to the historical MEDAR database [*MEDAR-Group*, 2002], at a mean depth of 520 m in the southern half of the western Alboran Sea. If the same reasoning is applied to the extreme minima of θ observed in ES, then the entire Mediterranean layer in the eastern approach of the Strait could be forced to overflow CS and leave the Mediterranean.

A further proof of the effect of the Strait of Gibraltar on the dynamics of the deep layer in the Alboran Sea was provided by the comparison of the outputs of the same numerical model applied to two different domains: the first domain included the Strait but it was closed in the second one. In the first case, the isotherm 12.85 °C, which is a good proxy of the WMDW in the Alboran basin, was shallower and it was even shallower across the eastern mouth of the Strait, thus reinforcing the Bernouilli suction as the mechanism responsible for the uplift of the WMDW.

As long as the aspiration is induced by the high velocities occurring in the Strait, the tidal currents must be considered. They were not included in the previous study and numerical models that ignore the tidal forcing would underestimate the Mediterranean ventilation. The effect of tides was assessed in Chapter IV by employing two numerical models of different spatial extension. In both cases, the same approach of comparing the outputs produced by runs with and without tides in the forcing terms was the basic tool of analysis. The regional model, whose domain included the Gulf of Cadiz, Strait of Gibraltar and Alboran Sea, reproduced the well-known tidally induced increase of the long-term exchange and a greater mixing in the case of the tidal run. Furthermore, the interface layer was shallower and thicker in the eastern part of the Strait, a result of the tidally enhanced mixing in the Tangier Basin, from where the water is later advected to the east. The shoaling and thickening of the interface means that more deep water has been brought toward the surface layer than in the case of non-tidal run. This in turn causes a colder and saltier Atlantic Jet, which was 0.37°C colder and 0.47 units saltier across the eastern boundary of the Strait in the tidal run. Despite the weakening of this signature as the Jet proceeds eastwards, it is still noticeable in the Almeria-Oran front in the eastern boundary of the Alboran Sea.

The basin-scale model, which included the whole Mediterranean basin and the Gulf of Cadiz, provided two worth noting results. The first one deals with the volume of water colder than 13°C (a good proxy of the WMDW in the Alboran Sea) flowing westwards through the eastern boundary of the Strait (TAC in Figure 1), which was 28% higher in the tidal run, thus suggesting that the drainage of WMDW is particularly favored by tides. Although the WMDW volume flowing out the Mediterranean has high interannual variability, it is

noteworthy that the tidal run always provided greater flows than the non-tidal run. The second is related to the effects that the mentioned differences of the Atlantic Jet density observed between tidal and non-tidal runs in the regional model could have on the formation of WMDW in the Gulf of Lion. Three proxies of the deep water formation in this area, namely, the Mixed Layer Depth (MLD), the surface area susceptible to participate in the deep convection (DCA), and the deep water formation rate, were estimated and compared in the two runs. Except for the first year, the three variables are always greater in the tidal run, which is the expected outcome for a less buoyant incoming Atlantic Jet (colder and saltier) found in the tidal run of the regional model. These variables also display a great year-to-year variability, as it does the volume of WMDW flowing out through the eastern boundary of the Strait mentioned above. These two processes seem to be related, reaching the outflow of WMDW its maximum a year after the greatest WMDW formation event.

One of the local effects of tides in the Strait discussed in Chapter IV is the enhanced mixing and consequent thickening of the interfacial layer. Considering that the Mediterranean is a deep, nutrient rich water, its mixing with the overlying Atlantic water fertilizes the Atlantic Jet, which will be more enriched than in the experiment without tidal forcing. Once more, in Chapter V the outputs of two identical biogeochemical models run with and without tides are compared. The comparison indicates that tides increase the productivity of the Alboran Sea in about 40%, and that the increase is even greater between the Strait and 3°W (the western Alboran Sea) where it reaches a 60%. The hypothesis of tidal flows in the Strait fertilizing the Atlantic inflow is examined by computing the transports of nutrient toward the Alboran Sea through the eastern boundary of the Strait. The nutrient flow is highly time-dependent in the tidal simulation: nitrate transport oscillates between 350-550 mmol NO_3 m^{-2} in this case, while it is much less variable in the non-tidal experiment (200-250 mmol NO_3 m^{-2}). The important point is, however, that the mean nutrient flux is nearly 75% greater in the tidal case, which explains the large increase of productivity obtained in the tidal simulation.

Tides could also fertilize the inflowing water also by diapycnal mixing driven by the eastwards propagation of the internal tidal bore generated at

the sill, which is reproduced by the tidal simulation. The topic was investigated conducting a new experiment in which the physics was as in the non-tidally forced simulation but with a modified set of ecosystem equations in which biochemical tracers are nudged towards their values in the tidal run within the Strait. Results from this experiment do not show significant differences with respect to the tidal simulation, thus indicating that the increased productivity observed in the Alboran Sea is driven by the intensification of nutrient transport through the Strait, while tidally driven flows in the Alboran Sea would not have much relevance.

A detailed description of the water masses exchanged through the Strait was the subject of the Chapter VI of this dissertation. In addition to WMDW and LIW, TDW and WIW have been recently proposed to be part of the outflow. Together with the two Atlantic waters NACW and SAW, they sum up to six water masses involved in the exchange. The relative contribution of each of this water masses to the exchange has been addressed by a cluster analysis of their hydrological properties. The observations from the Gibraltar International Campaign (see Chapter VI for details) indicate that the water masses east of CS have a rather clear spatial distribution, with the WMDW stacked up in the south and the TDW and LIW occupying preferably the northern area, although the latter is found at mid depth at all latitudes. On the other hand, westwards of CS the spatial differentiation of the Mediterranean waters is greatly reduced or, even, vanishes due to the strong mixing taking place in the Tangier basin. Here the cluster algorithm revealed a mixed water with similar proportions of the three prevailing Mediterranean water masses (WMDW, LIW and TDW; in this case WIW was not present), which prevent us to establish reliable distinctions between them. Therefore, from the main sill of Camarinal to the west, it seems reasonable to speak of a unique Mediterranean Water. The analysis of the zonal evolution of the densest water indicates that both the potential temperature and the salinity decrease as we proceed toward the west, and that the same applies to the NACW when we move from west to east in this case. Both of them underwent the main changes in the surroundings of CS when crossing the sill, thus confirming the great mixing occurring in this area.

The mentioned erosion of NACW signal and the fading of the spatial differentiation between the Mediterranean Waters are also visible in the

repeated CTD transects collected in the two bounding sections of the Strait within the frame of the INGRES projects. This collection of data supports the analysis of GIC data explained above and confirms the presence of four Mediterranean Water masses in the eastern part of the Strait that reduces to a unique Mediterranean water in the western part. Time variability has been analyzed with this dataset and rather clear seasonal fluctuations were found for SAW and NACW in the western section, which were related to the annual solar cycle and with the upwelling season in the Gulf of Cádiz, respectively. The four Mediterranean waters are well distinguished in the eastern section, although the data also highlights the intermittency of the WIW, which was not detected in year 2012, just the year of the GIC experiment. Coinciding with the absence of WIW, a slightly warmer and fresher LIW was detected and the WMDW showed a relative θ maximum, which was also insinuated in the mixed Mediterranean water at the western section. These features point at a mild 2010-2011 winter without WIW production. On the other hand, the WMDW showed its absolute minimum of potential temperature in year 2009, which would be an indicator of the extraordinary WMDW formation in the Gulf of Lion this year [*Salat et al.*, 2010]. Overall, the analysis of the temporal fluctuations illustrates the relatively high interannual variability of the presence and location of the Mediterranean water masses in the Strait of Gibraltar at its eastern approach, a variability that is smoothed out in the western exit due to the strong mixing in the Tangier basin.

VIII. MAIN CONCLUSIONS

The dynamics of the Strait of Gibraltar is basic for the final suction of deep waters from the near Alboran basin, which at the same time is favored by the quasi-permanent anticyclonic gyre in the Western Alboran Sea (Chapter III).

The tidal dynamics, disregarded in previous model studies, has to be resolved or at least suitably parametrized in regional and basin scale models to better reproduce some relevant features of the long-term exchange and, quite probably, other important processes taking place far away from the Strait such as the deep water formation in the Gulf of Lion (Chapter V).

The same applies to the primary productivity in the Alboran Sea, which is more realistically replicated when the tides in the Strait were included in the model. In fact, it was the tidal-induced mixing in the Strait that explain the difference, the internal waves irradiated into the Alboran Sea being of secondary importance (Chapter VI).

Regarding the spatial distribution of water masses in the Strait, up to four Mediterranean waters are detected in the outflow at the eastern part of the Strait, although one of them, the WIW, may be absent. Their signatures fade out slowly as they proceed to the west and change rather rapidly after crossing the sill of Camarinal; westwards of the sill it is more realistic to speak of a unique Mediterranean water. Seasonal signals are more evident in the Atlantic waters, while interannual variability is more important in the Mediterranean waters (Chapter VII).

IX. RESUMEN EN ESPAÑOL

IX.a. Breve Resumen

La presente tesis se ha desarrollado como una "tesis por compendio de publicaciones". Un total de cuatro artículos científicos, listados en la sección I, dan cuerpo al documento, éstos han sido publicados (a y b), aceptados para su publicación (c) o se encuentran en proceso de revisión (d), todos ellos en revistas científicas pertenecientes al primer cuartil en el área de oceanografía. Cada uno de los trabajos publicados conforma un capítulo de éste documento, en ellos se estudia el proceso de ventilación de las aguas profundas Mediterráneas que residen en la cuenca del Mar de Alborán, desde donde son absorbidas antes de fluir a través del Estrecho de Gibraltar. Asimismo se analiza cual es el efecto que ejerce el forzamiento mareal dentro del Estrecho de Gibraltar en éste y otros procesos relacionados en las cuencas contiguas.

Los trabajos que avalan esta tesis se han desarrollado en el Estrecho de Gibraltar a lo largo de los últimos años en el marco de los proyectos INGRES, llevados a cabo por el Grupo de Oceanografía Física de la Universidad de Málaga. El principal objetivo de esta memoria ha sido conocer los mecanismos y procesos involucrados en la ventilación de las aguas profundas del Mar de Alborán, qué papel juegan las estructuras de escala regional y el forzamiento mareal en el Estrecho de Gibraltar, o cuál es la estructura espacio-temporal de las masas de agua que participan en el intercambio de flujos en el Estrecho. La respuesta a estas cuestiones ofrece una nueva visión tanto de la dinámica como de las propiedades del flujo de salida antes de fluir definitivamente hacia el Océano Atlántico. Así mismo se evalúa la implicación que la dinámica mareal en el Estrecho pueda tener en los procesos biogeoquímicos del Mar de Alborán.

IX.b. Estado de la cuestión y Metodología

Las primeras referencias al origen del flujo saliente del Mar mediterráneo se encuentran en el trabajo de *Stommel et al.* [1973], quienes indican la succión de Bernouilli como el fenómeno por el cual el agua Mediterránea profunda puede ascender en el Mar de Alborán, en gran parte debido a las altas velocidades que se dan en el umbral del Estrecho de Gibraltar. En el mismo trabajo se observa que las isotermas tienden a apilarse contra la pared sur de la plataforma continental del Mar de Alborán occidental, a este respecto los autores exponen que dicha estructura no puede ser explicada simplemente por un efecto de succión de Bernouilli y especulan sobre la posibilidad de que sea un giro geostrófico permanente el responsable de dicho patrón. Poco después *Bryden and Stommel* [1982] ampliaron este tema y sugirieron que el Giro Oeste de Alborán (WAG de sus siglas en inglés) estaría involucrado en el proceso de ventilación del Agua Mediterránea Profunda Occidental (WMDW en adelante, de sus siglas en inglés) aportando energía para la aspiración de éste agua hacia el Estrecho. Por otro lado *Kinder et al.* [1986], *Parrilla et al.* [1986] y *Preller* [1986] en diferentes trabajos concluyen que la intensificación de la corriente en el margen sur de la cuenca es el resultado de la disminución de profundidad en la batimetría sobre la vorticidad potencial. Para resolver la cuestión de si el agua profunda fluía o no a través del Estrecho de Gibraltar fueron relevantes los datos recogidos durante la campaña *Gibraltar Experiment* (entre Octubre de 1985 y Octubre de 1986, más detalles en *Kinder and Bryden* [1987]) a partir de los cuales se pudo comprobar que existía una relación entre el flujo saliente y una temperatura potencial (θ en adelante) menor de 12.9°C en el umbral de Camarinal [*Pettigrew*, 1989]. Además, *Kinder and Bryden* [1990] haciendo uso de todos los datos recogidos hasta el momento analizaron la variabilidad temporal y concluyeron que el WMDW podía fluir sobre el umbral de Camarinal (CS, en la Figure 1) en cada ciclo de marea.

El tema fue de nuevo investigado por *García Lafuente et al.* [2007], dónde se evidencia la evacuación directa de WMDW a partir de observaciones recogidas en el umbral de Espartel (ES en la Figure 1). Este trabajo también mostró que existe un ciclo estacional del flujo saliente, siendo este menos frío y menos salado en invierno que en primavera-verano. En particular este trabajo muestra una caída en la θ medida en el umbral de Espartel poco después de Marzo de 2005, un mes que fue especialmente frío dentro de un

duro invierno en el que se favorecieron las condiciones climáticas para la formación de una gran cantidad de WMDW [*López-Jurado et al.*, 2005; *Schröder et al.*, 2006]. Los autores asocian este mínimo detectado en Espartel con el consecuente ascenso de WMDW más antigua y ligeramente menos pesada a profundidades desde donde su succión es más directa poco después del evento de convección en el Golfo de León. El papel de las estructuras de mesosescala en el Mar de Alborán ha sido previamente estudiado por *García Lafuente et al.* [2009], en este trabajo se encuentra una correlación significante entre la θ medida en Espartel y el coeficiente temporal del segundo modo empírico identificado en un análisis de funciones empíricas ortogonales de datos de altimetría en el Mar de Alborán, cuyo patrón espacial capturaba la estructura del WAG.

En la memoria que nos ocupa el primero de los mecanismos relacionados con la ventilación de aguas profundas estudiado es su relación con las estructuras de escala regional. A lo largo del Capítulo III ("*The Western Alboran Gyre helps ventilate the Western Mediterranean Deep Water through Gibraltar* ") se analiza una serie temporal de cinco años de duración que ha recogido datos de θ en el umbral de Espartel (ES en Figure 1), estas observaciones se corresponden con una medida de la WMDW en el flujo de salida. El sensor de temperatura se colocó cerca del fondo para asegurar que se estaba midiendo el agua más densa que fluye hacia fuera del Estrecho, es decir la WMDW. Por otro lado, para detectar las estructuras superficiales en el mar de Alborán, tales como los dos giros anticiclónicos característicos de ésta cuenca [*Viúdez et al.*, 1996], y su evolución temporal se han usado datos de altimetría. De este modo podemos investigar la posible relación entre el Giro Occidental de Alborán (WAG de sus siglas en ingles) y la evacuación de WMDW, mediante la medida de éste agua en el umbral de Espartel. Además la profundidad desde la cual este agua profunda podría ser succionada se ha estudiado a partir de datos históricos de CTD (sensor de Conductividad, Temperatura y Profundidad) de la base de datos MEDATLAS [*MEDAR-Group*, 2002]. Un último experimento se ha realizado usando un modelo numérico ejecutado con dos configuraciones distintas, en una de ellas el Estrecho de Gibraltar se cerró a conveniencia para comparar sus salidas con las de la simulación que incluía el Estrecho de Gibraltar. La comparación de las salidas

de estos dos modelos esclarece el papel que la dinámica en el Estrecho juega en la aspiración de WMDW.

En el capítulo IV se investiga cuáles son las consecuencias de incluir el forzamiento mareal en el Estrecho de Gibraltar, en la cuenca de Alborán e incluso a mayor escala, en el Mar Mediterráneo. Para ello se han ejecutado dos modelos numéricos diseñados a tal fin: el primero se trata de un modelo regional (engloba el Estrecho de Gibraltar y sus cuencas cercanas), mientras que el segundo es un modelo a escala de cuenca (Mar Mediterráneo). Ambos modelos se ejecutaron dos veces, con y sin forzamiento mareal. El modelo regional muestra correctamente el conocido efecto de las mareas en los flujos intercambiados a través del Estrecho [*Bryden et al.*, 1994]. Por otro lado la modificación de las propiedades hidrológicas como consecuencia de la inclusión de mareas puede ser valorada mediante la comparación de ambas simulaciones. Dicha modificación tiene consecuencias relevantes en el fenómeno de formación de agua profunda que ocurre en el Golfo de León ya que el agua Atlántica, que será modificada en las distintas aguas Mediterráneas, ha sido pre-condicionada por primera vez debido a la mezcla inducida por las mareas en el Estrecho. Esta hipótesis se investiga extensamente mediante el modelo a escala de cuenca siguiendo el mismo procedimiento que en el caso del modelo regional. De este modo se estudia el papel de la marea en el proceso de convección, que da lugar a la formación de WMDW en el Golfo de León, así como en la ventilación de éste agua en el Mar de Alborán.

El siguiente punto a tratar estudia cómo afectan las mareas en el Estrecho de Gibraltar a los patrones de productividad primaria en el Mar de Alborán.

El flujo de entrada de agua Atlántica hacia el Mar Mediterráneo, llamado normalmente chorro Atlántico, condiciona la circulación superficial del Mar de Alborán. El patrón superficial normal en la zona consiste en dos giros anticiclónicos, el ya mencionado WAG y el Giro de Alborán Este (EAG por sus iniciales en inglés) [*Seco*, 1959; *Donguy*, 1962; *Lanoix*, 1974]. El chorro Atlántico fluye alrededor de estos giros y da lugar a intensos frentes de densidad, ampliamente descritos en la bibliografía [*Tintore et al.*, 1988; 1991; *Viúdez et al.*, 1996], al encontrarse con un agua más densa y más salada. Asociada a esta actividad de frentes datos de satélite han evidenciado altas

concentraciones de clorofila a lo largo del chorro Atlántico [*Navarro et al.*, 2011], lo que sugiere una productividad primaria sostenida por la circulación ageostrófica en el frente [*Oguz et al.*, 2014]. Este patrón es más evidente en la parte occidental del Mar de Alborán, donde los vientos de poniente provocan afloramientos a lo largo de la costa española y dan lugar a floraciones de fitoplancton [*Sarhan et al.*, 2000; *Ramírez et al.*, 2005; *Reul et al.*, 2005; *Macías et al.*, 2007; 2008]. Estos procesos son esenciales para explicar por qué el Mar de Alborán es la sub-cuenca más productiva del Mar Mediterráneo [*Uitz et al.*, 2012]. La dinámica de frentes y su implicación en la productividad biológica ha sido recientemente investigado por *Oguz et al.* [2014] usando un modelo numérico 3D. Sin embargo este modelo no incluye mareas, lo cual puede ser un inconveniente si tenemos en cuenta que las corrientes mareales pueden fertilizar las aguas entrantes superficiales a través de una mayor mezcla vertical en el lado Oeste del umbral de Camarinal [*García Lafuente et al.*, 2013]. Además, la gran interacción entre las corrientes mareales y la abrupta topografía del Estrecho de Gibraltar origina una serie de transiciones hidráulicas [*Sánchez Garrido et al.*, 2011] que favorecen los movimientos verticales, particularmente en la cuenca de Tánger, aguas abajo del umbral de Camarinal (TB en la Figure 1), así como la mezcla entre las aguas Atlánticas, relativamente pobres en nutrientes, y las aguas Mediterráneas, profundas y ricas en nutrientes previamente succionadas desde la cuenca de Alborán. Una buena parte de estas aguas podrían retornar hacia el Mediterráneo cuando la marea invierte y favorecer así la producción primaria en la capa fótica, ayudando a mantener la alta productividad observada en la zona norte. Sin embargo este tema no ha sido estudiado hasta el momento.

La cuestión se aborda en el Capítulo V (*Modeling the impact of tidal flows on the biological productivity of the Alboran Sea*) mediante la implementación de un modelo de circulación de alta resolución acoplado a un modelo de ecosistemas. Siguiendo el mismo procedimiento descrito para el Capítulo V, un experimento numérico de referencia en el cual no se incluye el forzamiento mareal (pero reproduce la circulación básica en el área del Estrecho de Gibraltar y el Mar de Alborán) se compara con una simulación similar con mareas. De esta forma se estudia el efecto que la dinámica mareal dentro del Estrecho puede tener en los procesos biológicos del mar de Alborán.

Por último se aborda el análisis y la identificación de las masas de agua que forman parte de los flujos entrante y saliente. A éste respecto *Millot et al.* [2006] sugiere que además de las dos maas de agua Mediterránea tradicionalmente consideradas en el flujo de salida, el Agua Intermedia Levantina (LIW en adelante) y la WMDW, otras massas de agua participan en éste flujo. En este estudio Millot pone de manifiesto la presencia del Agua Densa del Tirreno (TDW), formada por la mezcla entre WMDW residente en el Tirreno con LIW procedente de la cuenca Este del Mediterráneo. Según los resultados de Millot la TDW habría sido detectada en el flujo de salida en los años 2003 y 2004. En la misma línea *Millot* [2009] sugiere la participación de una cuarta agua Mediterránea, el agua intermedia de Invierno (WIW), que se forma por la pérdida de temperatura del Agua Atlántica Modificada (MAW) durante el invierno en la plataforma continental de la región noroccidental del Mar Mediterráneo. La WIW se identifica en un diagrama θ-S por un mínimo de salinidad en el intervalo de densidad $28<\sigma_\theta<29$, y estaría posicionada entre la NACW y las otras tres aguas Mediterráneas (WMDW, LIW y TDW). Más recientemente [*Millot*, 2014] reconsidera la idea incidiendo en la hipótesis de un flujo saliente formado por diferentes proporciones de las cuatro aguas Mediterráneas, que serían aun distinguibles incluso después de sobrepasar el umbral de Camarinal en su recorrido hacia el Océano Atlántico. El autor basa sus conclusiones en el análisis de la pendiente de las líneas de mezcla definidas en un diagrama θ-S. Sin embargo la identificación de las diferentes masas de agua Mediterráneas más allá del umbral de Camarinal es un resultado controvertido [*García Lafuente et al.*, 2011]. La cuestión es ampliamente tratada en el Capítulo VI *(Mediterranean waters along and across the Strait of Gibraltar, characterization and zonal modification*) en el cual se examinan las masas de agua que fluyen a través del Estrecho de Gibraltar, cuál es su distribución y variabilidad temporal.

Las características termohalinas de las aguas Mediterráneas que fluyen a través del Estrecho se diferencian sutilmente, y además su presencia o posición en una sección determinada es muy variable y depende en gran medida de la fase de la marea. La campaña oceanográfica *Gibraltar International Campaign*, (ver el capítulo VI para más detalles) se llevó acabo con el objetivo de tomar nuevas medidas en el Estrecho mediante un MVP (Moving Vessel Profiler), este instrumento permite un muestreo de alta resolución espacial, además de favorecer la realización de los transeptos en un corto periodo de tiempo, y por

lo tanto minimiza la mencionada variabilidad en el conjunto de datos tomados. Las medidas se procesaron usando un análisis de clúster específicamente desarrollado para dicho conjunto de datos. El método clasifica cada medida del CTD en un cluster en función de la distancia a unos centroides previamente definidos por unas características θ-S-σ que se corresponden con cada una de las posibles masas de agua que pueden formar parte en algún momento del flujo a través del Estrecho. La variabilidad temporal se ha planteado por medio de una colección de medidas de CTD en los extremos Este y Oeste del Estrecho de Gibraltar (ES y TAC den la Figure 1), dichas secciones se han venido repitiendo desde 2005 en el marco de los proyectos INGRES.

Los detalles específicos sobre la metodología en cada caso pueden encontrarse en los capítulos correspondientes.

IX.c. Resultados más significativos

De manera resumida, la investigación desarrollada a lo largo de esta memoria se ha llevado a cabo del siguiente modo; el punto de partida ha sido el estudio de la influencia que las estructuras de escala regional pueden tener en la evacuación del agua Mediterránea profunda a través del Estrecho de Gibraltar y hasta el Océano Atlántico. Seguidamente el punto anterior se completa con la evaluación de las consecuencias que la inclusión del forzamiento mareal en el Estrecho de Gibraltar tiene tanto en la ventilación de las capas profundas del Mar de Alborán como en la formación de agua profunda en el Golfo de León. El siguiente paso consiste en dilucidar cuál es el papel que la dinámica del Estrecho tiene en la productividad primaria de las aguas superficiales en el Mar de Alborán, particularmente en su parte noroccidental. Por último se presenta una caracterización detallada de las masas de agua que participan en los flujos intercambiados. En su conjunto esta memoria resuelve satisfactoriamente cuestiones como de dónde y cómo es aspirada el agua profunda, cual es la contribución de la marea en tal proceso, como afecta este forzamiento mareal al sistema físico-ecológico y cuáles son las masas de agua que participan en la ventilación del agua profunda. Los principales resultados se discuten a continuación.

En el CapítuloIII se ha estudiado el papel que desempeña el WAG en la aspiración de agua profunda y se ha aclarado que este giro anticiclónico facilita su drenaje hacia el Océano Atlántico. Para ello se han estudiado las series de tiempo de θ obtenidas con un sensor de conductividad-temperatura desplegado cerca del fondo en Espartel que monitoriza el agua más densa que fluye hacia fuera del Mediterráneo. Simultáneamente mediante datos de altimetría se ha ideado un índice para seguir la evolución de la intensidad del WAG, el cual se ha comparado con la serie de θ. El resultado es una alta correlación entre ambas variables, con un desfase de dos semanas entre el índice del WAG y la θ medida en Espartel. Este resultado sugiere que el WAG facilita el ascenso de la WMDW que reside en la parte más profunda del Mar de Alborán occidental.

Además se ha estimado la profundidad desde la cual estas aguas son aspiradas. Siguiendo a *García Lafuente et al.* [2011], la θ mínima promedio observada en el umbral de Espartel se correspondería con una θ=12.98°C en el umbral de Camarinal. Dicha isoterma se encuentra entre 300 y 600 m de profundidad en el extremo Este del Estrecho (sección TAC en la Figure 1) y, de acuerdo con la base de datos históricos de MEDATLAS [*MEDAR-Group*, 2002], a unos 520 m de profundidad en la mitad sur del Mar de Alborán occidental. Si este mismo procedimiento se aplica a los extremos de la mínima θ observada en el umbral de Espartel se puede deducir que toda la capa Mediterránea cerca de la sección Este del Estrecho podría ser succionada, superar el umbral de Camarinal y abandonar el Mediterráneo.

Por otro lado se ha estudiado cómo influye la dinámica del Estrecho de Gibraltar en la capa profunda del Mar de Alborán por medio de la comparación de las salidas del mismo modelo numérico aplicado a dos dominios diferentes, en el primer caso se incluye el Estrecho mientras que en el segundo éste se cerró. En el primer caso la isoterma de 12.85°C, que es un buena representación del WMDW en la cuenca de Alborán, resultó ser más somera sobretodo en la zona más cercana al extremo Este del Estrecho. Dicho resultado indica que la succión por efecto Bernouilli es el mecanismo responsable de la aspiración del WMDW.

Debido a que el proceso de aspiración de aguas profundas está claramente inducido por las altas velocidades que tienen lugar en el Estrecho de Gibraltar, las corrientes mareales deben ser consideradas. Estas corrientes

no se han incluido en los estudios anteriores, sin embargo los modelos numéricos que no tienen en cuenta el forzamiento mareal podrían estar subestimando la ventilación en el Mar Mediterráneo. El efecto de las mareas se desarrolla en el Capítulo IV haciendo uso de dos modelos numéricos con diferente escala espacial, en ambos casos se procede comparando las salidas de una simulación con mareas con respecto a otra que no incluye el forzamiento mareal. El modelo regional incluye el Golfo de Cádiz, el Estrecho de Gibraltar y el Mar de Alborán, este modelo reproduce el incremento del intercambio a largo término inducido por las mareas así como una mayor mezcla en el caso de la simulación con mareas. Además, la capa interfacial es más somera y de mayor espesor en la parte Este del Estrecho, como resultado de la mayor mezcla en la cuenca de Tánger en presencia de mareas. Desde aquí esta agua será posteriormente advectada hacia el Este. El asomeramiento y el mayor esperor de la interfase implica que más agua profunda se ha transportado a las capas superficiales que en el caso de no incluir mareas. Ello a su vez causa un chorro Atlántico más frío y más salino, 0.37°C más frío y 0.47 unidades más salado a lo largo de la sección Este del Estrecho (sección TAC en la Figure 1) en la simulación que incluye mareas. Esta señal puede reconocerse incluso en el frente Almería-Orán en el extremo oriental del Mar de Alborán a pesar de su erosión a medida que el chorro Atlántico fluye hacia el Este.

El modelo a escala de cuenca incluye el Mar Mediterráneo y el Golfo de Cádiz. A partir de éste modelo se han obtenido dos resultados significativos. El primero de ellos tiene que ver con el volumen de agua que se acumula por debajo de los 13°C (un límite que representa bien el WMDW en el Mar de Alborán) que fluye hacia el Oeste a través del extremo oriental del Estrecho de Gibraltar (TAC en la Figura Figure 1), dicho volumen es un 28% mayor en la simulación con mareas, lo cual sugiere que el drenaje de WMDW está favorecido por la acción de las mareas. A pesar de que el volumen de WMDW que fluye hacia fuera del Mediterráneo tiene una gran variabilidad interanual, hay que destacar que la simulación con mareas arroja siempre mayores flujos que en el caso de no incluir mareas. El segundo resultado relaciona los efectos mencionados anteriormente en el chorro Atlántico (más denso en la simulación de mareas) con la formación de WMDW en el Golfo de León. Se han definido tres variables que evalúan la formación de agua profunda en éste área, la profundidad de la capa de mezcla (MLD de sus siglas en ingles), el

área superficial que puede participar en el proceso de convección profunda (DCA de sus siglas en ingles), y el ratio de formación de agua profunda. Estas variables se calcularon y compararon en ambas simulaciones. El resultado indica que, excepto en el primer año, las tres variables mencionadas son siempre mayores en la simulación que incluye el forzamiento mareal, como se espera que sea para un chorro Atlántico con menos flotabilidad (más frío y más salado) visto en el modelo regional. Además las variables mencionadas muestran fluctuaciones anuales importantes, al igual que lo hace el volumen de WMDW que fluye a través de la sección Este del Estrecho comentado anteriormente. Estos dos procesos parecen estar relacionados, tal es así que el flujo saliente de WMDW es máximo un año después del mayor evento de formación de WMDW.

Uno de los efectos locales de las mareas en el Estrecho discutida en el Capítulo IV es el incremento en la mezcla y el consecuente mayor espesor de la capa interfacial. Considerando que el agua Mediterránea es un agua profunda, rica en nutrientes, su mezcla con el agua Atlántica situada sobre ella fertilizaría el chorro Atlántico, que estaría más enriquecido que en el experimento sin forzamiento mareal. De nuevo, en el Capítulo V se comparan las salidas de dos modelos biogeoquímicos ejecutados con y sin mareas. Dicha comparación indica que las mareas provocan un aumento de la productividad del Mar de Alborán de alrededor de un 40%, y que este incremento es incluso mayor en el área que queda entre el Estrecho y 3°W (el Mar de Alborán Occidental) donde este aumento puede alcanzar el 60%. La hipótesis de que los flujos mareales en el Estrecho pueden fertilizar el flujo Atlántico de entrada se estudia mediante el cálculo del transporte de nutrientes hacia el Mar de Alborán a través de la sección Este del Estrecho (TAC en la Figura 1). El flujo de nutrientes varía ampliamente con el tiempo en la simulación con mareas, el transporte de nitrato oscila entre 350-550 mmol NO_3 m^{-2} en dicho caso, mientras que es mucho menos variable en el experimento que no incluye forzamiento mareal (200-250 mmol NO_3 m^{-2}). El resultado más interesante, sin embargo, es que el flujo medio de nutrientes es aproximadamente un 75% mayor en el caso de considerar las mareas, lo cual explicaría el gran incremento de productividad que se obtiene en la simulación con mareas.

La marea también podría fertilizar el agua que fluye hacia el Mediterráneo mediante mezcla diapicna, por medio de la propagación hacia el Este de ondas internas generadas en el umbral, las cuales reproduce el modelo con mareas satisfactoriamente. Esta posibilidad se ha investigado mediante el desarrollo de un nuevo experimento en el cual la física se mantiene como en la simulación no forzada con mareas mientras que los trazadores biogeoquímicos se modifican para que tiendan hacia sus valores dentro del Estrecho en el modelo con mareas. Los resultados de este experimento no muestran diferencias significativas con respecto a la simulación inicial con mareas, con lo cual se concluye que el incremento de productividad que se observa en el Mar de Alborán se debe a la intensificación del transporte de nutrientes a través del Estrecho, mientras que otros flujos mareales en el Mar de Alborán como la propagación de ondas internas no son significativos.

Una detallada caracterización de las masas de agua que se intercambian a través del Estrecho es el objetivo del Capítulo VI de ésta memoria. Además de la WMDW y la LIW, recientemente se ha propuesto que también el TDW y el WIW forman parte del flujo de salida. Junto a estas aguas Mediterráneas fluyen en sentido opuesto dos aguas Atlánticas, la SAW y la NACW, en total suman hasta seis masas de agua participando en el intercambio. La contribución relativa de cada una de estas seis masas de agua al intercambio se ha abordado por medio de un análisis de cluster de sus propiedades hidrológicas. Las observaciones obtenidas en la *Gibraltar International Campaign* (ver el Capítulo VI para más detalles), muestran que las masas de agua al Este del umbral de Camarinal se distribuyen espacialmente de una forma mucho más clara. La WMDW se apila contra la pared Sur y la TDW y la LIW ocupan preferiblemente el área norte, aunque la LIW se encuentra a profundidades medias en todas las latitudes. Por otro lado, al Oeste del umbral de Camarinal la diferenciación espacial de las Aguas Mediterráneas deja de ser tan clara, e incluso desaparece debido a la mezcla que tiene lugar en la cuenca de Tánger. En esta zona el algoritmo únicamente detecta un agua muy mezclada con proporciones similares de las tres masas de agua Mediterráneas predominantes (WMDW, LIW y TDW, en esta campaña la WIW no se encontraba presente en ninguna de las secciones), lo cual impide distinguir adecuadamente entre ellas. Por lo tanto, desde el umbral de Camarinal hacia el Oeste, parece razonable referirse a una única agua

Mediterránea. El análisis de la evolución zonal del agua más densa indica que ambas, la θ y la salinidad disminuyen a medida que nos desplazamos hacia el Oeste, y lo mismo ocurre con el NACW a medida que fluye de Oeste a Este. Ambas experimentan los cambios más significantes en los alrededores del umbral de Camarinal, lo cual da cuenta de la importante mezcla que tiene lugar en la zona.

La erosión de la señal de la NACW y la desaparición de la diferenciación espacial entre las aguas Mediterráneas se detecta también en las repeticiones de las secciones CTD llevadas a cabo en las dos secciones de los extremos Este y Oeste del Estrecho en el marco de los proyectos INGRES (Figure 1, TAC y TES respectivamente). Estos datos apoyan los resultados obtenidos en el análisis de los datos de la *Gibraltar International Campaign* detallados en el párrafo anterior, y confirman la presencia de hasta cuatro masas de agua Mediterránea en la sección Este, que se reducen a una única masa de agua Mediterránea en la parte Oeste. La variabilidad temporal analizada con este conjunto de datos muestra que tanto la SAW como la NACW presentan variabilidad estacional en la sección Oeste, debida al ciclo solar anual y la estación de afloramiento en el Golfo de Cádiz respectivamente. Las cuatro aguas Mediterráneas definidas anteriormente se pueden distinguir claramente en la sección Este, no obstante los datos resaltan la intermitencia de la WIW, que no se detectó en 2012, tal y como se observó el mismo año en los datos de la *Gibraltar International Campaign.* Coincidinendo con la ausencia de WIW la LIW que se midió fue ligeramente más cálida y más dulce, y la WMDW se caracterizó por un máximo relativo, la misma señal se insinúa también en la mezcla de aguas Mediterráneas de la sección Oeste. Estas características apuntan a un invierno suave en 2010-2011 en el que probablemente no se formó WIW. Por el contrario, la WMDW presenta un mínimo absoluto de temperatura potencial en el año 2009, lo cual podría ser un efecto de la extraordinaria formación de WMDW que tuvo lugar en el Golfo de León tal año [*Salat et al.*, 2010]. La serie temporal ha mostrado que, sobre todo, las aguas Mediterráneas tienen una alta variabilidad interanual que afecta tanto a su presencia como a su localización en la sección Este del Estrecho de Gibraltar, una variabilidad que se suaviza en el contorno Oeste debido a la intensa mezcla que ocurre en la cuenca de Tánger.

IX.d. Principales conclusiones de esta memoria

La dinámica del Estrecho de Gibraltar es fundamental en la ventilación de las aguas profundas del Mar de Alborán, la cual a su vez es facilitada por la presencia casi permanente del giro anticiclónico del Mar de Alborán Occidental (Capítulo III).

En el capítulo III no se tiene en cuenta la dinámica mareal, sin embargo en el capítulo IV se concluye que esta debe ser resulta en los modelos a escala regional y de cuenca que pretenden reproducir algunas características relevantes del intercambio a largo término y, muy probablemente, otros importantes procesos que tienen lugar más allá del Estrecho, como la formación de agua profunda en el Golfo de León.

El mismo razonamiento se aplica a la productividad primaria en el Mar de Alborán la cual se reproduce satisfactoriamente cuando el forzamiento mareal se incluye en un modelo regional físico-ecológico (Capítulo V). Más específicamente se encuentra que la diferencia entre tener o no en cuenta las mareas puede suponer hasta un 60% más de producción primaria en la cuenca Oeste de Alborán.

Con respecto a la distribución espacial de las masas de agua en el Estrecho (Capítulo VI), hasta cuatro masas de agua Mediterráneas se han detectado en el flujo saliente en la sección del contorno Este del Estrecho, a pesar de que una de ellas, la WIW, puede no estar presente en determinados años. La señal de estas aguas se suaviza lentamente a medida que fluyen hacia el Oeste, y lo hacen abruptamente una vez sobrepasan el umbral de Camarinal. Según lo anterior, al Oeste del umbral sería más apropiado hablar de una única agua Mediterránea. Con respecto a la variabilidad temporal se observa que las señales estacionales son más evidentes en las aguas Atlánticas, mientras que la variabilidad interanual es más notable en las aguas Mediterráneas.

X. List of Abbreviations

AC: Algeciras-Ceuta

AS: Alboran Sea

AWs: Atlantic waters

CS: Camarinal Sill

CT: Conductivity-Temperature

CTD: Conductivity-Temperature-Depth

DCA: Deep Convection Area

ES: Espartel Sill

GIC: Gibraltar International Campaing

GMSM: Global Mediterranean Sea Model

LIW: Levantine Intermediate Water

MAW: Modified Atlantic Water

MLD: Mixed Layer Depth

MVP: Moving vessel profiler

MWs: Mediterranean waters

NACW: North Atlantic Central Water

RSGM: Regional Strait of Gibraltar Model

SAW: Surface Atlantic Water

SoG: Strait of Gibraltar

TDW: Tyrrhenian Dense Water

WAG: Western Alboran Gyre

WIW: Winter Intermediate Water

WMDW: Western Mediterranean Deep Water

θ: Potential temperature

σ_θ: Potential density

XI. References

Bryden, H. L., J. Candela, and T. H. Kinder (1994), Exchange through the Strait of Gibraltar, *Progress in Oceanography*, *33*(3), 201-248, doi:http://dx.doi.org/10.1016/0079-6611(94)90028-0.

Bryden, H. L., and H. M. Stommel (1982), Origin of the Mediterranean Outflow, *Journal of Marine Research*, *40*, 55-71.

Donguy, J. (1962), Hydrologie en mar d'Alboran, *Cah. Oceanogr*, *14*, 573-578.

García Lafuente, J., E. Bruque Pozas, J. C. Sánchez Garrido, G. Sannino, and S. Sammartino (2013), The interface mixing layer and the tidal dynamics at the eastern part of the Strait of Gibraltar, *Journal of Marine Systems*, *117–118*(0), 31-42, doi:http://dx.doi.org/10.1016/j.jmarsys.2013.02.014.

García Lafuente, J., J. Delgado, A. Sánchez Román, J. Soto, L. Carracedo, and G. Díaz del Río (2009), Interannual variability of the Mediterranean outflow observed in Espartel sill, western Strait of Gibraltar, *Journal of Geophysical Research: Oceans*, *114*(C10), C10018, doi:http://dx.doi.org/10.1029/2009JC005496.

García Lafuente, J., A. Sánchez Román, G. Díaz del Río, G. Sannino, and J. C. Sánchez Garrido (2007), Recent observations of seasonal variability of the Mediterranean outflow in the Strait of Gibraltar, *Journal of Geophysical Research: Oceans*, *112*(C10), C10005, doi:http://dx.doi.org/10.1029/2006JC003992.

García Lafuente, J., A. Sánchez Román, C. Naranjo, and J. C. Sánchez Garrido (2011), The very first transformation of the Mediterranean outflow in the Strait of Gibraltar, *Journal of Geophysical Research: Oceans*, *116*(C7), C07010, doi:http://dx.doi.org/10.1029/2011JC006967.

Kinder, T. H., and H. L. Bryden (1987), The 1985"1986 Gibraltar Experiment: Data collection and preliminary results, *Eos, Transactions American Geophysical Union*, *68*(40), 786-794, doi:10.1029/EO068i040p00786.

Kinder, T. H., and H. L. Bryden (1990), Aspiration of Deep Waters through Straits, in *The Physical Oceanography of Sea Straits*, edited by L. J. Pratt, pp. 295-319, Springer Netherlands, doi:10.1007/978-94-009-0677-8_14.

Kinder, T. H., D. C. Chapman, and J. A. Whitehead (1986), Westward Intensification of the Mean Circulation on the Bering Sea Shelf, *Journal of Physical Oceanography*, *16*(7), 1217-1229, doi:10.1175/1520-0485(1986)016<1217:WIOTMC>2.0.CO;2.

Lanoix, F. (1974), *Project Alboran; etude hydrologique et dynamique de la mer d'Alboran: d'après les travaux effectués dans le cadre du project Alboran (Juillet et*

Aout 1962), Sous-comite Oceanographique de l'Organisation du Traite de l'Atlantique Nord.

López-Jurado, J. L., C. González-Pola, and P. Vélez-Belchí (2005), Observation of an abrupt disruption of the long-term warming trend at the Balearic Sea, western Mediterranean Sea, in summer 2005, *Geophysical Research Letters*, *32*(24), n/a-n/a, doi:10.1029/2005GL024430.

Macías, D., M. Bruno, F. Echevarría, A. Vázquez, and C. M. García (2008), Meteorologically-induced mesoscale variability of the North-western Alboran Sea (southern Spain) and related biological patterns, *Estuarine, Coastal and Shelf Science*, *78*(2), 250-266, doi:http://dx.doi.org/10.1016/j.ecss.2007.12.008.

Macías, D., G. Navarro, F. Echevarría, C. M. García, and J. L. Cueto (2007), Phytoplankton pigment distribution in the northwestern Alboran Sea and meteorological forcing: A remote sensing study, *Journal of Marine Research*, *65*(4), 523-543, doi:10.1357/002224007782689085.

MEDAR-Group (2002), MEDAR 200 2Database Mediterranean and Black Sea cruise Inventory, Observed Data, Analysed Data and Climatological Atlas (4CD-ROMs).

Millot, C. (2009), Another description of the Mediterranean Sea outflow, *Progress in Oceanography*, *82*(2), 101-124, doi:http://dx.doi.org/10.1016/j.pocean.2009.04.016.

Millot, C. (2014), Heterogeneities of in- and out-flows in the Mediterranean Sea, *Progress in Oceanography*, *120*(0), 254-278, doi:http://dx.doi.org/10.1016/j.pocean.2013.09.007.

Millot, C., J. Candela, J.-L. Fuda, and Y. Tber (2006), Large warming and salinification of the Mediterranean outflow due to changes in its composition, *Deep Sea Research Part I: Oceanographic Research Papers*, *53*(4), 656-666, doi:http://dx.doi.org/10.1016/j.dsr.2005.12.017.

Navarro, G., Á. Vázquez, D. Macías, M. Bruno, and J. Ruiz (2011), Understanding the patterns of biological response to physical forcing in the Alborán Sea (western Mediterranean), *Geophysical Research Letters*, *38*(23), n/a-n/a, doi:10.1029/2011GL049708.

Oguz, T., D. Macias, J. Garcia-Lafuente, A. Pascual, and J. Tintore (2014), Fueling Plankton Production by a Meandering Frontal Jet: A Case Study for the Alboran Sea (Western Mediterranean), *PLoS ONE*, *9*(11), e111482, doi:10.1371/journal.pone.0111482.

Parrilla, G., T. H. Kinder, and R. H. Preller (1986), Deep and intermediate mediterranean water in the western Alboran Sea, *Deep Sea Research Part A. Oceanographic Research Papers*, *33*(1), 55-88, doi:http://dx.doi.org/10.1016/0198-0149(86)90108-1.

Pettigrew, N. R. (1989), Direct measurements of the flow of western Mediterranean deep water over the Gibraltar sill, *Journal of Geophysical Research: Oceans*, *94*(C12), 18089-18093, doi:10.1029/JC094iC12p18089.

Preller, R. H. (1986), A numerical model study of the Alboran Sea Gyre, *Progress in Oceanography*, *16*(3), 113-146, doi:http://dx.doi.org/10.1016/0079-6611(86)90031-5.

Ramírez, T., D. Cortés, J. M. Mercado, M. Vargas-Yañez, M. Sebastián, and E. Liger (2005), Seasonal dynamics of inorganic nutrients and phytoplankton biomass in the NW Alboran Sea, *Estuarine, Coastal and Shelf Science*, *65*(4), 654-670, doi:http://dx.doi.org/10.1016/j.ecss.2005.07.012.

Reul, A., V. Rodríguez, F. Jiménez-Gómez, J. M. Blanco, B. Bautista, T. Sarhan, F. Guerrero, J. Ruíz, and J. García-Lafuente (2005), Variability in the spatio-temporal distribution and size-structure of phytoplankton across an upwelling area in the NW-Alboran Sea, (W-Mediterranean), *Continental Shelf Research*, *25*(5–6), 589-608, doi:http://dx.doi.org/10.1016/j.csr.2004.09.016.

Salat, J., P. Puig, and M. Latasa (2010), Violent storms within the Sea: dense water formation episodes in the NW Mediterranean, *Adv. Geosci.*, *26*, 53-59, doi:10.5194/adgeo-26-53-2010.

Sánchez Garrido, J. C., G. Sannino, L. Liberti, J. García Lafuente, and L. Pratt (2011), Numerical modeling of three-dimensional stratified tidal flow over Camarinal Sill, Strait of Gibraltar, *Journal of Geophysical Research: Oceans*, *116*(C12), C12026, doi:http://dx.doi.org/10.1029/2011JC007093.

Sarhan, T., Garcı, amp, x, J. a Lafuente, M. Vargas, J. M. Vargas, and F. Plaza (2000), Upwelling mechanisms in the northwestern Alboran Sea, *Journal of Marine Systems*, *23*(4), 317-331, doi:http://dx.doi.org/10.1016/S0924-7963(99)00068-8.

Schröder, K., G. P. Gasparini, M. Tangherlini, and M. Astraldi (2006), Deep and intermediate water in the western Mediterranean under the influence of the Eastern Mediterranean Transient, *Geophysical Research Letters*, *33*(21), n/a-n/a, doi:10.1029/2006GL027121.

Seco, E. (1959), La capa de velocidad cero en el mar de Alborán, *Rev. Ceincas*, *25*, 765-779.

Stommel, H., H. Bryden, and P. Mangelsdorf (1973), Does some of the Mediterranean outflow come from great depth?, *PAGEOPH*, *105*(1), 879-889, doi:10.1007/BF00875837.

Tintoré, J., D. Gomis, S. Alonso, and G. Parrilla (1991), Mesoscale Dynamics and Vertical Motion in the Alborán Sea, *Journal of Physical Oceanography*, *21*(6), 811-823, doi:10.1175/1520-0485(1991)021<0811:MDAVMI>2.0.CO;2.

Tintore, J., P. E. La Violette, I. Blade, and A. Cruzado (1988), A Study of an Intense Density Front in the Eastern Alboran Sea: The Almeria–Oran Front, *Journal of Physical Oceanography*, *18*(10), 1384-1397, doi:10.1175/1520-0485(1988)018<1384:ASOAID>2.0.CO;2.

Uitz, J., D. Stramski, B. Gentili, F. D'Ortenzio, and H. Claustre (2012), Estimates of phytoplankton class-specific and total primary production in the Mediterranean Sea from satellite ocean color observations, *Global Biogeochemical Cycles*, *26*(2), n/a-n/a, doi:10.1029/2011GB004055.

Viúdez, Á., J. Tintoré, and R. L. Haney (1996), Circulation in the Alboran Sea as Determined by Quasi-Synoptic Hydrographic Observations. Part I: Three-Dimensional Structure of the Two Anticyclonic Gyres, *Journal of Physical Oceanography*, *26*(5), 684-705, doi:10.1175/1520-0485(1996)026<0684:CITASA>2.0.CO;2.

Whitehead, J. A. (1985), A laboratory study of gyres and uplift near the Strait of Gibraltar, *Journal of Geophysical Research: Oceans*, *90*(C4), 7045-7060, doi:10.1029/JC090iC04p07045.

Agradecimientos

Agradezco a mis directores no solo la ayuda inestimable en el desarrollo de esta tesis sino también el apoyo permanente y la motivación que día a día me han transmitido. Especial reconocimiento merece mi director y tutor Jesús, que más allá de brindarme esta oportunidad me ha acompañado en la experiencia de ser doctorando prácticamente de la mano desde la primera vez que embarqué en el pequeño *Odón de Buen*.

A mis compañeros del grupo de Oceanografía Física por estar ahí, en especial a José Carlos y Simone que continúan respondiendo día sí y día también a mis innumerables dudas. A todos con los que en algún momento he compartido jornadas de mar abierto y saben de cuántos colores puede ser una persona.

El Dr. Gianmaría Sannino me tutorizó durante algunos meses de estancia, a él y a su grupo de "Climate Modelling and Impacts" de ENEA les agradezco profundamente la calidez con la que me acogieron.

Esta Tesis Doctoral se ha realizado gracias a la concesión de una beca de Formación de Personal Investigador (BES-2011-043421) de la Subdirección General de Formación e Incorporación de Investigadores del Ministerio de Ciencia e Innovación, en el marco del Proyecto INGRES-3 (CTM2010_21229) “Flujo Mediterráneo en Gibraltar, influencia en la ventilación de las aguas Mediterráneas y primera evolución y acoplamiento con las aguas centrales en el Golfo de Cádiz”.

El trabajo se ha realizado en el Departamento de Física Aplicada II de la Universidad de Málaga y parcialmente, gracias a las ayudas para la realización de estancias breves concedidas por la mencionada subdirección, en el departamento de Climate Modelling, del Ente per la Nuove Tecnologie, l’Energia e l’Ambiente (ENEA), centro de investigación en Roma (Italia).